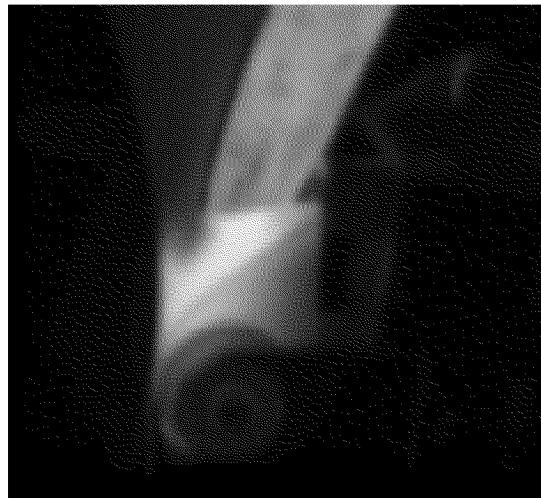


Effective Automated Tape Winding Process with On-Line Bonding under Transient Thermal Conditions



Yves Marcel Pierre Toso
Ingénieur mécanicien EPFL

SWISS FEDERAL INSTITUTE OF TECHNOLOGY ZURICH
IMES, Center of Structure Technologies

*En lui vous aussi, après avoir entendu
la parole de la vérité, l'Évangile de votre
salut, en lui vous avez cru et vous avez été
scellés du Saint-Esprit qui avait été promis.**

* Ephésien 1.13, La Sainte Bible, Nouvelle Edition de Genève, Quatrième Edition, ISBN 2-8260-1211-8, 1992

Acknowledgements

At this point, I would like to express my gratitude to all the people who helped me during the course of my work.

I am particularly grateful to my thesis supervisor Prof. Dr. Paolo Ermanni for having given me the opportunity to finish it, for his advices, for his help to improve it, for his availability and for having allowed me to work with considerable freedom.

I especially acknowledge my thesis co-advisor Prof. Dr. Dimos Poulidakos for his advices, comments and tips during the development of the thermal model and the redaction of Chapter 4.

I thank Prof. Dr. Markus Meier and Prof. Dr. Gerhard Ziegmann for supporting me during the starting phase of this thesis.

I acknowledge Prof. Dr. Dieter Landolt, Prof. Dr. Jan-Anders Månson, Dr. Pierre-Etienne Bourban, Dr. Vishal Mallick and Dr. Dietrich Reinhard for their support during the duration of the Swiss Priority Program on Materials Research: Cost-Effective Composites for the Transportation Industry.

I am thankful to Dr. Thomas Schweizer for his help during the rheometric measurements, Mr. Willy Surer for his aid during the measurements of the specific heat capacity of the fiber reinforced polypropylene and Mr. Christian Florin for his advices in the domain of infrared-measurements.

I thank my colleagues Dr. Marion Uebersax-Dumortier, Dr. Stephan Busato, Mr. Andreas Endruweit, Mr. Nicolas Goudemand and Mr. Thierry Luthy for their diverse helps. I am thankful to all my colleagues for bearing me and for contributing to the good environment during this study.

I acknowledge Mr. Gerhard Kuhn for his help during the various experimental investigations and for the maintenance of the machines. Thanks are also due to the secretary, the current and alumni technicians of the Center of Structure Technologies: Mrs. Helen Götz, Mrs. Sabine Ohlendorf-Ritter, Mr. Freddy Bürki, Mr. Hans-Rudi Nef and Mr. Hans-Peter Eigenmann.

I'm thankful to Mr. Mauro Beretta and Mr. Alfio Cerini who helped me to develop the new compaction assembly during their diploma thesis.

Finally, I will particularly thank my parents, my brother and my friends for their encouragements and bearing me during all the duration of the current work.

Table of Contents

CHAPTER 1 Introduction	1
1.1. Background	1
1.2. State of the art	2
1.3. Objectives	2
1.4. Critical issues	3
1.5. Approach	3
1.6. Overview of the Ph.D. thesis	4
CHAPTER 2 The Automated Tape Winding (ATW) and The Automated Tape Placement (ATP) Processes	7
2.1. Introduction	7
2.2. The process	7
2.2.1. A process example	7
2.2.2. The incoming tape	9
2.2.3. The nip point, line or curve	10
2.2.4. Setup configurations	10
2.2.5. Selection of the adequate incoming tape and of the appropriate components	17
2.2.6. Parts examples	17
2.3. Modeling	18
2.3.1. Heat transfer in composite materials	19
2.3.2. Strength development at polymer interfaces	20
2.3.3. Intimate contact	23
2.3.4. Polymer chain diffusion (autohesion, healing or self-diffusion)	24
2.3.5. Void consolidation	25
2.3.6. Void growth	28
2.3.7. Crystallization kinetics (from the melt)	29
2.3.8. Melting kinetics	33
2.3.9. Degradation kinetics	33
2.3.10. Bondline thickness	34
2.4. Process simulation	35
2.5. Nomenclature	36

CHAPTER 3	Experimental Investigations of the Automated Tape Winding Process with On-Line Bonding	39
3.1.	Introduction	39
3.2.	Experimental setup	42
3.3.	Specimen preparations and characterization methods	44
3.3.1.	Preparation of the specimens for the mechanical characterization	44
3.3.2.	Mechanical characterization	44
3.3.3.	Preparation of the polished cross-sections	45
3.3.4.	Void content characterization	46
3.4.	Results of the short beam shear tests	46
3.4.1.	Variation of the interlaminar shear strength in the axial direction of the cylinder	46
3.4.2.	Reference cylinder	47
3.4.3.	Variation of the interlaminar shear strength with the nitrogen flow temperature and the compaction force applied to the nip line	48
3.4.4.	Variation of the interlaminar shear strength with the nitrogen flow temperature and the winding pitch	50
3.4.5.	Variation of the interlaminar shear strength with the nitrogen flow temperature and the winding speed	52
3.5.	Measurements with the pyrometer	55
3.5.1.	Discussion on the polymer chain diffusion	57
3.5.2.	Discussion on the polymer degradation	58
3.6.	Micrograph analysis	59
3.7.	Conclusion	61
CHAPTER 4	Thermal Phenomena in the Automated Tape Winding Process	63
4.1.	Introduction	63
4.2.	Theory	66
4.3.	Numerical simulation	69
4.3.1.	Approach	69
4.3.2.	Discretization and solution procedure	71
4.3.3.	Material parameters	75
4.3.4.	Results	75
4.4.	Experimental determination of the heat transfer in the vicinity of the gas torch	76
4.4.1.	Setup	77
4.4.2.	Measurement and evaluation method	79
4.4.3.	Results	82

4.5. Experiments for the validation of the simulation	85
4.5.1. Setup	85
4.5.2. Experiments	87
4.5.3. Results	87
4.6. Comparison between experiments and simulations	90
4.7. Conclusion and outlook	94
4.8. Nomenclature	94

CHAPTER 5 Heating Strategies for the Automated Tape Winding (ATW) Process

97

5.1. Introduction	97
5.2. Process	99
5.3. Theory	100
5.3.1. Heat transfer	100
5.3.2. Degree of polymer chain diffusion	101
5.4. Model	102
5.5. Validation	103
5.6. Heating strategies	106
5.6.1. Convection heat input of the torch	106
5.6.2. Influence of the initial mandrel temperature	109
5.7. Conclusion	112
5.8. Nomenclature	113

CHAPTER 6 Development of a New Compaction Tool for the Fabrication of Reinforcement Frames of a Railway Coach

115

6.1. Introduction	115
6.2. Test geometry	116
6.3. Tape compaction concepts	118
6.3.1. Utilization of a tape-tension system	118
6.3.2. Utilization of a solid compaction roller	120
6.3.3. Utilization of a deformable compaction roller	122
6.3.4. Utilization of a compaction shoe	123
6.3.5. Utilization of a deformable band	124
6.3.6. Evaluation of the different compaction concepts	126
6.4. Development of the new compaction head	127
6.4.1. Choice of the band	127
6.4.2. Number of rollers guiding the band	127
6.4.3. Rotation of the compaction assembly	128
6.4.4. Description of the new setup	128
6.5. Fabrication of reinforcement frames for a railway coach	130

6.6. Results	132
6.6.1. Preparation of the specimens for the mechanical tests	132
6.6.2. Evaluation of some specimens for each frames	133
6.6.3. Evaluation of the best frame	133
6.7. Conclusion	134
6.8. Nomenclature	135
CHAPTER 7 Conclusions and Outlook	137
7.1. Conclusions	137
7.2. Outlook	139
APPENDIX A	141
A.1. Development for the determination of the convective heat transfer coefficient	141
A.2. Nomenclature	143
APPENDIX B	145
B.1. Degree of polymer chain diffusion	145
B.2. Determination of the mechanical relaxation time of the polypropylene matrix	146
B.3. Determination of the molecular weight	150
B.4. Numerical determination of the degree of polymer chain diffusion during the process	151
B.5. Remarks	152
B.6. Nomenclature	152
REFERENCE	155
CURRICULUM VITAE	165

Version Abrégée

Le sujet de cette thèse est l'enroulement automatique de bandes thermoplastiques renforcées par fibre. Ses objectifs sont: 1) d'étudier scientifiquement ce procédé avec des bandes faites en polypropylène renforcé par fibre de verre, afin d'optimiser la résistance interlaminaire des produits et d'améliorer ses coûts de fonctionnement, 2) de faciliter l'enroulement sur des géométries complexes.

La première tâche de ce travail fut d'assembler plusieurs composants, afin de créer une installation permettant d'étudier expérimentalement l'enroulement automatique de bandes. Un grand nombre de cylindres fut fabriqué avec cette installation en variant les paramètres de fabrication suivants: la température du flux d'azote, la force de compression, le pas d'enroulement, la puissance de l'unité de chauffage du canal de préchauffage et la vitesse d'enroulement. Ils permirent d'observer l'influence des paramètres de fabrication sur la résistance interlaminaire des échantillons produits. Cette étude montre que plusieurs combinaisons de paramètres permettent d'obtenir des cylindres possédant une résistance interlaminaire satisfaisante. Toutefois la résistance interlaminaire des cylindres produits par enroulement est plus petite ou équivalente à 80% de celle d'un cylindre post-consolidé dans un autoclave.

Un programme numérique fut écrit afin d'approfondir les recherches. Il permet de simuler les phénomènes thermiques transitoires qui ont lieu durant le procédé. Une méthode fut également développée dans le but de définir une partie des constantes (le coefficient de convection dans la région du point de contact et la température du flux d'azote en dehors de la couche limite thermique) qui permettent de déterminer des conditions aux bords du modèle.

Des simulations furent réalisées pour deux combinaisons de paramètres de fabrication. Ces dernières furent choisies en considérant les résultats de la recherche expérimentale. Les cylindres fabriqués avec la première combinaison possèdent une faible résistance interlaminaire tandis que ceux de la seconde combinaison en ont une bonne. Afin d'acquérir des données permettant de valider le programme de simulation, des mesures de température furent réalisées avec deux pyromètres durant la fabrication de cylindres. Les résultats numériques obtenus montrent une bonne concordance avec les valeurs expérimentales.

Ensuite, les paramètres d'un modèle décrivant le degré de diffusion des chaînes de polymère furent déterminés. Le modèle fut adapté pour les calculs non-isothermiques et intégré dans le programme de simulation thermique. Les prédictions du nouveau modèle furent comparées à des mesures expérimentales pour les deux combinaisons de paramètres de fabrication et de conditions aux bords qui furent utilisées précédemment. Elles montrent pour les exemples utilisés que la différence entre la résistance interlaminaire des cylindres enroulés et celle du cylindre post-consolidé dans un autoclave est due à un degré de diffusion des chaînes de polymère insuffisant. Plusieurs simulations furent effectuées avec une nouvelle stratégie de chauffage en conservant les paramètres de fabrication utilisés précédemment. Elles permirent de déterminer des conditions de fabrication qui conduisent à la fabrication de cylindres possédant une résistance interlaminaire maximale. Le programme de simulation fut également utilisé pour décrire une nouvelle stratégie de chauffage qui permettrait de ne pas utiliser le chauffage au point de contact.

Un nouvel outil de compression fut développé, afin de permettre l'enroulement de bandes sur des géométries complexes. Sur un mandrin représentant un wagon, un anneau de référence fut consolidé en autoclave et des anneaux furent fabriqués par le procédé qui est étudié. Des mesures de résistance interlaminaire furent effectuées sur des échantillons de chaque anneau. Elles permirent de déterminer l'anneau enroulé qui avait la meilleure résistance interlaminaire moyenne. Pour ce dernier, le degré de soudage fut estimé sur une grande partie de la circonférence. Ces dernières mesures montrent que le nouvel outil peut être utilisé pour le procédé d'enroulement de bandes thermoplastiques renforcées par fibre.

Abstract

This thesis deals with the automated tape winding process. Its objectives are twofold: 1) to investigate scientifically the automated tape winding process with fiber reinforced polypropylene tapes in order to process products with optimized interlaminar shear strength and to ameliorate its economic efficiency, 2) to facilitate the laying of the tape on complex geometries.

In order to investigate the automated tape winding process, a setup is assembled and modified. The experimental investigations study the influence of nitrogen temperature, compaction force, winding pitch, heating power of the preheating device and processing speed on the interlaminar shear strength of tape wound cylinders. They show that various sets of process parameters enable to fabricate parts with a good interlaminar shear strength. It is however approximately equal to 80% of that of a reference cylinder that is post-processed in an autoclave.

A numerical program is developed to pursue the investigations. It simulates the transient thermal phenomena during the entire automated tape winding process. In order to provide accurate input values for the model, a method to evaluate the heat flow parameters of the hot gas torch (i.e. the outside flow temperature and the convective heat transfer coefficient) is developed and used.

Simulations are performed with two sets of process parameters. During the previous experimental investigations, they permit to produce parts with low and high interlaminar shear strength. Concurrently to the numerical simulations, a comprehensive experimental program with two pyrometers is carried out to provide the on-line temperature data that serve to validate the numerical simulations. The comparison of experimental measurements and simulation predictions shows good agreements for the two sets of parameters.

The parameters of a standard model determining the degree of polymer chain diffusion are evaluated. The model is adapted for non-isothermal calculations and integrated in the transient thermal simulation program. Experimental results and predictions of the new model are compared and discussed for the two sets of process parameters that are used to validate the thermal simulation program. They show that the low degree of bond strength of the best tape wound cylinders is caused for the current investigations by an insufficient degree of polymer chain diffusion. Considering the same process parameters, a heating strategy is presented that permits to process cylinders with a complete degree of polymer chain diffusion and then to produce cylinders with optimum interlaminar

properties. The simulation program is also used to describe another heating strategy that disregards the very sensitive nip heating.

In order to enable the automated tape winding on various geometries, a new compaction head is developed. Frames over a mandrel representing a train coach model are wound. A reference frame is also consolidated in an autoclave. The interlaminar shear strength of the best tape wound frame and that of the reference frame are compared and discussed. They demonstrate that the new tool can be used for the automated tape winding process.

CHAPTER 1

Introduction

1.1. Background

The demand of lightweight solutions is continuously increasing in the transportation and offshore industries, as well as in the sport world. Composite materials can provide solutions for those industries. They can be used to reduce the weight of parts, because fiber orientation and content can be adapted specifically to the load cases.

In addition, fiber reinforced thermoplastic composites can be reprocessed, recycled and repaired when failure occurs through polymer chain pull out. Various polymers can be used as matrix system for composite applications. Selection criteria include cost-effectiveness, chemical and/or mechanical properties.

Various processes can produce fiber reinforced thermoplastic parts: hand lay-up with autoclave molding, fusion bonding, press molding, diaphragm forming, liquid composite molding, roll forming, automated tape placement, filament winding and automated tape winding.

Among the several manufacturing processes investigated in the past in the composite laboratory, the automated tape winding with on-line bonding is very promising. In comparison with the other techniques, it has a large potential in terms of economical attractiveness and implementation of tailored design

solutions in the finished parts. Due to its high level of automation, the labor work is extremely reduced, the precision of the fiber orientation is high, the reproducibility and the security during the process are enhanced.

1.2. State of the art

Up to now, few components are fabricated with the automated tape winding process. Ahrens et al. ^[3] show the utilization of this process to produce motor overhang bandages. Stover ^[86] presents the industrial fabrication of shafts.

Researchers have performed theoretical investigations on this process with APC-2. Already in 1991, Ghasemi Nejhad et al. ^[28] present a thermal analysis of the automated tape winding process. Later, James and Black ^[41] compare steady-state thermal simulation results with infrared thermography measurements.

Most of the experimental investigations ^{e.g. [2]} also use carbon fiber reinforced poly-ether-ether-ketone (PEEK). Few other studies employ other material combinations. Lauke et al. ^[50] propose a method to measure the interlaminar shear strength of curved samples. Their samples are made of polyamide 12 (PA12) reinforced with glass fiber. Funck ^[26] optimizes the process speed with glass fiber reinforced polypropylene. Mondo and Parfrey ^[62] investigate the performance of carbon fiber reinforced poly-phenylene-sulfide (PPS).

Further, few researches try to improve the complexity of the parts that can be produced with this process. Mazumdar and Hoa ^[59] show the development of a technique for the fabrication of elliptical springs for automotive suspensions. Steiner ^[82] presents the fabrication of a two-dimensional double curved component. Romagna ^[71] describes a method to fabricate reinforcements for a railway coach.

1.3. Objectives

Hence, the objectives of this Ph.D. thesis are twofold: 1) to investigate scientifically the automated tape winding process with fiber reinforced polypropylene tapes in order to process products with optimized interlaminar shear strength and to ameliorate its economic efficiency, 2) to facilitate the laying of the tape on more complex geometries.

1.4. Critical issues

The automated tape winding process is very promising, but also very challenging. As tape bonding takes place during tape lay-up, the available process window is small.

Since it exists transient conditions during the automated tape winding process, the small process window is changing. When the process parameters are not adapted to the variations of the process conditions, the laminate respectively part quality will be affected.

In order to fabricate lightweight products, the laminate quality must be maximized. For the automated tape winding process, the intralaminar quality is mainly dependent on the quality of the incoming tape. Therefore the main sensible properties depending on the process are the interlaminar bond properties. This signifies that the interlaminar bond properties must be optimized for the entire laminate with appropriate transient process conditions.

The range of application of a process technique is related to the complexity of the parts that can be produced. During the placement of tapes on complex paths and/or geometries, the form of the nip varies rapidly. In order to bond correctly the tape to the substrate, the compaction system(s) must press the tape on its entire width for all the nip geometries.

1.5. Approach

The research approach of this thesis is considering experimental and theoretical investigations.

Experimental investigations

The aim of the experimental investigations is to find various sets of processing parameters that permit to process cylinders having a good interlaminar shear strength (degree of bond strength) for a fiber reinforced polypropylene. Considering the experimental results, realistic boundary conditions and transient validation data are then determined.

Simulations analyses

The main work of the present study is to develop a three-dimensional transient thermal model for the automated tape winding process. The parameters of a model describing the development of polymer chain diffusion must be also determined. The model has to be adapted for the case of non-isothermal calculations and integrated in the thermal simulation program. Heating strategies must be determined with this new simulation tools.

Convection heat transfer in the nip

In order to provide accurate input values for the simulation program, a method to evaluate the heat flow parameters of the hot gas torch (i.e. the outside flow temperature and the convective heat transfer coefficient) has to be developed and used.

Compaction tools

In order to extend the potential of the automated tape winding process, this study aims to develop a new compaction tool. It has to allow the tape winding of an incoming tape on different support shapes.

1.6. Overview of the Ph.D. thesis

Chapter 2 presents the basic principles of the automated tape winding process, the terminology that is employed, various setup components in order to give an overview of the setup configurations, and various models that describe the thermal and physical phenomena occurring during the process.

In Chapter 3, a setup is assembled and modified in order to study the influence of process parameters on the quality of the produced cylinders. A short beam shear apparatus is used to evaluate the interlaminar shear strength (ILSS). The experimental investigations determine various sets of process parameters that lead to a good degree of bond strength. The maximum ILSS-values of tape wound specimens are however lower than that of a reference that is post-processed in an autoclave. Investigations are performed in order to analyze possible causes of the difference between the ILSS of tape wound and post-processed specimens.

Chapter 4 first describes the development of a transient thermal simulation program for the automated tape winding process. In order to provide accurate input values for the model, a method to evaluate the heat flow parameters of the hot gas torch (i.e. the outside flow temperature and the convective heat transfer coefficient) is also developed. The simulation program is validated with two sets of process parameters that are used in Chapter 3. They have been selected considering parts with low and high interlaminar shear strength values. The simulation and experimental results are compared and discussed.

In Chapter 5, a model evaluating the development of the degree of polymer chain diffusion is integrated in the transient thermal simulation program. Experimental results and predictions of the new model are compared and discussed for the two sets of process parameters that are used in Chapter 4. Two heating strategies are also presented.

The development a new compaction assembly is detailed in Chapter 6. Unlike other compaction tools, it enables to apply a compaction force on various geometries. Frames over a mandrel representing a train coach model are wound. A reference frame is also consolidated in an autoclave. The interlaminar shear strength of the best tape wound frame and that of the reference frame are compared and discussed.

Chapter 7 lists the main achievements of this study and presents the outlook for the automated tape winding process.

CHAPTER 2

The Automated Tape Winding (ATW) and The Automated Tape Placement (ATP) Processes

2.1. Introduction

This research work deals with the automated tape winding process. The basic principles and the physical phenomena occurring during this process are similar to those of the automated tape placement process. Therefore this chapter gives an overview of both processes.

Section two presents the main process steps, terminology and major setup components. Section three introduces different models that describe the thermal and physical phenomena occurring during those processes. It details the thermodynamics and the polymer diffusion through an interface. Those models are used in Chapter 4 and Chapter 5. Section four provides finally general considerations over the simulation of those processes.

2.2. The process

2.2.1. A process example

The fabrication of a cylinder is described below in order to explain the basics of the automated tape winding process. The manufacturing process is divided in four stages: the preparation, the start, the process and the post-process.

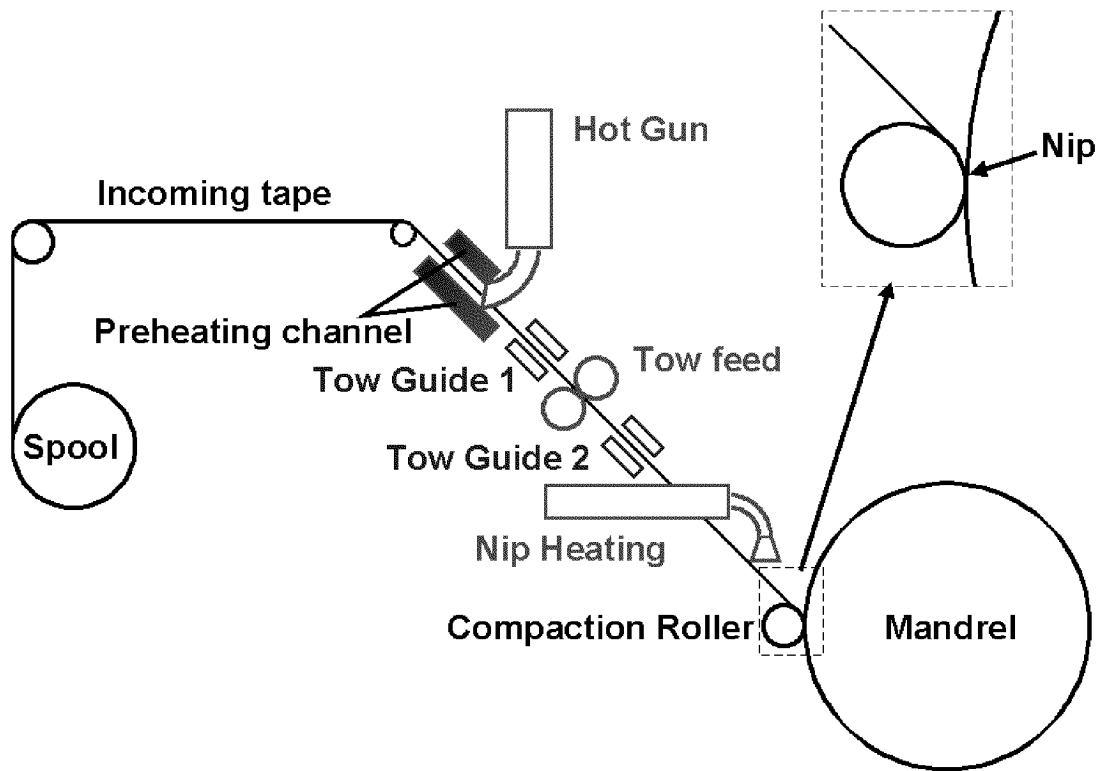


Figure 2.1: Sketch of an automated tape winding setup at the ETH

The preparation of the setup begins with the mounting of the spool on the spool holder. Then the tape is pulled manually up to the second tow guide (Figure 2.1). The winding machine is turned on. The motion axes of the winding machine are set. The winding program is loaded. The preheating channel and the nip heating are warmed up.

The start procedure consists to feed the tape (at least up to the nip), to fix the incoming tape on the mandrel, to start the winding program and to apply the compaction force with the compaction roller.

During the process, the spool supplies the composite material. The latter is warmed up in the preheating channel and by the nip heating. The incoming tape is compacted with the compaction roller at the nip. It is laid on different paths to fill free volumes. When the laying direction needs to be changed abruptly, the process can be stopped and restarted. The laid material composes the substrate, and its quantity increases as the process is going on.

The basic principle of the process is to bond (weld) on-line the incoming tape to the substrate (see sections 2.3.2, 2.3.3 and 2.3.4). The compaction force at the nip enforces the contact between the incoming tape and the substrate. The composite material must be warmed up in order to allow the bonding process.

The process is terminated, when the desired quantity of composite material is laid on the planned locations. At this time, the winding program stops automatically. Then the incoming tape is cut and the compaction force is removed. Note that the substrate forms now the cylinder.

Generally the cylinder and the mandrel constitute a single part at the end of the process. Therefore, a post-processing stage is necessary. The demolding is the action of separating the mandrel and the cylinder.

2.2.2. The incoming tape

The tapes are composed of fiber material and thermoplastic matrix: e.g. carbon fiber and poly-ether-ether-ketone or glass fiber and polypropylene (Figure 2.2).

The advantages of tapes are that the fibers are pre-impregnated and the matrix pre-consolidated. This means that the fibers and the thermoplastic matrix are bounded, and that the void content is low. This enables to concentrate the research effort on the placement of the tape and the bonding between the substrate and the incoming tape. The latter is described in sections 2.3.2, 2.3.3 and 2.3.4.

The disadvantage of the tapes is that they are expensive. The utilization of more usual preforms (bundles and yarns) permits therefore to reduce the material costs. On the other hand, the fibers need to be impregnated and the thermoplastic matrix consolidated in the bundles and yarns with matrix powder and fibers. The impregnation is the process that describes the evolution of the binding between the fibers and the matrix. The consolidation process depicts the reduction of the void content until the voids vanish.

The impregnation and the consolidation stages must be performed on-line prior to the nip in the automated tape winding and the automated tape placement processes. They necessitates large compaction pressure and large energy inputs to heat the perform material closed to or above the melting temperature of the thermoplastic matrix. The elevated temperature of the matrix is required to facilitate the deformations of the thermoplastic matrix and of the composite material.

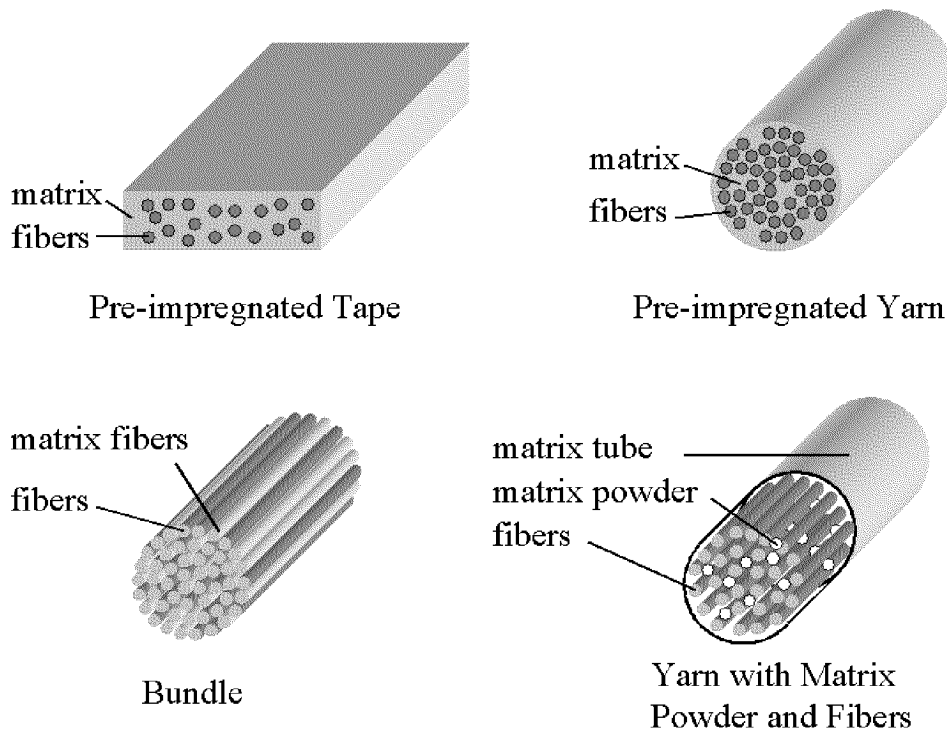


Figure 2.2: Different types of preforms

2.2.3. The nip point, line or curve

The nip is the location where the incoming tape comes into contact with the support or the substrate. In two-dimensional analysis, it is a point. In three-dimensional analysis, the shape of the support (substrate) determines its form. It can be a line or a curve.

2.2.4. Setup configurations

Typical setup configurations are shown in Figure 2.1 and Figure 2.3. They are composed of following major components:

- motion control(s)
- assembly(ies) to apply the compaction force
- heat source(s) and cooling system(s)
- guiding system
- support

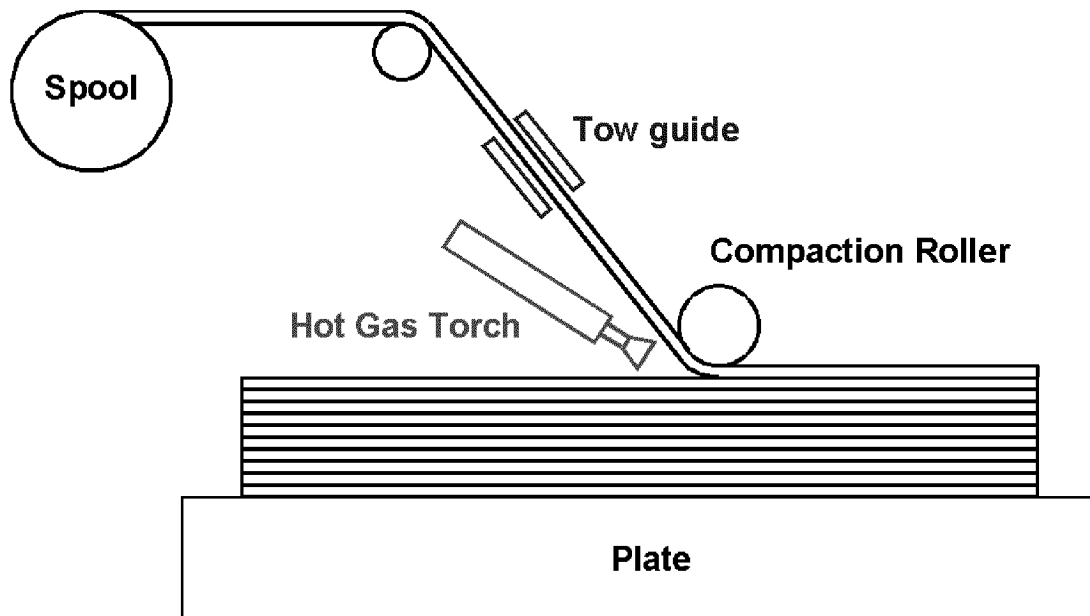


Figure 2.3: Sketch of an automated tape placement setup

Motion control

The motion control is performed with a numerically controlled machine. During the process, a program drives the position of the nip and therefore the fiber orientations in the substrate. It determines also the process speed(s) and the duration of the process.

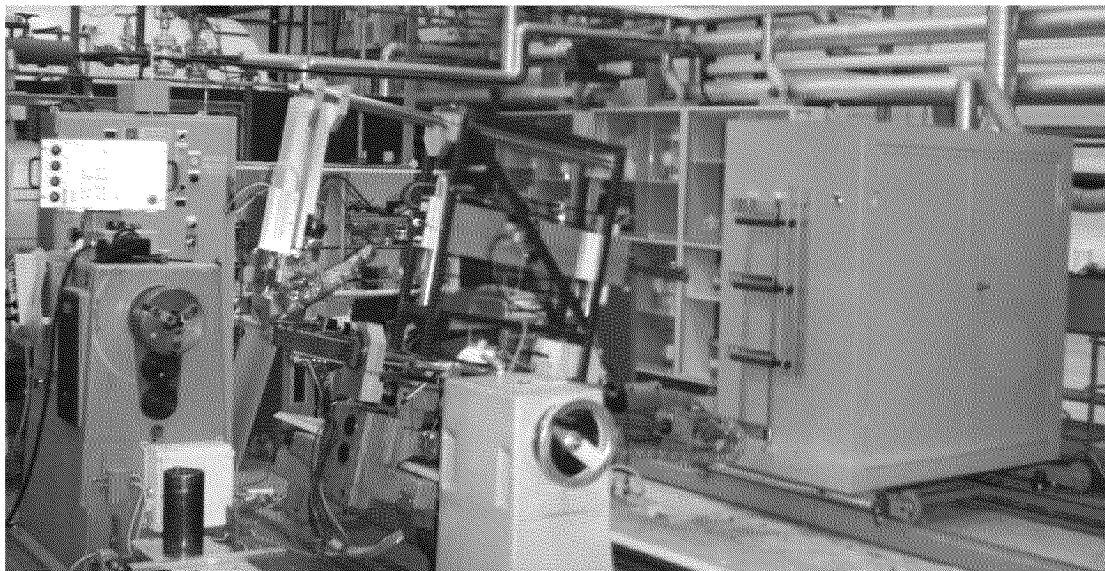


Figure 2.4: Automated tape winding setup at the ETH

The automated tape winding process can be performed with a winding machine (Figure 2.4) or a robot controlling the rotation of the mandrel (Figure 2.5). The automated tape placement process can be done with a tape placement machine (Figure 2.6) or with a robot.

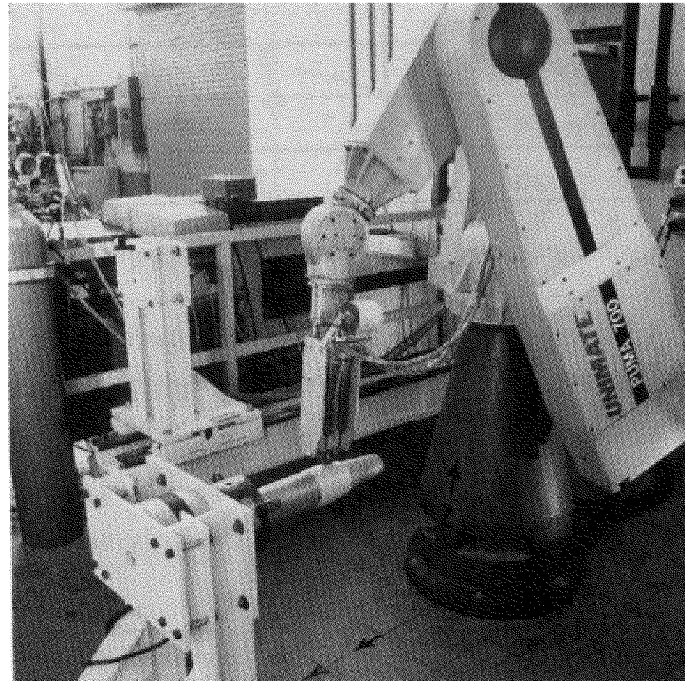


Figure 2.5: Automated tape winding with a robot ^[82]

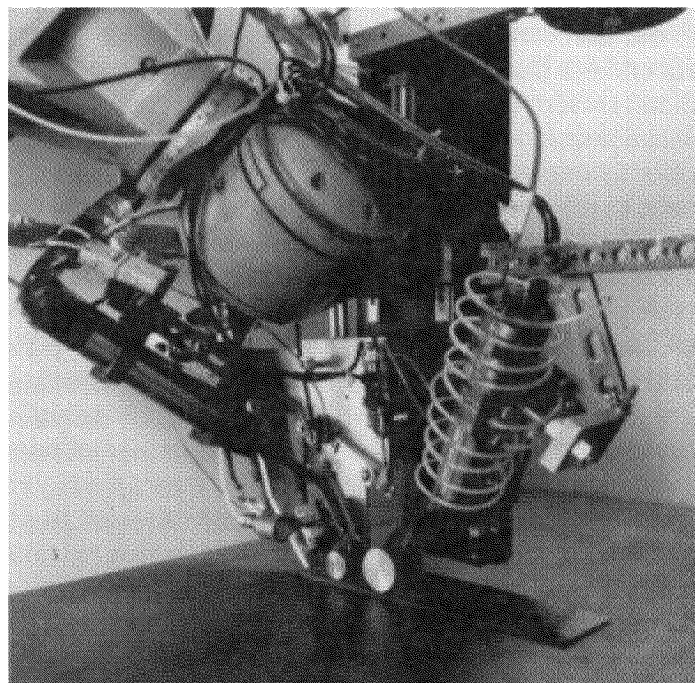


Figure 2.6: Prototype of the tape placement setup at the Center for Composite Materials ^[70]

Compaction assembly

The task of the compaction components is to bring the tape and the substrate into contact, and to smooth the surface irregularities on the merging surfaces. Two methods can be employed during the automated tape winding processes: to locally apply a compaction force or to use a setup to pull the tape. In the case of the automated tape placement, only a compaction force can be applied to the nip, as the tape would slip when it is tugged on an automated tape placement setup.

A pressure cylinder and a compaction tool are the two main components used when a compaction force is applied to the nip. The first component is usually hydraulic or pneumatic. Its role is to generate a defined compaction force. This force is transmitted to the composite material by a roller, a shoe or a special system^[95]. Since there are no standards, their dimensions vary in the literature.

Tension in the preform can be converted to a compaction pressure when the part has a curvature and when the tape is held at both ends. Lauke et al.^[49] use a magnetic brake, and Romagna^[71] a tension unit. It has to be remarked that the tension can also introduce internal stresses in the laminate as shown by Funck^[26].

Heat sources and cooling systems

The task of the heat sources and of the cooling systems is to control the process temperature of the composite material. They use the three principles of heat transfer: convection, radiation and conduction (Table 2.1).

Heat sources are distinguished with respect to their locations. Figure 2.7 shows various heat exchange locations: dQ_1/dt preheating of the incoming tape, dQ_2/dt preheating (cooling) of the substrate, dQ_3/dt nip heating, dQ_4/dt tape heating (cooling), dQ_5/dt mandrel heating (cooling), dQ_6/dt post-heating (cooling) and dQ_7/dt substrate cooling with the environment.

Type of Heat Sources	Convection	Radiation	Conduction	Locations
Hot Air ^[47]	X			1, 2, 3, 5, 6
Hot Nitrogen ^[10]	X			1, 2, 3, 5, 6
Flame ^[35]	X			3
CO ₂ laser ^[26]		X		3
Infrared Panel ^[47]		X		1, 2, 6
Infrared Lamp ^[71]		X		3
Water and Oil			X	5
Compaction Roller			X	4
Compaction Shoe			X	4
Guiding Component			X	1
Environment	X	X		1, 2, 5, 6, 7

Table 2.1: Principle used by various heat sources and their available locations

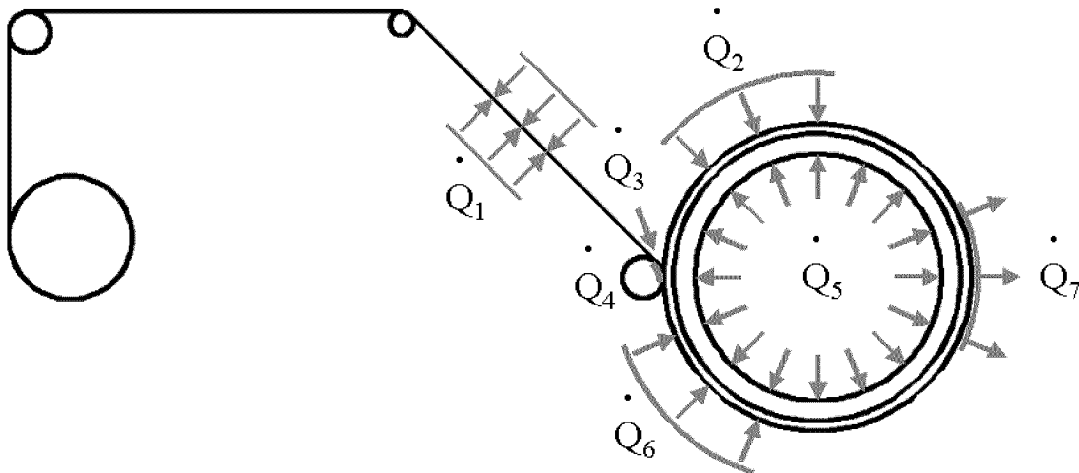


Figure 2.7: Various locations of the heat sources and heat losses

Guiding elements for the incoming tape

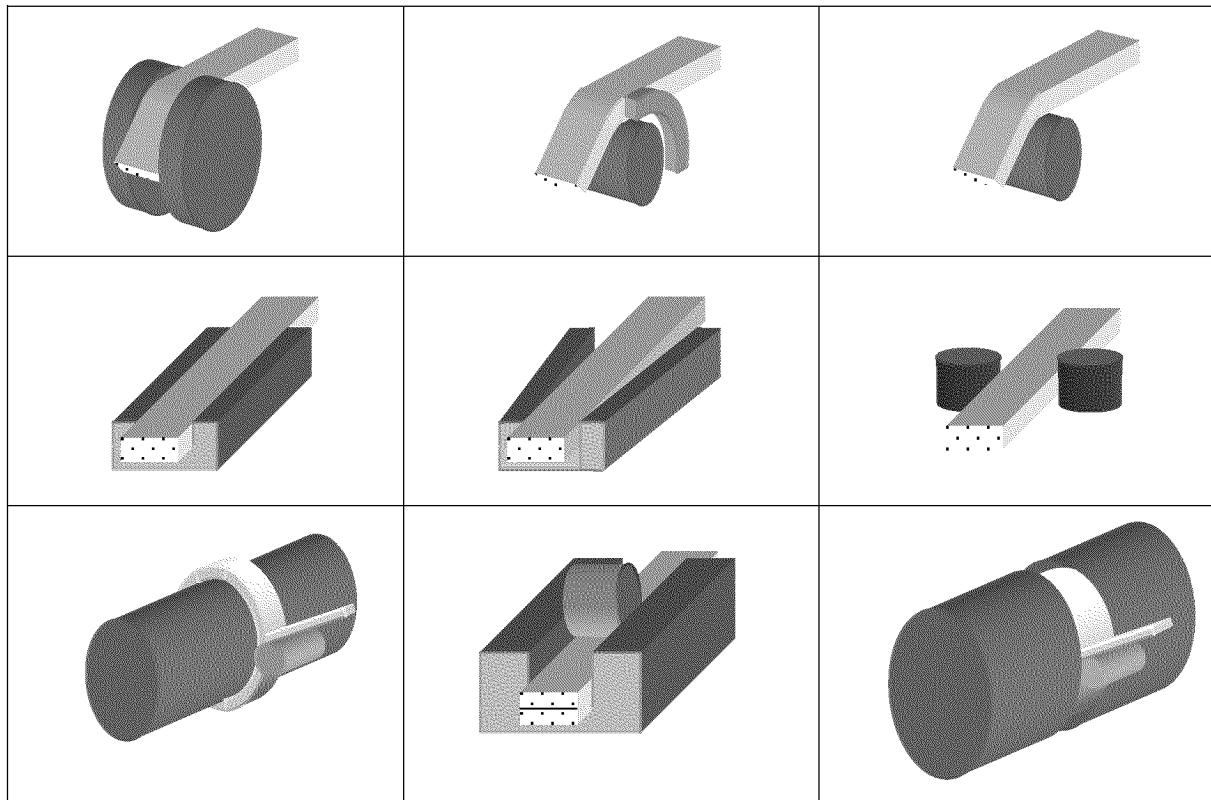


Figure 2.8: Different guiding elements

The guiding system is composed of different guiding elements (Figure 2.8). It leads the incoming tape from its delivery system to the nip. The quality of the product depends directly on the precision of the guiding system, because it prevents the creation of voids and discrepancies between the programmed fiber orientations and those in the final product. They are caused by discrepancies between the programmed nip location and the effective one. The latter are due to process-induced forces that deviate the incoming tape from its track.

Support

The support is the element on which the composite material is laid. It is generally called mandrel in the automated tape winding process. Various names are used in the automated tape placement process: e.g. base, table, plate or mandrel.



Figure 2.9: Elements of a shaft : metallic end and thermoplastic reinforced tube

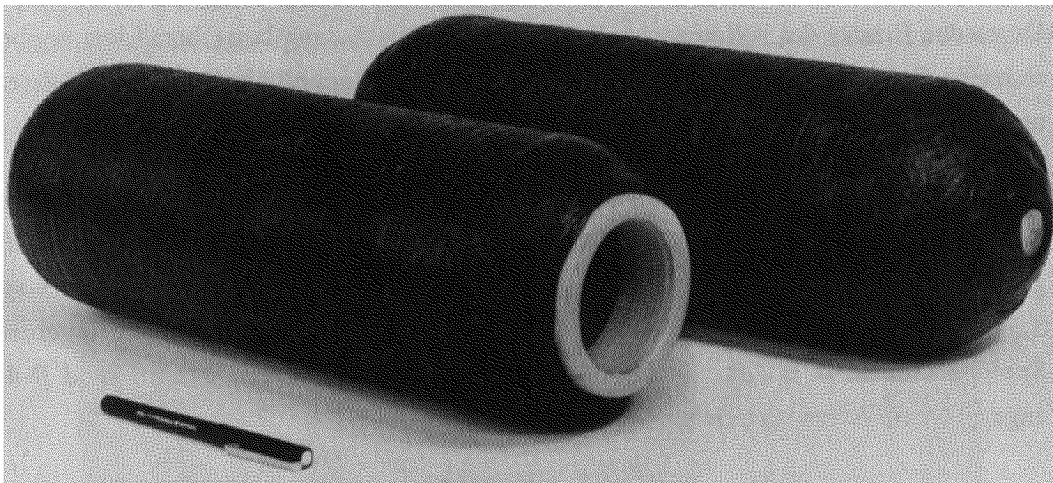


Figure 2.10: High pressure tanks ^[26]

At the end of the process, the support can be removed or integrated in the final product : a metallic cylinder is the support used to produce the hollow composite tube of shafts (Figure 2.9), and the composite material is directly laid on the liner of high pressure tanks (Figure 2.10).

2.2.5. Selection of the adequate incoming tape and of the appropriate components

The composite material determines the type of the incoming tape that can be used. The support, the motion control and the guiding system must fulfill the lay down requirements. The process conditions are chosen in relation with the lay down and with the composite material. They determine the locations and the power of the heat input(s) and of the cooling source(s). They fix also the type(s) and the power of the compaction assembly(ies).

Optimum process conditions can be determined experimentally or with simulations. Various models are available to simulate the various phenomena occurring during the automated tape winding and the automated tape placement processes (see section 2.3).

2.2.6. Parts examples

Most of the experimental and theoretical investigations study the process in relation with the fabrication of simple geometries: rings, cylinders, plates and flat strips.

Since composite products have usually complex shapes and/or are subjected to complex solicitations, the automated tape placement and automated tape winding processes should be able to produce parts with complex shapes and/or complex fiber orientations to be viable processes.

The challenge is to lay correctly the tape, i.e. to adapt the process parameters to the different process configurations and variations. The guiding of the tape must ensure the correct placement of the tape and avoid its slipping. The compaction apparatus must apply a sufficient compaction force over the nip (point, line or curve). The heat inputs and cooling sources must guarantee appropriate thermal conditions.

Some investigations pay attention to this challenge. Funck ^[26] fabricates high-pressure resistant tanks with the automated tape winding process. They could replace the iron tanks that are employed to transport gases. He also presents a hyperbolic element. Romagna ^[71] winds rings and external layers on a train coach mandrel. Mazumdar and Hoa produce elliptical rings ^[59]. Steiner ^[82] studies the laying over a mandrel with concave and convex curvatures.

2.3. Modeling

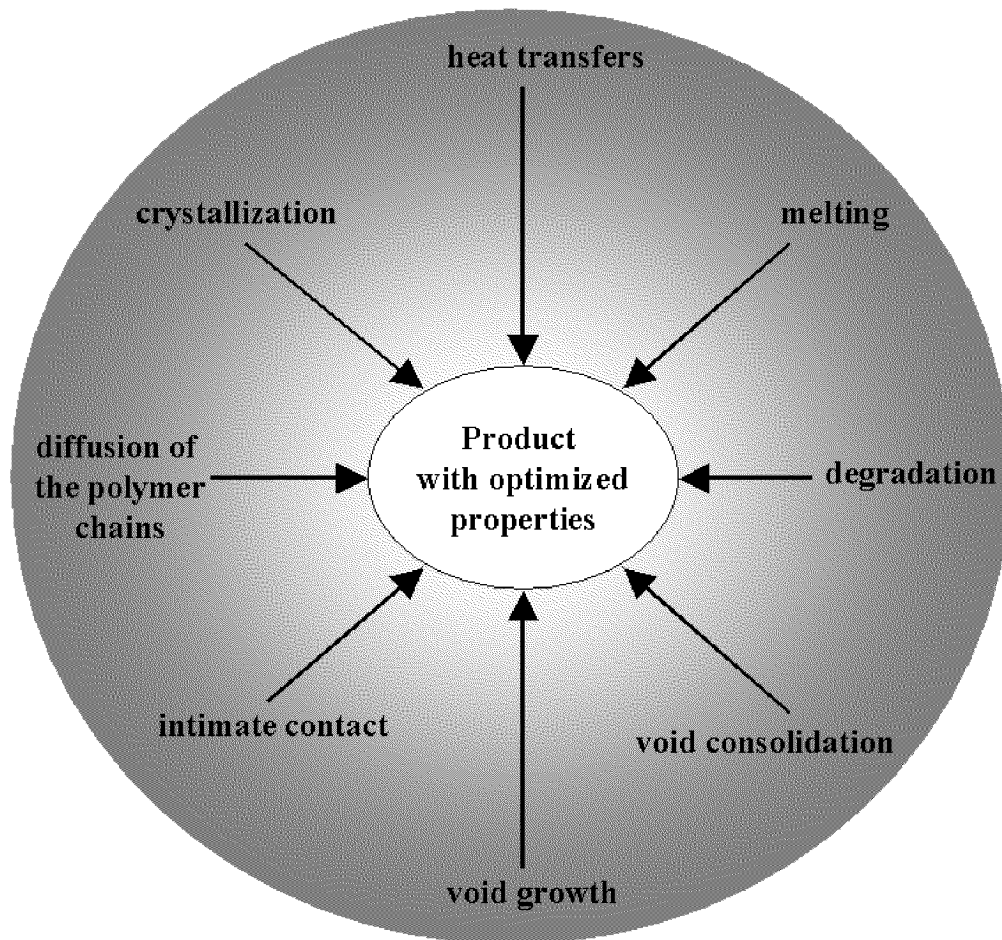


Figure 2.11: Phenomena taking place during the processes

Several phenomena occur during the tape placement and tape winding processes (Figure 2.11). This section presents an overview over known models related to those phenomena.

Since the tape is already pre-impregnated, this section does not consider impregnation phenomena. The development of process-induced internal stresses and residual stresses after processing are not treated, because they are not the topic of this research.

2.3.1. Heat transfer in composite materials

General formulation

The heat diffusion equation describes the heat transfer in a solid structure. Since the composite materials are anisotropic, it must take into account material parameters that are dependent on the direction of the coordinate systems. Its general form in Cartesian coordinates is given by :

$$\frac{\partial}{\partial x}\left(K_x \frac{\partial T}{\partial x}\right) + \frac{\partial}{\partial y}\left(K_y \frac{\partial T}{\partial y}\right) + \frac{\partial}{\partial z}\left(K_z \frac{\partial T}{\partial z}\right) + \dot{q} = \rho C \frac{\partial T}{\partial t} + v_x \frac{\partial T}{\partial x} + v_y \frac{\partial T}{\partial y} + v_z \frac{\partial T}{\partial z} \quad (2.1)$$

Most of the investigations of the tape winding and tape placement processes consider steady-state conditions. In this case, the temperature distribution is independent of the time, the time derivative term in Equation 2.1 is equal to zero, and the convection-like terms are utilized to simulate the displacement of the composite material.

However, transient analyses are necessary when it is expected that the temperature will vary with time. In the modeling of those analyses, the time derivative term of Equation 2.1 can not be neglected. The simulation method determines whether the convection-like terms can be neglected or not.

The rate of energy in Equation 2.1 is generally related to the energy released during the crystallization and to the energy absorbed during the melting of the thermoplastic matrix. Some few studies employ this term. Its influence depends among other on the thermoplastic content, the type of thermoplastic, the degree of crystallinity and the fraction of thermoplastic that can be crystallized.

Boundary conditions

It exists three types of thermal boundary conditions: contact (Equation 2.2), convection (Equation 2.3) and radiation (Equation 2.4). In normal terrestrial environment, the radiation and convection boundary conditions are coupled. The radiation and contact boundary conditions can be coupled when the beams can be transmitted through the contact elements.

$$T = T_{surface} \quad (2.2)$$

$$\dot{q} = \alpha \Delta T \quad (2.3)$$

$$\dot{q} = \varepsilon \varepsilon_0 (T_{surface_1}^4 - T_{surface_2}^4) \quad (2.4)$$

2.3.2. Strength development at polymer interfaces

Crack healing and bonding (welding) are related processes that determine among others the strength development at polymer interfaces. They are however fundamentally not similar (Wool [98]). Crack healing is the healing of two fractured surfaces that contain the remnants of the deformation zone through which the crack propagated. Bonding involves the contact of two surfaces that had not previously been in contact. This section describes both of them, to avoid any misunderstanding.

Crack healing

Wool and O'Connor [96] study the crack healing process of polymer surfaces. They divide it in five stages : the surface rearrangement, the surface approach, the wetting, the diffusion and the randomization.

- The surface rearrangement is related to the roughness or topology of the surfaces that would come into contact and its changes with time, temperature and pressure. Wool [98] gives the example of fractured polymers, where the rearrangement of fibrillar morphology and other factors can affect the rate of healing.
- Generally, space separates two different surfaces. Therefore, a force must be applied to bring them into contact. This phenomenon is called surface approach. It takes into consideration the time-dependent contact of the different parts of surfaces to create the interface [98].
- According to Butler et al. [12], the wetting phenomenon occurs when the surfaces are close enough for the establishment of intermolecular forces. In other words, the surface asperities are on a small enough scale for the intermolecular forces to have enough effect on the interface to deform the asperities and to establish full contact.

- The polymer chains can diffuse through interfaces between two surfaces in the direction of the bulk material. This diffusion phenomenon takes place only when the material temperature is higher than the glass transition temperature.
- Wool ^[98] mentions that the randomization stage refers to the equilibration of the non-equilibrium conformations of the chains near the surfaces and to the restoration of the molecular weight distribution and random orientation of chain segments near the interface.

Bonding or welding

Mantel et al. ^[55] introduce a simplification for the welding (bonding) of polymer surfaces that is well accepted in the simulations of the tape placement and tape winding processes. Since the two merging surfaces were not fractured during the welding process, it doesn't consider the rearrangement of the fibrillar morphology or other factors following a crack. Further, they neglect the effect of two stages : the wetting and the randomization.

The wetting stage can be disregarded, when the asperities between the two merging surfaces are on a scale significantly larger than the range where intermolecular forces have an effect, because an outside force must be applied to deform the asperities in order to establish interfacial contact. The surface approach is prevalent when the roughness is large enough to necessitate an external force to cause flow or deformation of the asperities. According to Butler et al. ^[12], the effects of wetting are overshadowed by external forces and the wetting phenomenon can be assumed to be instantaneous.

The randomization can be included in the stage of the diffusion of chains, when only the mechanical properties of the bond are considered. This is justified by results of experimental works on different polymers ^{[16],[19],[36],[43],[45]&[52]}, since they show that the strength development with a perfect contact between the two merging surfaces can be described by a single stage. The diffusion of chains is assumed to be the prominent phenomenon, because it takes place prior to the randomization.

Mantel et al. ^[55] consider only two stages: the intimate contact and the autohesion (self-diffusion, healing or polymer chain diffusion). The intimate contact corresponds to the surface approach of the crack healing process. The autohesion, the self-diffusion, the healing and the polymer chain diffusion refer to the same phenomenon.

The authors use dimensionless values to relate the bond quality to the intimate contact and the polymer chain diffusion.

$$D_b(t) = \sum_{i=1}^{\infty} (D_{ic}(i \Delta t) - D_{ic}((i-1)\Delta t)) D_{pcd}(t - i \Delta t) \quad (2.5)$$

Butler et al. ^[12] give also an integral form of this equation :

$$D_b(t) = D_{ic}(0) D_{pcd}(t) + \int_0^t D_{pcd}(t-t') \dot{D}_{ic}(t') dt' \quad (2.6)$$

The degree of intimate contact D_{ic} is the fraction of the interface where the spatial gaps between the two merging surfaces have been removed.

$$D_{ic}(t) = \frac{\sum S_{contacts}(t)}{S_{interface}} \quad (2.7)$$

During the processes using thermoplastic fiber reinforced tapes or sheets, it can vary with the elapsed process time. In this case, it is equal to zero when there is no contact between the two surfaces that should merge. Then it increases with time when a force is applied to flatten the non-uniform asperities of those surfaces. Finally, it remains constant when it has reached a value of 1. It can only decrease when a force is applied to separate those two surfaces and when this force exceeds the strength of the current bond.

Once the spatial gaps have been closed on a fraction of the interface, the diffusion of the polymer chains in the opposite bulk begins through it. The degree of polymer chain diffusion D_{pcd} characterizes the normalized strength development due to this diffusion (Equation 2.8).

$$D_{pcd}(t) = \frac{\sigma(t)}{\sigma_{\infty}} \quad (2.8)$$

2.3.3. Intimate contact

To analyze the development of the intimate contact, Mantel et al. ^[55] represent the irregular ply surface by a surface consisting of a series of rectangles (Figure 2.12). According to this model, the degree of intimate contact defined in Equation 2.7, becomes :

$$D_{ic}(t) = \frac{b(t)}{w_0 + b_0} \quad (2.9)$$

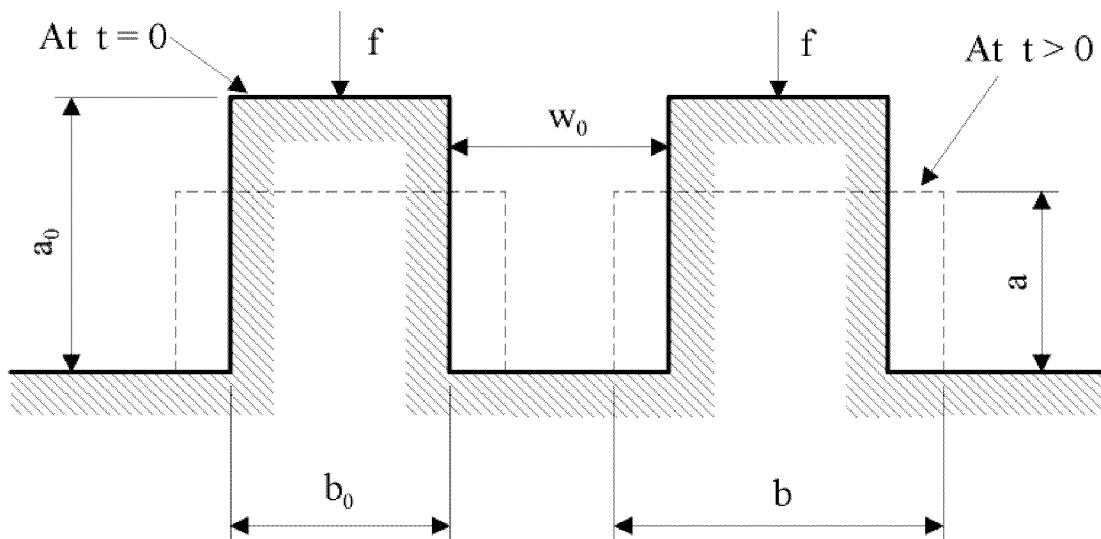


Figure 2.12: Rectangular elements representing the uneven surface at different times

Since the value of $b(t)$ can generally not be measured during the process, Mantel et al. ^[57] transform this equation with respect to the following assumptions : the volume ($V = a_0 b_0$) of each surface element remains constant, the flow of the surface irregularities is laminar, the pressure between the two adjacent surface elements is the ambient pressure, and the edge of the element moves with a speed of db/dt .

$$D_{ic}(t) = \frac{1}{1 + \frac{w_0}{b_0}} \left[1 + 5 \frac{P_{app}}{\mu_{mf}} \left(1 + \frac{w_0}{b_0} \right) \left(\frac{a_0}{b_0} \right)^2 t \right] \quad (2.10)$$

Mantel et al. ^[57] give a more general form of Equation 2.10:

$$D_{ic}(t) = \frac{1}{1 + \frac{w_0}{b_0}} \left[1 + 5 \left(1 + \frac{w_0}{b_0} \right) \left(\frac{a_0}{b_0} \right)^2 \int_0^t \frac{P_{app}}{\mu_{mf}} dt \right] \quad (2.11)$$

According to Equation 2.10 and Equation 2.11, the degree of intimate contact depends on the original surface irregularities, the applied pressure and the rheometric viscosity of the composite material. The latter varies with the temperature.

2.3.4. Polymer chain diffusion (autohesion, healing or self-diffusion)

In different studies ^{[9],[19]&[45]}, the diffusion of polymer chains through an interface in terms of strength development is discussed. In those researches, the intimate contact is disregarded. It can be neglected, when the duration to obtain a constant degree of intimate contact is much smaller than the duration of the diffusion of the polymer chains through the interface. Note that the strength measurements can be compared only when the value of the degree of intimate contact is constant.

Based on the reptation theory, Bastien and Gillespie ^[9] determine the strength development through diffusion of chains for three different cases: isothermal (Equation 2.12), non-isothermal with the minor chain length as the criterion for fracture (Equation 2.13), and non-isothermal with the interpenetration distance as the criterion for fracture (Equation 2.14):

$$\frac{\sigma(t)}{\sigma_\infty} = \left(\frac{t}{t_{rep}} \right)^{1/4} \quad (2.12)$$

$$\frac{\sigma(t)}{\sigma_\infty} = \left[\sum_{i=0}^{t/\Delta t} \left(\frac{t_{i+1}^{1/2} - t_i^{1/2}}{t_{rep}^{1/2}} \right) \right]^{1/2} \quad (2.13)$$

$$\frac{\sigma(t)}{\sigma_\infty} = \sum_{i=0}^{t/\Delta t} \left(\frac{t_{i+1}^{1/4} - t_i^{1/4}}{t_{rep}^{1/4}} \right) \quad (2.14)$$

According to the authors, the time increment Δt must be such that convergence of the results is achieved. Note that the above mentioned equations are valid only for :

$$0 \leq t \leq t_{rep} \quad (2.15)$$

Those equations were developed in relation with the reptation theory that describes the chains motion in amorphous polymers. However, since Cho and Kardos^[16] show with a semi-crystalline PEEK that the strength continues to increase with the fourth root of the time, when the degree of crystallinity stays approximately constant, it is to be expected that Equation 2.12 to Equation 2.14 remain valid for the semi-crystalline polymers.

2.3.5. Void consolidation

Pitchumani et al.^[67] combine a thermal analysis with models for different phenomena : the void consolidation, the degradation of the polymer, the intimate contact and the strength development due to the diffusion of polymer chains through an interface. In this article, they also develop the void consolidation model that describes the reduction of the intralaminar voids inside a tow during the thermoplastic tow placement process. This process takes place under every compaction element, when a tow is laid. Since this model is the only one used in the simulation of the placement of fiber reinforced thermoplastic tape, it is presented below.

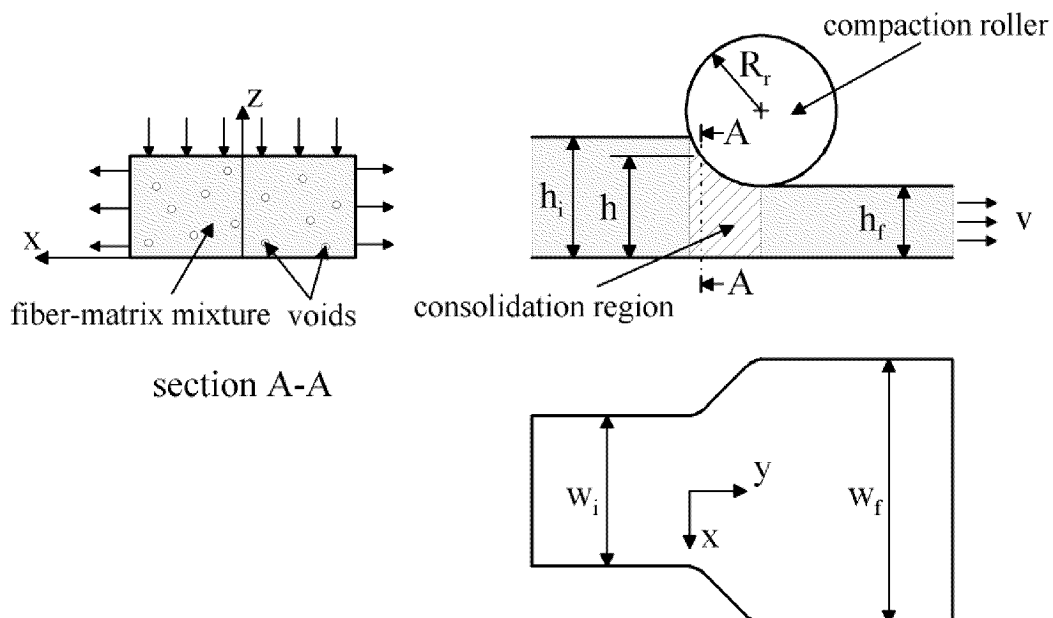


Figure 2.13: Enlarged view of the region under a compaction roller^[67]

Macroscopic relations

First, they consider that the tow is deformed macroscopically according to Figure 2.13. Then, they use the continuity and momentum equations with the assumption that the density and the pressure are functions of time and x only. It results that :

$$h \frac{\partial \rho^*}{\partial t} + \frac{\partial}{\partial x} \left(\rho^* \int_0^h \left[v_{x0} + \frac{dp}{dx} \int_0^z \frac{\xi}{\mu} d\xi + c_1(x) \int_0^z \frac{1}{\mu} d\xi \right] dz \right) + \rho^* \frac{dh}{dt} = 0 \quad (2.16)$$

where v_{x0} and $C_1(x)$ are constants of integration that can be determined from the velocity profile.

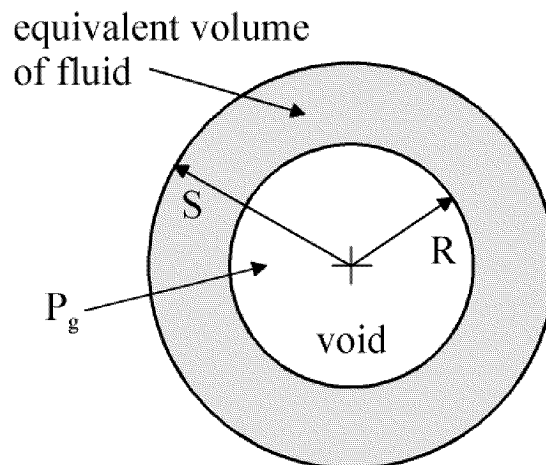


Figure 2.14: Microscopic void compression model used to determine the bubble radius as a function of the local pressure and temperature^[67]

The density of the fiber-matrix-voids mixture is scaled with respect to the mixture without voids :

$$\rho^* = \frac{\rho}{\rho_f} \quad (2.17)$$

Since the void consolidation happens under a compaction roller (Figure 2.13), the variation of the height can be determined geometrically with $dy/dt=v$:

$$\frac{dh}{dt} = -v \frac{\left[R_r^2 - (R_r - h - h_f)^2 \right]^{1/2}}{R_r - h - h_f} \quad (2.18)$$

Microscopic relations

Pitchumani et al. ^[67] also model the reduction of microscopic bubbles (voids), because it cannot be determined directly from the density. This latter and its time derivative may be written :

$$\rho^* = \frac{S^{*3} - R^{*3}}{S^{*3}} = \frac{S_0^{*3} - 1}{S_0^{*3} - 1 + R^{*3}} \quad (2.19)$$

$$\frac{\partial \rho^*}{\partial t} = \frac{-3R^{*2} (S_0^{*3} - 1)}{(S_0^{*3} - 1 + R^{*3})^2} \frac{\partial R^*}{\partial t} \quad (2.20)$$

As it can be remarked, the above model is not completely defined, because one relation is missing. Therefore, the authors introduce the balance between the pressure inside and outside the voids, the surface tension and the resin viscosity. This relation governs the void collapse.

$$4 \left(\frac{R^{*3}}{S_0^{*3} + R^{*3} - 1} - 1 \right) \frac{dR^*}{dt} + (p_g - p_f) \frac{R^*}{\mu} - \frac{2\sigma}{\mu R_0} = 0 \quad (2.21)$$

$$S^* = \frac{S}{R_0} \quad (2.22)$$

$$R^* = \frac{R}{R_0} \quad (2.23)$$

Boundary conditions

Finally, boundary conditions are needed to determine the different constants. Pitchumani et al. ^[67] use a general form for the velocity at the tow-substrate interface and at the tow-roller contact :

$$\left(\frac{\partial v_x}{\partial z}\right)_{z=0} = \frac{K_b}{\mu} v_x(z=0) \quad (2.24)$$

$$\left(\frac{\partial v_x}{\partial z}\right)_{z=h} = \frac{K_t}{\mu} v_x(z=h) \quad (2.25)$$

The value K/μ defines the type of boundary conditions. A value of ∞ implies a no-slip condition, whereas a value of 0 corresponds to a perfect slip condition. In real processes, the conditions lie between these two extremes.

The last boundary conditions can be obtained with the pressure. When the tow is laid on a surface, they are given by :

$$p(x = \pm w/2) = p_{atm} \quad (2.26)$$

2.3.6. Void growth

Pitchumani et al. ^[68] extend the void consolidation model discussed above for the void growth process. The latter occurs when the fiber-matrix-voids mixture is in regions outside the compaction elements. Since the tape is exposed to atmospheric pressure in their model, Equation 2.21 becomes :

$$4 \left(\frac{R^{*3}}{S_0^{*3} + R^{*3} - 1} - 1 \right) \frac{dR^*}{dt} + (p_g - p_{atm}) \frac{R^*}{\mu} - \frac{2\sigma}{\mu R_0} = 0 \quad (2.27)$$

This equation defines directly the growth of the voids, when they don't coalesce.

2.3.7. Crystallization kinetics (from the melt)

Crystallization kinetics of thermoplastics and compounds with thermoplastics describe the phase transition between the molten state and the crystalline state of the matrixes. Since amorphous thermoplastics never have crystals, it can only happen in semi-crystalline materials.

Karger-Kocsis resumes works performed on polypropylene ^[44]. Two types of investigations can be distinguished : overall and microscopic studies. The overall crystallization kinetics describes the macroscopic effects of the crystallization on physical properties like the heat generation/release, the absorption of radiation and the density. The microscopic studies deal with the microscopic development of the crystals.

Since the topics of this study are based on the macroscopic scale, this chapter begins with an outline of the well-known basic overall models that are used to describe the crystallization kinetics from the melt. Then, it presents the models employed in the simulations of the tape winding and the tape placement processes.

Generally, the experimental works try to fit the data with a model so that they can be used in simulations or be compared with literature data. There exists a large number of models. However, they are generally developed from one of the basic models : Avrami, Tobin, Malkin and Ozawa.

Basic models

The best known model is the one of Avrami ^{[6]-[8]} (Equation 2.28 and Equation 2.29) that is valid for isothermal crystallization. This model has two parameters : n and k . Their values depend on the form of the crystal and on the type of crystallization (see Table 2.2).

In the heterogeneous crystallization, a fixed number of growing nuclei is initially present in the polymer melt. The crystallization is called homogeneous, when no nuclei are present at the start, and when the number of nuclei increases with time.

$$\gamma(t) = 1 - \exp(-kt^n) \quad (2.28)$$

$$\frac{1}{(1-\gamma)} \frac{d\gamma}{dt} = k^{1/n} n \left(\ln \left(\frac{1}{1-\gamma} \right) \right)^{(n-1)/n} \quad (2.29)$$

Crystal growth	Form	Nucleation	Exponent (n)	Rate Constant (k)
One-dimensional	beam	heterogeneous	1	G A N
		homogeneous	2	1/2 G A I
Two-dimensional	cylinder	heterogeneous	2	$\pi G^2 D N$
		homogeneous	3	$(\pi/3) G^2 D I$
Three-dimensional	sphere	heterogeneous	3	$(4/3) \pi G^3 N$
		homogeneous	4	$(\pi/3) G^3 I$

Table 2.2: Parameter of the Avrami equation and their significations ^[21]

Since experimental data cannot be acceptably fitted with the Avrami model, Tobin develops a new relation ^{[87]-[89]} (Equation 2.30 and Equation 2.31). Those equations imply two terms. The first one models the heterogeneous crystallization and the second one the homogeneous crystallization. Therefore, they can directly predict the crystallization when the heterogeneous and homogeneous crystallization happen simultaneously.

$$\frac{\gamma(t)}{1-\gamma(t)} = k^* N^* t^{n^*} + k^* I^* \int_0^t (t-w)^{n^*} (1-\gamma(w)) dw \quad (2.30)$$

$$\dot{\gamma}(t) = k^* n^* N^* t^{n^*-1} [1-\gamma(t)]^2 + k^* n^* I^* [1-\gamma(t)]^2 \int_0^t (t-w)^{n^*-1} (1-\gamma(w)) dw \quad (2.31)$$

Malkin et al. ^{[53]&[54]} derive a more general relation that is based on a free growth function $S'(\gamma)$ (Equation 2.32). It should be noted that if the generality of the $S'(\gamma)$ is not limited, Equation 2.29 can be regarded as a particular case of Equation 2.32.

$$\frac{d\gamma}{dt} = [c_1 + c_2 S'(\gamma)] (1-\gamma) \quad (2.32)$$

The aim of Malkin et al. ^{[53]&[54]} was also to develop a model for the non-isothermal analysis of the crystallization kinetics. Therefore, they assume that $S'(\alpha) = D \alpha$ and transform Equation 2.32 to Equation 2.33. They show the validity of Equation 2.33 by comparing its prediction with the one of Equation 2.29. For the examples that are presented, very good correspondence has been found.

$$\gamma(t) = 1 - \frac{c_3 + 1}{c_3 + \exp(c_4 t)} \quad (2.33)$$

The model of Ozawa ^[66] describes the crystallization kinetics for a constant cooling rate (Equation 2.34 and Equation 2.35). Equation 2.34 appears very similar to Equation 2.28 for the Avrami model. However, the description of the crystallization depends directly on the temperature and indirectly on the time through the cooling rate “a”.

$$\gamma(T) = 1 - \exp\left(-\frac{k(T)}{a^n}\right) \quad (2.34)$$

$$\frac{d\gamma}{dt} = -(1-\gamma)\frac{dk(T)/dT}{a^{n-1}} \quad (2.35)$$

Crystallization kinetics models in relation with the tape laying and tape winding processes

Ghasemi Nejhad et al. ^[29] apply the model of Seferis et al. ^[76] (Equation 2.36 to Equation 2.39). It is a modified form of the Equation 2.28: it uses two Avrami functions and an initial crystallization level. The first function aims to take into account the heterogeneous crystallization and the second one the homogeneous crystallization. The global crystallization is the sum of both influences (Equation 2.36). To predict it during annealing processes, Equation 2.38 contains an initial level. Equation 2.39 gives the parameter k_i in function of the temperature. Since the parameter n_i is normally constant, this relation allows to predict the crystallization kinetics when the temperature of the thermoplastic varies.

$$\gamma(t) = w_{het}\gamma_{het}(t) + w_{hom}\gamma_{hom}(t) \quad (2.36)$$

$$w_{het} + w_{hom} = 1 \quad (2.37)$$

$$\ln\left[\frac{1}{1-\gamma_i(t)}\right]^{1/n_i} = \ln\left[\frac{1}{1-\gamma_i(t=0)}\right]^{1/n_i} + \int_0^t [k_i(T(t))]^{1/n_i} dt \quad (2.38)$$

where $i = \text{“het”}$ or “hom”

$$k_i(T) = c_{1i} T \exp\left(-\frac{c_{2i}}{T - T_g + C} - c_{3i} \left(\frac{T}{(T_m^0 - T)}\right)^2\right) \quad (2.39)$$

Mantel and Springer ^[56] give two crystallization kinetics models. The first one is originally developed by Velisaris and Seferis ^[92]:

$$\gamma(t) = w_{het} \gamma_{het}(t) + w_{hom} \gamma_{hom}(t) \quad (2.40)$$

$$\gamma_i(t) = 1 - \exp \left[-c_{1i} \int_0^t T \exp \left(-\frac{c_{2i}}{T - T_g + C} - c_{3i} \left(\frac{T}{(T_m^0 - T)} \right)^2 \right) n_i t_i^{n_i - 1} dt_i \right] \quad (2.41)$$

where $i = \text{“het”}$ or “hom”

The second one is the model of Ozawa whose parameters are determined by Lee and Springer ^[51] for carbon fiber reinforced polyetheretherketone (AS4/APC-2). Sarrazin and Springer ^[75] take also into account the influence of the crystallization with the model of Ozawa and those parameters.

Somnez and Hahn ^[80] adopt the model of Choe and Lee ^[17] (Equation 2.42 to Equation 2.44). The final relation has the form of Equation 2.31. Temperature dependent functions replace the value of knN^* and knI^* . The goal of this modification is to be able to take into account the temperature variations during processes.

$$\dot{\gamma}(t) = \dot{\gamma}_{het}(t) + \dot{\gamma}_{hom}(t) \quad (2.42)$$

$$\dot{\gamma}_{het}(t) = k_{het} \exp \left(-\frac{3E}{RT} \right) \exp \left(-\frac{3\psi_1 T_m^0}{T(T_m^0 - T)} \right) t^2 [1 - \gamma(t)]^2 \quad (2.43)$$

$$\dot{\gamma}_{hom}(t) = k_{hom} \exp \left(-\frac{4E}{RT} \right) \exp \left(-\frac{(3\psi_1 + \psi_2) T_m^0}{T(T_m^0 - T)} \right) [1 - \gamma(t)]^2 \int_0^t (t-w)^2 [1 - \gamma(w)] dw \quad (2.44)$$

James and Black ^[42] use the model of Muzzy et al. ^[64] describing the crystallization kinetics in term of volumetric changes. It assumes heterogeneous nucleation and a temperature-dependent growth of spherulites.

$$\gamma(t) = \frac{4 \pi R^2 \gamma_{max}}{V} \frac{dR}{dt} = \frac{4 \pi R^2 \gamma_{max}}{V} \frac{b_0}{h} k^* T \exp \left(\frac{-\Delta I}{k^* T} \right) \exp \left(\frac{-\Delta F}{k^* T} \right) \quad (2.45)$$

$$\frac{-\Delta I}{k^* T} = \frac{4b_0 \sigma_s \sigma_e (T_m^0)^2}{k^* \Delta H_f \rho_c T^2 (T_m^0 - T)} \quad (2.46)$$

$$\frac{-\Delta F}{k^* T} = \frac{E}{(c_2 + T - T_g) R} \quad (2.47)$$

2.3.8. Melting kinetics

Melting is the reverse phenomenon to crystallization. It can also only happen in semi-crystalline materials. The melting kinetics describes the phase transition between the crystalline state and the molten state. Only few studies on its relation with the thermoplastics and compounds with thermoplastic can be found.

Maffezzoli et al. ^[61] model it for polyetheretherketone (PEEK) and carbon fiber reinforced PEEK (APC-2). Mantel and Springer ^[56], Sarrazin and Springer ^[75] and Somnez and Hahn ^[80] implement this model in their simulations.

$$\frac{d\gamma}{dt} = k (1 - \gamma)^n \quad (2.48)$$

$$k = k_0 \exp\left(\frac{E}{RT}\right) \quad (2.49)$$

2.3.9. Degradation kinetics

In a polymer, the chain structures are modified by its interaction with its environment (i.e. temperature and radiation), and the chain lengths are reducing up to their disappearance. This phenomenon, called degradation, is very slow under normal environmental conditions.

During the tape winding and tape placement processes, the polymer chains are heated at temperature closed to or above the melting temperature. Under such conditions, the degradation can not be always neglected, because the properties of the polymer change with its advancement.

Some thermodynamic investigations ^{[23],[70]& [80]} integrate the model of Nam and Seferis ^[65] that it is based on weight loss measurements (Equation 2.50 - Equation 2.54). It predicts the degradation of PEEK in nitrogen.

$$\delta = \frac{M_0 - M}{M_0 - M_f} \quad (2.50)$$

$$\frac{d\delta}{dt} = k_\delta(T) f(\delta) \quad (2.51)$$

$$k_\delta = k_{\delta_0} \exp\left(\frac{E_\delta}{R T}\right) \quad (2.52)$$

$$f(\delta) = w_1 (1 - \delta) + w_2 \delta (1 - \delta) \quad (2.53)$$

$$w_1 + w_2 = 1 \quad (2.54)$$

Don et al. ^[22] implement the model of Day et al. ^[20] in their simulations of the tape placement process. It is also grounded on weight loss measurements and Equation 2.50 is still valid.

$$g(\delta) = [-\ln(1 - \delta)]^{1/2} \quad (2.55)$$

$$g(\delta) = k_{\delta_0} \exp\left(\frac{-E_\delta}{RT}\right) t \quad (2.56)$$

2.3.10. Bondline thickness

Chao and Gillespie ^[14] developed a coupled model for polymer chain diffusion and bondline thickness. They show that both phenomena affect the bond strength of a thermoplastic composite joint.

They determine experimentally an asymptotic strength value that depends on the bondline thickness :

$$\sigma_\infty(b_{lt}(t)) = 47.66 - 44.06b_{lt}(t) \quad (2.57)$$

where

$$b_{it}(t) = \sqrt{\left\{ \int_0^t \frac{1}{\eta(T)} dt \left[\frac{2(P_a - P_0)}{X_0^2} \right] + \frac{1}{Z_0^2} \right\}^{-1}} \quad (2.58)$$

Note that the first equation is only valid for their material combination (AS4/PEEK with amorphous PEI).

2.4. Process simulation

All phenomena described in section 2.3 are dependent on the temperature, its gradients or both. Process simulation is therefore based on reliable modeling of the thermal phenomena occurring during the process.

Each of those models must be coupled to the thermal model, when they influence significantly the heat transfers. This can be the case for the melting kinetics and the crystallization kinetics, the void consolidation and the void growth, and the degradation of the thermoplastic matrix. The melting process absorbs heat. The crystallization releases heat. The void consolidation or the void growth changes the thermal conductivity. The chemical reactions occurring during the degradation absorb or generate heat. Degradations can modify the thermal conductivity.

The automated tape winding and the automated tape placement are transient processes. Generally, transient simulations need be performed in order to describe them correctly. Steady-state or quasi-steady state simulations can be done when a control volume (area) can be defined and its boundary conditions can be determined. In such cases, the computation work is extremely simplified.

Since the simulations allow to describe the phenomena during the process, they enable to evaluate their influence in order to be able to determine optimum processing parameters or to design setups for the fabrication of specific products. They need to be validated in order to assess the quality of their results, to predict realistic optimum processing parameters and design appropriate setups.

2.5. Nomenclature

α	convective heat transfer coefficient
δ	degree of degradation
ε	emission coefficient
ε_0	constant of Stefan-Boltzmann ($5.67 \cdot 10^{-8} \text{ W/m}^2\text{K}^4$)
γ	degree of crystallinity or degree of melting
ρ	density
ρ_c	density of a full crystalline polymer
μ	dynamic viscosity
η	viscosity
σ	strength
σ	surface tension between air and thermoplastic melt
σ_e	end surface energy
σ_s	side surface energy
ψ	kinetic constant
A	cross-section
a	element height
a	cooling rate (Ozawa)
b	element width
b_0	monomolecular layer
b_{lt}	bondline thickness
C	heat capacity
C	constant
D	constant in the model of Malkin
D	degree
D	thickness (rate constant of the Avrami model)
E	activation energy
f	force
G	radial growth rate
h	instantaneous tow thickness under the consolidation roller
I	number of nuclei formed per unit volume and unit time
I^*	number of homogeneous nuclei formed per unit untransformed volume
K	thermal conductivity
K	friction factor in the velocity boundary condition
k	Avrami rate constant
k	kinetic constant
k^*	growth rate of the nuclei
k^*	Boltzmann's constant
M	mass
N	number of nuclei per unit volume

N^*	initial number of heterogeneous nuclei present
n	Avrami form parameter
n^*	form exponent
P	pressure
P_a	applied pressure
P_0	back pressure at free edges
p	pressure
Q	energy
q	energy per mass unit
R	radius
R_r	roller radius
R	universal gas constant
R	instantaneous void radius
R_0	initial void radius
S	surface
S	instantaneous radius of the resin shell surrounding a void in the consolidation model
S_0	initial radius of the resin shell surrounding a void in the consolidation model
$S'(\gamma)$	free growth function
T	temperature
T_m^0	equilibrium melting temperature
t	time
X_0	length of the joint
V	volume
v	velocity
w	distance between two adjacent elements
w	weighting factor
w	width
x, y, z	Cartesian coordinates
Z_0	initial thickness of the interlayer bondline
ΔF	activation energy for crystallization
ΔH_f	latent heat of fusion
ΔI	activation energy for flow

Subscript

δ	degradation
0	initial
app	applied
atm	atmospheric
b	bond strength
b	bottom
c	full crystalline polymer
f	fluid
f	final
i	initial
ic	intimate contact
g	gas
g	glass transition
het	heterogeneous
hom	homogeneous
max	maximum
mf	matrix-fiber
pcd	polymer chain diffusion
t	top
rep	reptation
x, y, z	Cartesian coordinates

CHAPTER 3

Experimental Investigations of the Automated Tape Winding Process with On-Line Bonding

3.1. Introduction

The automated tape placement and the automated tape winding processes with on-line bonding use similar techniques to produce composite parts. Due to their high level of automation, the labor work is extremely reduced, the reproducibility and the safety during the process are enhanced. They have a high flexibility, because several different components can be produced with the same setup when only the lay-up support or the mandrel is changed. They can be stopped and restarted without any penalty in the quality of the products.

Although those processes have a high potential, their complexities limit drastically their use. Various phenomena can occur : the melting of the thermoplastic matrix, the degradation of the polymer chains, the deformation of the incoming fiber reinforced material, the development of the intimate contact between the tape and the substrate, the diffusion of the polymer chains through the interfaces, the void consolidation and growth, the development of process induced stresses and the crystallization of the thermoplastic matrix. Further, the melting of the thermoplastic matrix, the deformation of the incoming material, the development of intimate contact and the void consolidation must happen during extremely short dwell times to produce parts that have good mechanical properties.

The experimental works allow to acquire several informations that can lead to a large use of those processes despite their complexity, i.e. to determine appropriate setups and setup components, the processing parameters that influence the quality of the parts, the sensibility of properties to the processing parameters and processing windows.

To obtain the above-mentioned information, testing methods like the short beam shear (SBS) ^[79], the interlaminar shear device (ISD) ^[50], the double cantilever beam (DCB) ^[2], the wedge peel ^{[31]&[37]} and the axial compression ^{[48]&[49]} can be employed to investigate the quality of parts produced. They basically rely on the characterization of the laminate properties along one of the three shear modes (Figure 3.1). Other methods to evaluate the laminate are the blocking force test ^[2], the fourier transform infra-red (FTIR) ^[2], the differential scanning calorimetry ^[2], the ultra-sonic C-scan ^[10], the micrographic pictures ^[18], the torque tube ^[24], the acid digestion ^[25], the tensile strength ^{[74]&[93]}, the hydroburst (for vessels) ^[25], the X-rays ^[27] and the dimension measurements ^{[58]&[60]}.

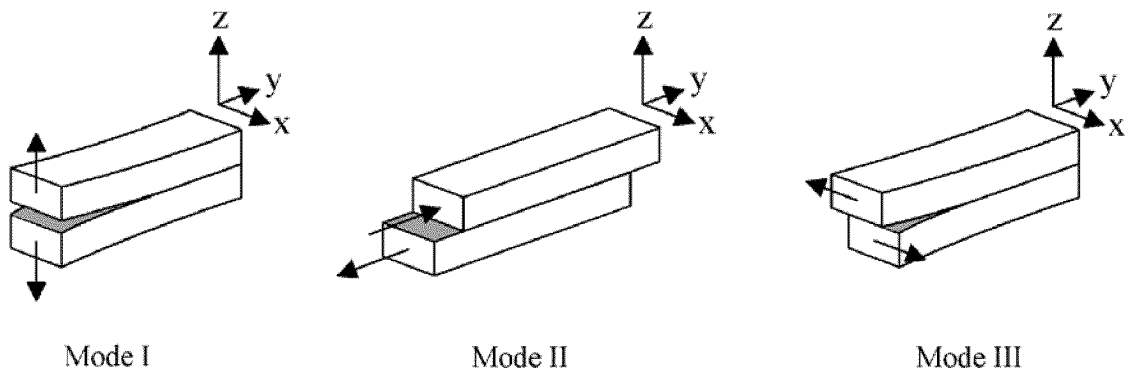


Figure 3.1: Different shear modes

According to experimental investigations e.g. ^{[26],[48],[49]&[82]}, the parameters that influence notably the shear strengths are the heat input, the process speed and the dwell time, the compaction force and the tension in the tape. Investigations reported in the literature make use of different material combinations, different setups and different testing methods. They prevent therefore accurate quantitative comparison. Qualitative analysis can however be used to identify trends. When only a process parameter varies, the bond strength increases in general with an increasing heat input, an increasing compaction force, or a decreasing process speed. Some investigations ^{[32]&[73]} show that the strength goes through a maximum value when the heat input increases. The decrease following the maximum is caused by the degradation of the polymer chains or the decomposition of the tape. Some other researchers ^{[37]&[95]} find also that the

strength does not always rise with an increasing compaction pressure. The influence of the tension in the tape must be carefully interpreted, since it can introduce internal stresses in the laminate, and affect the determination of the shear strength.

The degree of bond strength (measured shear strength divided by a reference shear strength) can also be used to compare the quality of the bonds obtained with different setups. This method needs however reference specimens that must be carefully chosen.

Mantel et al. ^[55] study the influence of the compaction pressure and applied temperature on the degree of bond strength. They use a reference made by press molding. Their best tape placed specimens have a degree of bond strength of approximately 92%. Mantel et al. ^[57] study the intimate contact, the bond strength and modulus of tape placed and pressed specimens. They normalized their results with respect to reference specimens obtained with the press molding process. Their analysis of C-scans shows that nearly optimum intimate contact can be reached with the tape laying process. They investigate the bond strength with the lap shear and the short beam shear tests. The strengths of their tape placed specimens are lower than 80 % of the reference specimens. Steiner ^[82] tests most of his samples with a short beam shear apparatus. He studies the interlaminar shear strength (ILSS) of cylinders wound from AS4/PEKK tapes. His reference is the ILSS of a plate that is fabricated in an autoclave (duration 20 minutes at 400°C with 0.69 MPa). He compares the ILSS and calculates the degree of bond strength, although the cylinders and the plate have different geometries and different numbers of layers. He shows that there exist processing parameters for the automated tape winding process that lead to the same ILSS-value than that of the plate. Rosselli et al. ^[73] manufacture IM7/APC-2 rings with an automated tape winding setup using a CO₂-laser. They post-process one of their rings in an autoclave under vacuum (duration 20 minutes at 380°C with 0.6 MPa). They use an interlaminar shear device to measure the ILSS. Their results show that the maximum ILSS of the wound rings is approximately 55% of that of the post-processed rings. Romagna ^[71] develops an automated tape winding setup. He uses a short beam shear apparatus to measure the ILSS of his specimens made from GF/PP. He post-processes a reference cylinder in an autoclave. He winds a cylinder that has 79% of the ILSS of a post-processed cylinder. Sun et al. ^[85] built a Karman filter and a state feedback controller to estimate and control the interlaminar bonding temperature during the process. In the experimental validation of their setup, they study the influence of the bonding temperature on the interlaminar shear strength. Various failure modes occur during the lap shear tests. Considering the specimens that break at the bond, the ILSS of their best specimens is 97% of that a reference specimen made by press molding.

Since the ILSS of a composite laminate is often the limiting design characteristic ^[72], the present experimental study follows the methodology used in the researches mentioned previously in order to investigate the influence of process parameters on the automated tape winding process under transient thermal conditions for a glass fiber reinforced polypropylene. Its objectives are to determine process parameters that permit to produce cylinders with a good interlaminar shear strength (degree of bond strength) and to provide informations like realistic sets of process parameters and database for the further theoretical works.

First, a large investigation window is defined. The nitrogen temperature, the compaction force, the winding pitch, the heating power of the preheating device and the processing speed are the processing parameters that are studied. The objectives of this first step are twofold : 1) to find different sets of processing parameters that results in the best ILSS, 2) to observe whether or not the winding pitch could influence the ILSS. Second, investigations are performed to discuss possible causes of the difference between the best ILSS of tape wound specimens and the reference ILSS.

3.2. Experimental setup

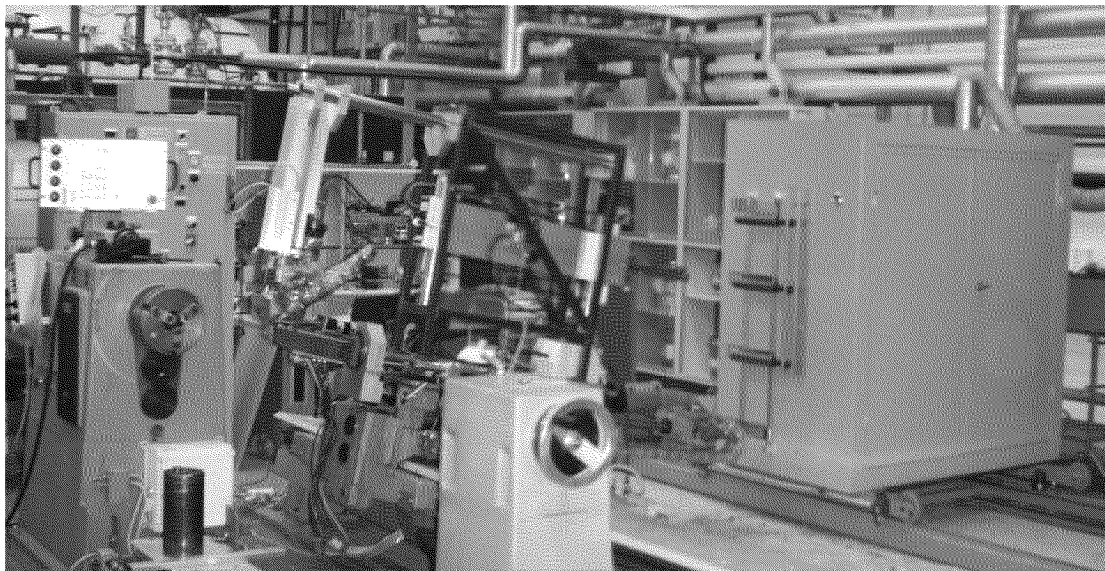


Figure 3.2: View of the winding machine

Elements of the setup are shown in Figure 3.2. It consists of a Baer WSE-II winding machine with a Baer TCS-84 control system, an ADC compaction

assembly, a PC, a data acquisition and control system, a pressure regulator and a pyrometer.

The Baer control system determines the processing speed and the winding paths. The ADC control cabinet fixes the parameters of the hot gas torch that are the nitrogen flow and its temperature at the outlet of the hot gas torch. A Labview program runs on a PC. It visualizes and stores the pressure and temperature data that are given by the pressure regulator and the pyrometer. The pressure regulator controls the force applied by the compaction roller of the ADC compaction assembly.

A sketch of the setup is given in Figure 3.3. It shows the location of the pyrometer spot. The pyrometer moves laterally with the compaction assembly to give the temperature of the incoming tape just before the nip line during the entire process. This temperature is chosen such that the measurements can be easily repeated. This won't be the case for a mixed temperature measurement (substrate and incoming tape), because they have different temperatures during the process, and because it is difficult to focus the pyrometer spot always on the same location. The knowledge of the incoming tape temperature just before the nip line is essential, because the phenomena at the nip line are directly dependent on this temperature.

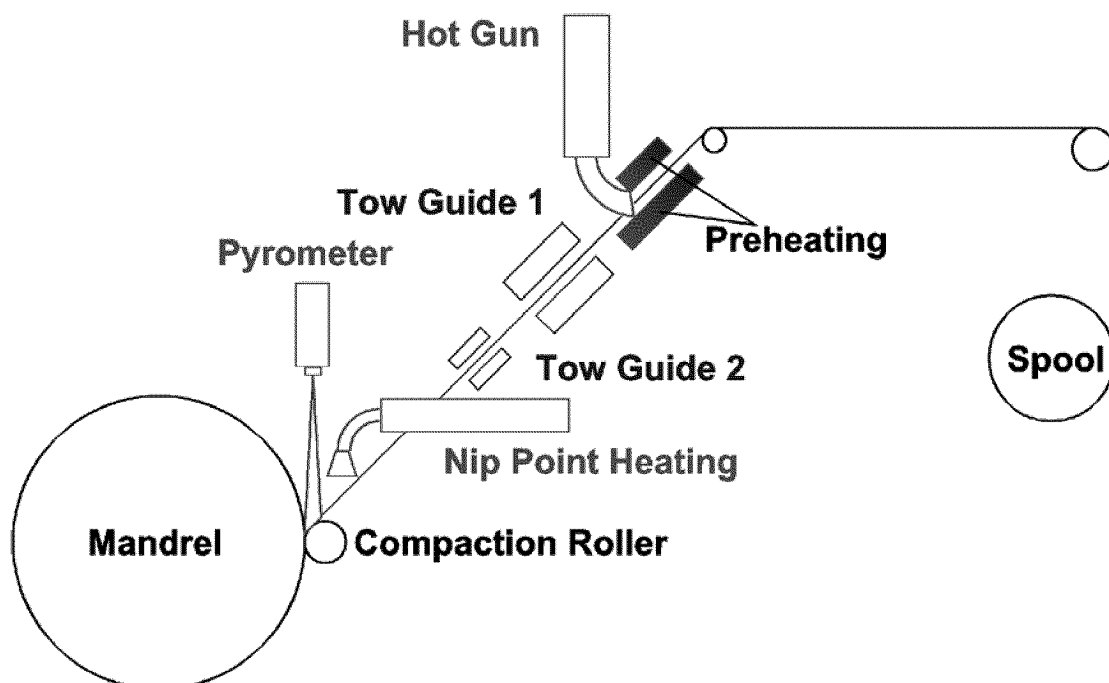


Figure 3.3: Sketch of the winding machine during the process

3.3. Specimen preparations and characterization methods

3.3.1. Preparation of the specimens for the mechanical characterization

A diamond saw with water cooling is used to fabricate specimens from cylinders in two steps : first rings are cut, second ring segments with identical arch length are made.

3.3.2. Mechanical characterization

The mechanical properties of the processed cylinders were characterized using a short beam shear apparatus (Figure 3.4 and Figure 3.5). Since relatively high deformations occur during the testing of the glass fiber reinforced specimens, a setup with rollers is chosen instead of the one described in the norm ATSM-D2344-89. The dimensions of the specimens are defined in the norm ASTM-D2291-83 (type C).

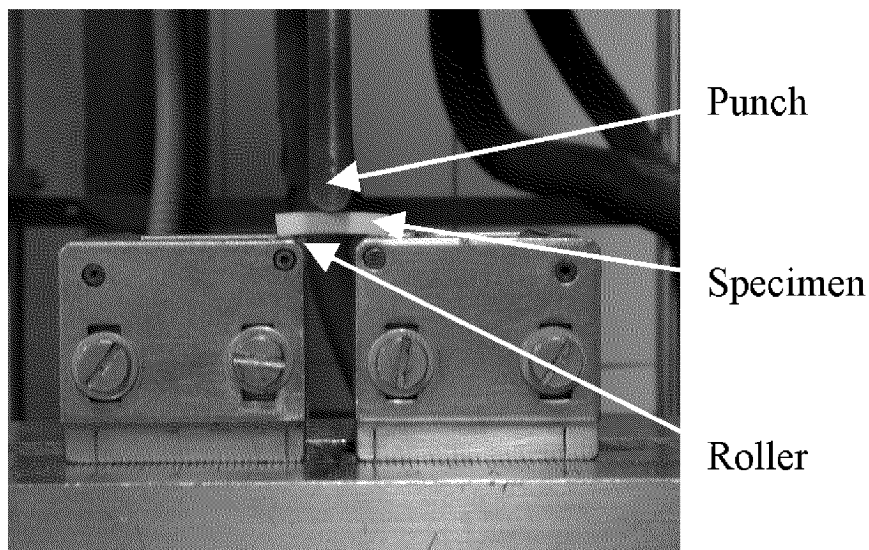


Figure 3.4: View of the short beam shear apparatus

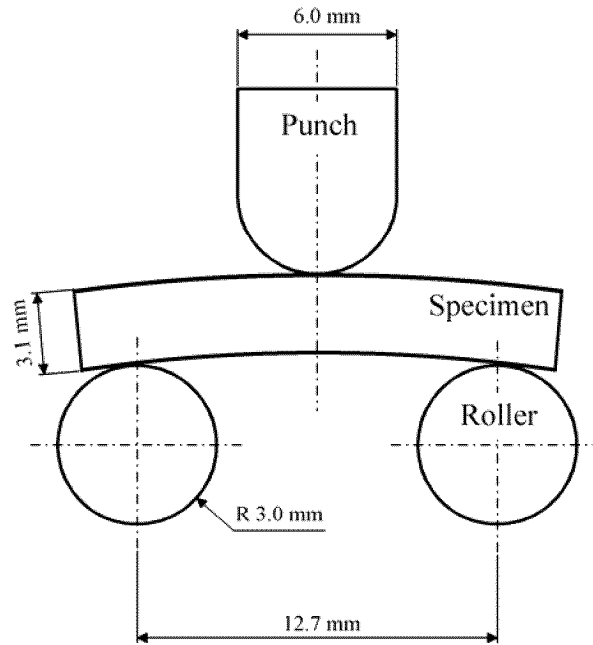


Figure 3.5: Dimension of the short beam shear apparatus

3.3.3. Preparation of the polished cross-sections

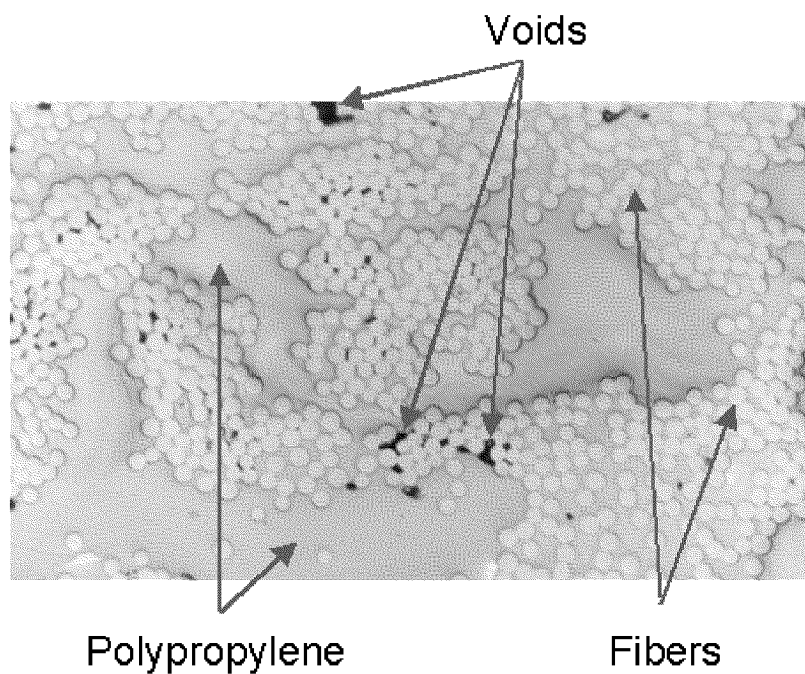


Figure 3.6: Example of a micrograph

Specimens prepared originally for the mechanical characterization are placed in a mold. Holders maintain them to prevent their displacement. Then, a thermoset resin is used to fill the mold. Once the thermoset resin is cured, the specimen and the thermoset resin form a small cylinder that is demolded. The thermoset resin acts as a holder for the polishing process. The latter is performed with various grinding and polishing media on a PEDEMAX-2 machine made by STRUERS.

3.3.4. Void content characterization

Polished cross-sections of the specimens are photographed under a microscope with a 100 times magnification. An example is shown in Figure 3.6. In that picture, the circles are the fibers, the gray areas are the polypropylene matrix and the black areas are the voids. The pictures are digitized to determine the void content with Equation 3.1.

$$\text{void content} = \frac{N_{\text{inside the voids}}}{N_{\text{of the picture}}} \quad (3.1)$$

where N is the number of pixels

3.4. Results of the short beam shear tests

3.4.1. Variation of the interlaminar shear strength in the axial direction of the cylinder

The first question arising during an experimental investigation studying the variation of a mechanical property in cylinders is : does the location, from which the specimens are coming, influences the result of the mechanical measurements ? For this reason, the changes of the interlaminar shear strength (ILSS) along the axial direction are studied for a cylinder.

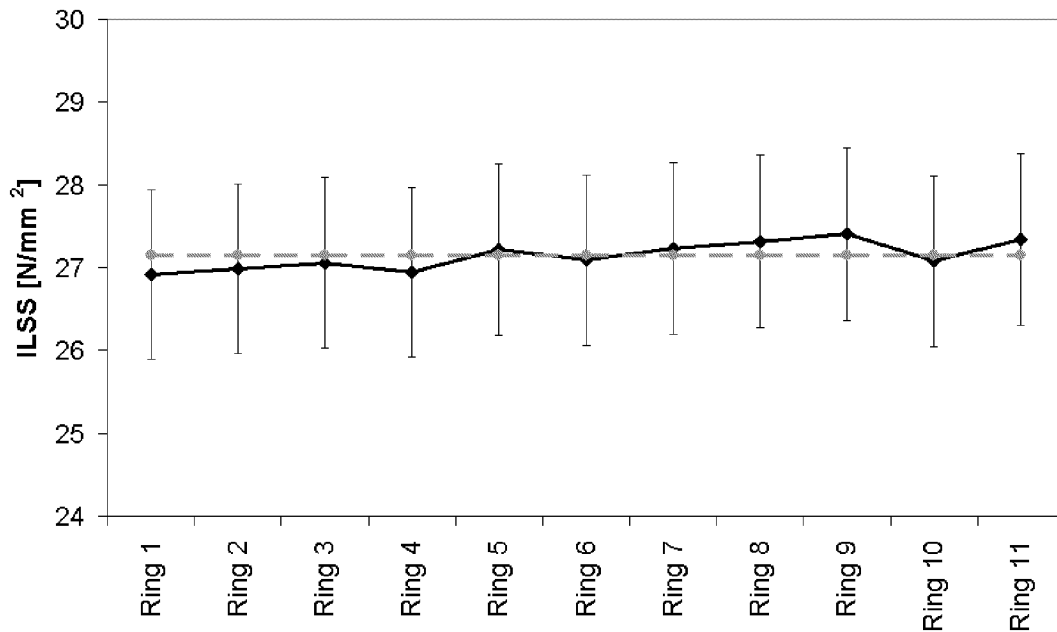


Figure 3.7: Variation of the ILSS along the axial direction

Eleven rings are cut from the cylinder. The domain covered by the rings is in the middle of the length of the cylinder. It represents approximately 2/3 of this length. Ten samples are then tested for each ring.

The mean ILSS for the eleven rings are shown in Figure 3.7. The error for each ring is $\pm 4\%$. The error for the 110 specimens is $\pm 6\%$. The variation of the mean ILSS of each ring is below 4%, i.e. the half of the error of each ring.

This result demonstrates that the ILSS can be considered as constant for the entire domain studied. Therefore, only specimens from a ring in this range will be tested in the next investigations.

3.4.2. Reference cylinder

In order to discuss the quality of the parts made with the tape winding process, a reference cylinder is fabricated in two steps. First, it is wound with the following processing parameters: nitrogen flow 2.81 m³/h, nitrogen temperature 700°C, force applied to the nip 276 N and processing speed 0.1 m/s. Second, the cylinder is post-processed in an autoclave under vacuum. The other parameters of the autoclave process are plotted in Figure 3.8.

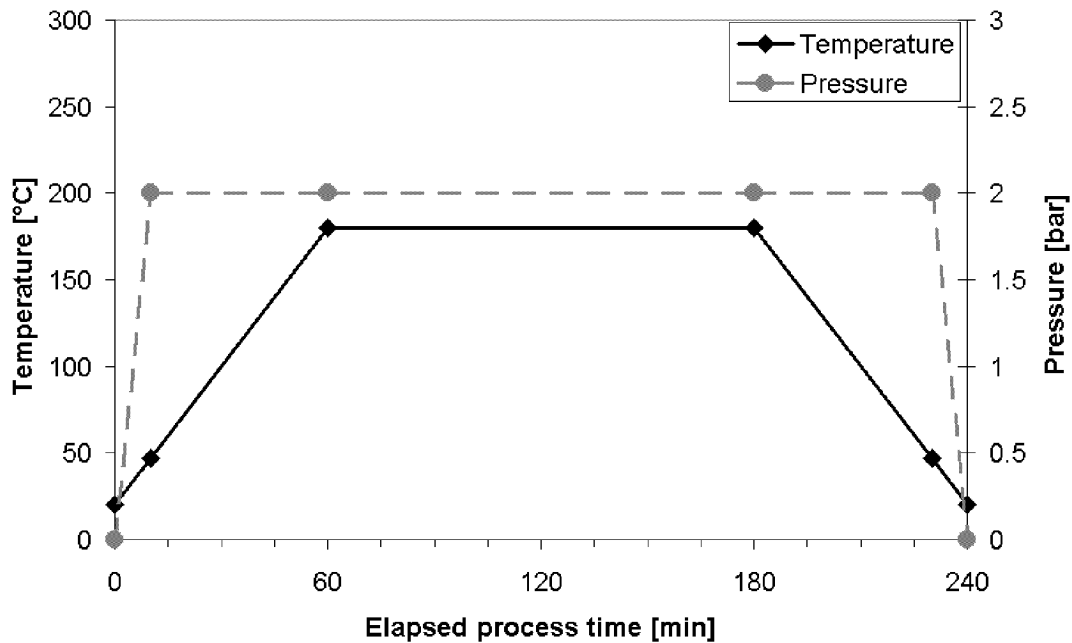


Figure 3.8: Parameters during the autoclave process

The results of ten short beam shear measurements show that the mean interlaminar shear strength of the post-processed cylinder is 34.78 N/mm^2 with an error of $\pm 4\%$.

3.4.3. Variation of the interlaminar shear strength with the nitrogen flow temperature and the compaction force applied to the nip line

The results of different experimental investigations prove that the temperature of the composite material ^[57] (heating power ^{[2]&[72]}) and the compaction force applied to the nip ^{[32],[38]&[55]} influence the mechanical properties of the laminate produced with the tape winding or the tape placement processes. Therefore, this investigation studies the variations of the interlaminar shear strength (ILSS) as function of these two parameters.

Winding speed 0.1 m/s , nitrogen flow $2.81 \text{ m}^3/\text{h}$ and winding pitch 5.7 mm are not changed during this investigation. Ten samples are tested for each set of process parameters. The mean ILSS as function of the nitrogen temperature at the torch outlet and of the compaction force applied to the nip is displayed in Figure 3.9. The results are also listed in Table 3.1.

The cylinder with the lowest ILSS is also the cylinder with the largest error. Since the range of ILSS is not the largest one in this cylinder, it is assumed that the large variations in percent come essentially from the low mean ILSS.

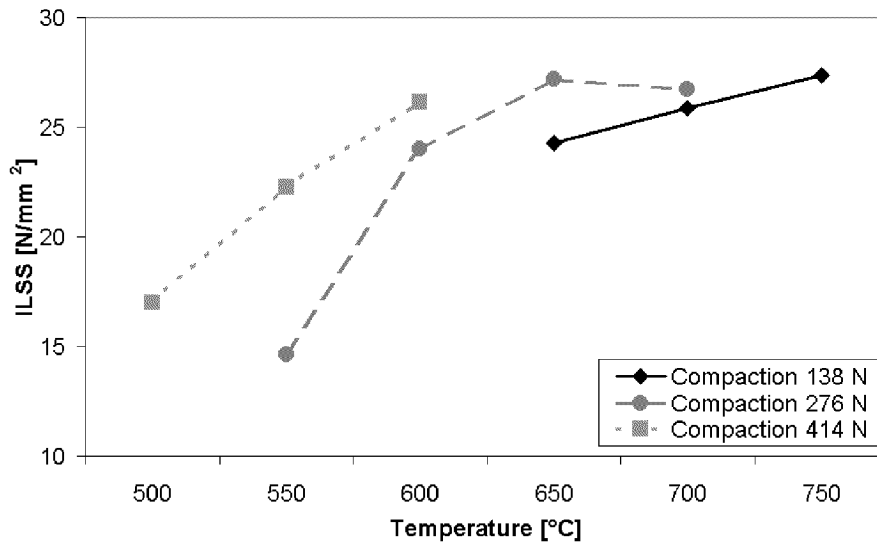


Figure 3.9: ILSS in function of the nitrogen flow temperature and of the compaction force applied to the nip

Nitrogen Flow Temperature	Compaction Force	ILSS	Error
°C	N	N/mm ²	%
650	138	24.28	4.50
700	138	25.85	2.00
750	138	27.38	3.70
550	276	14.66	10.10
600	276	24.01	4.50
650	276	27.20	4.30
700	276	26.74	6.00
500	414	17.01	6.00
550	414	22.27	3.50
600	414	26.14	6.00

Table 3.1: ILSS in function of the nitrogen flow temperature and of the compaction force applied to the nip

Figure 3.9 shows that the temperature range studied for each constant compaction force is relatively small: 100°C or 150 °C. The reason is that the experimental possibilities are bracket by inadequate bonding at the lowest

nitrogen temperature and by high tape deformations at the highest nitrogen temperature. When the bonding between the preform surfaces is insufficient, the cylinder delaminates at the end of the process. The tape can be correctly laid down and the temperature of the incoming tape can be measured by the pyrometer, when the width of the deformed tape is closed to the winding pitch. The reasons are that the previously laid composite material guides laterally the incoming tape, and that the program defines the position of the pyrometer spot.

The results presented in Figure 3.9 confirm results of Goedels^[32], who notices that the influence of the compaction force decreases with an increasing temperature. Comparing the vertical spaces between the curves can bring this through.

Considering the maximum ILSS for each compaction force (27.38, 27.20 and 26.14), Table 3.1 shows that the ILSS-variations are larger than the difference between the maximum and the minimum values of those ILSS. The maximum ILSS can be reached for each of the compaction force employed in this study by varying the nitrogen flow temperature. This result demonstrates that there exists a processing window that allows to process cylinders with the best achievable ILSS.

Finally, the influence of the nitrogen flow temperature and of the compaction force applied to the nip is relatively high as expected. The maximum ILSS obtained during this study are about 80% of that of the post-consolidated cylinder.

3.4.4. Variation of the interlaminar shear strength with the nitrogen flow temperature and the winding pitch

The work presented in this section is motivated by the upper limit mentioned above, i.e. the increase of the nitrogen flow temperature is limited when other process parameters are kept constant. Since this limit appears during the fabrication of cylinders using the sets of process parameters that produce the cylinders with the best interlaminar shear strength (ILSS), and the ILSS depends on the process temperature, this section aims to study the influence of the nitrogen flow temperature and of the winding pitch on the ILSS. This work enables to observe if the variation of the winding pitch results in change of the maximum ILSS that is achievable by increasing the nitrogen flow temperature, and then to show if it is possible to obtain ILSS for tape wound cylinders higher than 80% of that of the post-consolidated cylinder.

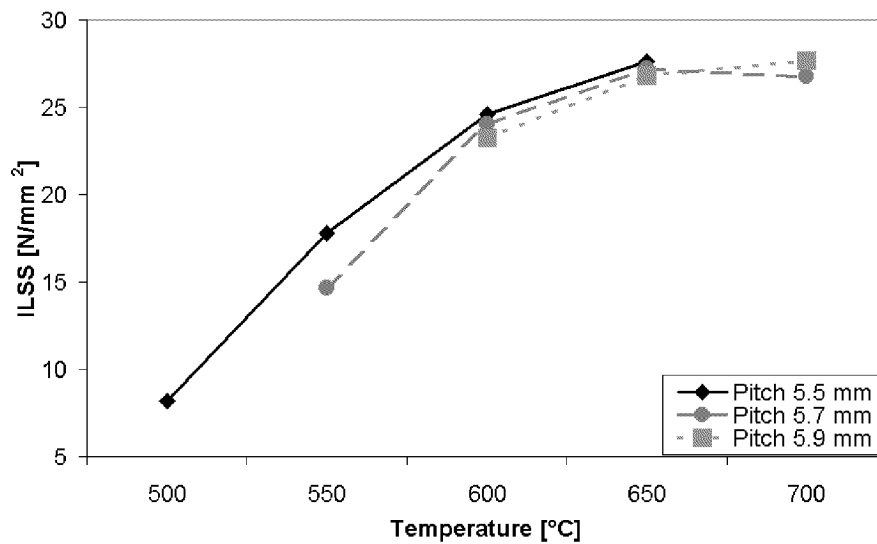


Figure 3.10: ILSS as function of the nitrogen flow temperature and of the winding pitch

The constant process parameters of this study are the winding speed 0.1 m/s, the nitrogen flow 2.81 m³/h and the compaction force applied to the nip 276 N. Ten samples are tested for each set of process parameters. The mean ILSS as function of the nitrogen temperature at the torch outlet and of the winding pitch is plotted in Figure 3.10. The results are given in Table 3.2.

Nitrogen Flow Temperature	Winding Pitch	ILSS	Error
°C	mm	N/mm ²	%
500	5.5	8.21	15.50
550	5.5	17.76	6.10
600	5.5	24.58	5.80
650	5.5	27.59	4.80
550	5.7	14.68	10.30
600	5.7	24.01	4.50
650	5.7	27.20	4.30
700	5.7	26.78	6.20
600	5.9	23.22	4.60
650	5.9	26.83	5.90
700	5.9	27.67	3.80

Table 3.2: ILSS as function of the nitrogen flow temperature and of the winding pitch

As in the previous section, the highest relative errors are encountered for the cylinders with the lowest ILSS.

The results presented in Figure 3.10 show that the increase of the winding pitch from 5.7 mm to 5.9 mm doesn't enable to increase the nitrogen flow temperature during the process. They point out that the deformation of the incoming tape is highly sensitive to the nitrogen flow temperature in the domain of the process parameters studied. This implies that the possibilities to increase the winding pitch in order to increase of the ILSS are small.

This investigation confirms that the best ILSS for each winding pitch is constant at about 80% of that of the post-consolidated cylinder.

3.4.5. Variation of the interlaminar shear strength with the nitrogen flow temperature and the winding speed

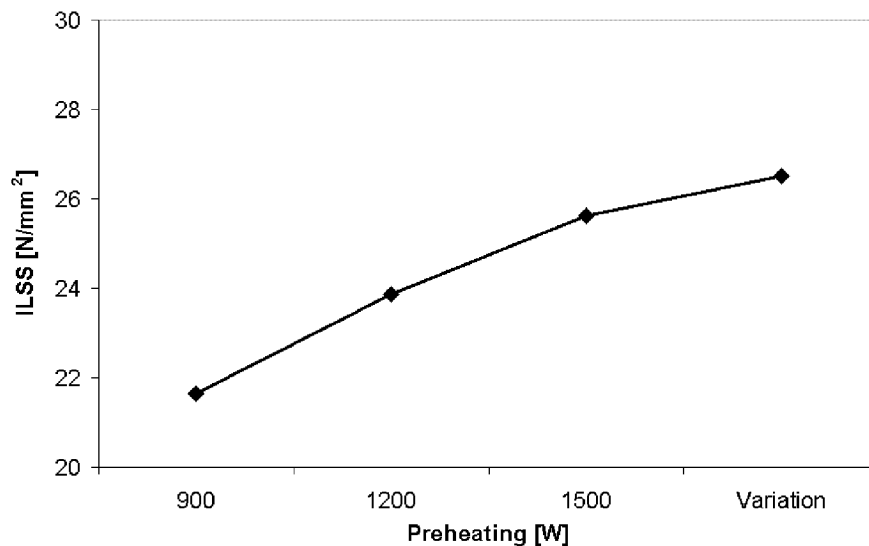


Figure 3.11: ILSS as function of the preheating power (winding speed 0.3 m/s)

Various authors ^{[18]&[48]} show that the winding speed is also one of the process parameters that influences the mechanical properties of the parts produced.

The winding speed is increased in two steps. First, a winding speed of 0.3 m/s is considered. Second, the winding speed is changed to 0.5 m/s. During this work, the preheating channel is used, because a higher heating power is required to warm up the incoming tape.

Considering that the incoming tape is a longer time in contact with the hot air in the preheating channel, the hot air gun power is the parameter that is varied for the winding speed of 0.3 m/s. The other process parameters are kept constant : the nitrogen flow 2.81 m³/h, the nitrogen flow temperature 700°C, the compaction force applied to the nip 276 N and the winding pitch 5.3 mm.

Preheating	ILSS	Error
W	N/mm²	%
900	21.65	3.60
1200	24.72	3.60
1500	25.63	3.30
Variation	26.51	1.40

Table 3.3: ILSS as function of the preheating power (winding speed 0.3 m/s)

For each set of process parameters, ten specimens are tested with the short beam shear apparatus. Figure 3.11 displays the mean ILSS for the different cylinders processed with a winding speed of 0.3 m/s. The short beam shear results are also listed in Table 3.3.

Once again the maximum ILSS is approximately equal to 80% of that of the post-processed cylinder. The limit can be reached with a speed three times faster than that in the two previous sections.

For the fabrication of the cylinders with a speed of 0.5 m/s, two heating parameters are varied : 1) the nitrogen flow temperature, 2) the power of the hot air gun. The other process parameters are the nitrogen flow 2.81 m³/h, the compaction force applied to the nip 276 N and the winding pitch 5.2 mm.

Ten specimens are tested for each set of process parameters. Figure 3.12 plots the results of the short beam shear tests for the different cylinders processed with a winding speed of 0.5 m/s. Table 3.4 lists them.

In Figure 3.12, the shape of the curve for the preheating power 2100 W is different than that for the preheating power 1500 W. Considering the errors of both curves, the differences are not significant.

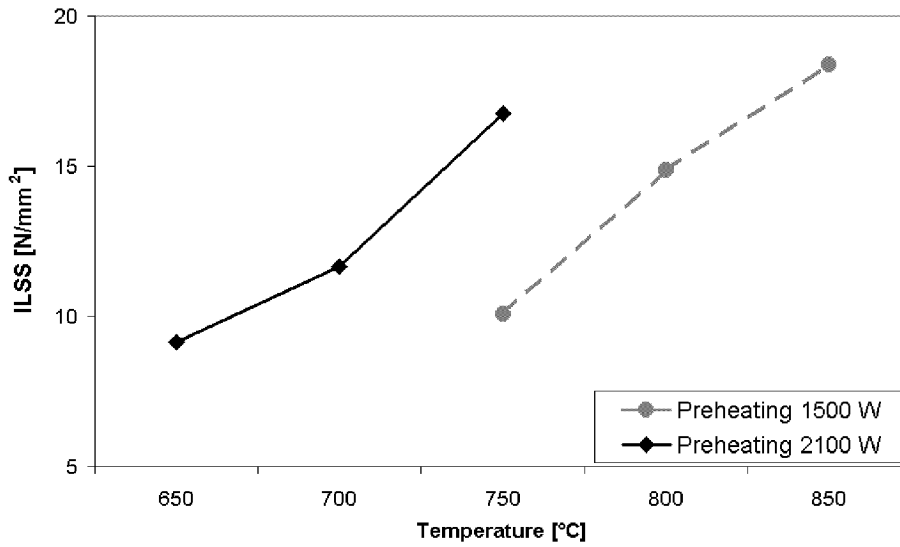


Figure 3.12: ILSS as function of the preheating power (winding speed 0.5 m/s)

As it can be seen in Figure 3.12, the highest plotted ILSS is lower than the limit of 80%. For the domain of process parameters studied, those results show that neither the variation of the preheating power nor that of the nitrogen flow temperature permit to produce a cylinder with an ILSS of about 80% of that of the post-processed cylinder. Therefore, a winding speed of 0.3 m/s is considered as the limit for the current setup.

Nitrogen Flow Temperature	Preheating Power	ILSS	Error
°C	W	N/mm²	%
750	1500	10.06	8.10
800	1500	14.86	10.60
850	1500	18.39	8.00
650	2100	9.15	14.00
700	2100	11.66	19.00
750	2100	16.77	6.00

Table 3.4: ILSS as function of the preheating power (winding speed 0.5 m/s)

3.5. Measurements with the pyrometer

Since the temperature of the incoming tape just before the nip gives informations on the welding temperature, and since it can enable in some cases to determine whether or not degradation takes place in this region, representative examples are presented in this section (Figure 3.13 and Figure 3.14).

Both diagrams show temperature measurements performed with the pyrometer. Figure 3.13 plots examples made during the fabrication of cylinders using a winding speed of 0.1 m/s and a winding pitch of 5.5 mm. Figure 3.14 displays measurements performed during processes using a winding speed of 0.3 m/s.

Figure 3.13 and Figure 3.14 are divided in eight time intervals of 123.5 s and 43.5 s. They correspond to the duration of the lay down of a layer during the tape winding process.

At the end of a layer, the incoming tape must go up the previous layer so as to start the next one. This causes instabilities in the guiding of the incoming tape. Since the axial position of the incoming tape isn't perfectly defined, the spot of the pyrometer isn't any more focused only on the incoming tape. Its measurements have no physical meaning. They are therefore not plotted in the graphs.

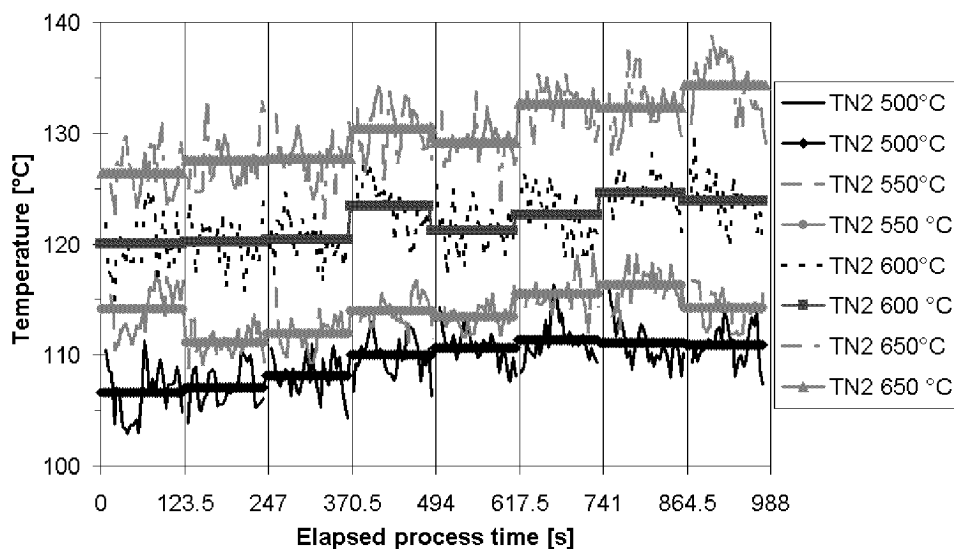


Figure 3.13: Temperature during the process (speed 0.1 m/s, winding pitch 5.5 mm)

The number of measurements is higher for the processes with a winding speed of 0.1 m/s. This allows to integrate them numerically prior to their representation in Figure 3.13, in order to reduce the noise.

This noise origins from the vibrations of the winding machine. Since they are transmitted to the holder of the pyrometer, the pyrometer spot moves relatively to the incoming tape during the process. The measured temperature changes, due to the high temperature gradients in the nip region.

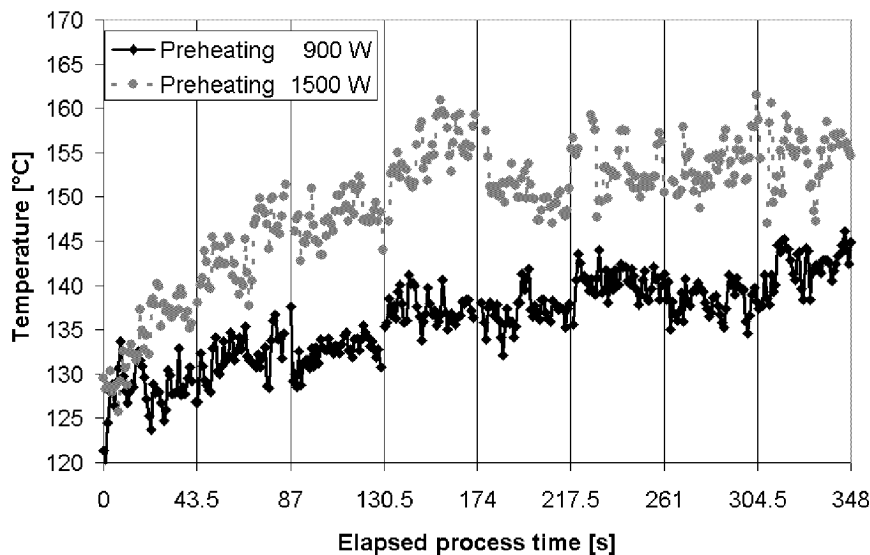


Figure 3.14: Temperature during the process (speed 0.3 m/s)

There are two curves for each nitrogen flow temperature in Figure 3.13. The first one displays the integrated measurements and the second one the mean layer temperatures. The measurements show that the second curves are representative of the incoming tape temperature during the lay-down of each layer, because this temperature is approximately constant.

The curves with the mean layer temperatures are not plotted in Figure 3.14, because the temperature of the incoming tape changes during the process. The measurements are not numerically integrated in Figure 3.14 in order to visualize the variations.

3.5.1. Discussion on the polymer chain diffusion

Figure 3.15 shows a measurement made with a differential scanning calorimeter. The large decrease between 25°C and 40°C is caused by instabilities related to the change from isothermal to isogradient measurements. The large increase between 200°C and 205°C is due to the reverse effect (isogradient to isothermal measurements). The low decrease between 40°C and 110 °C is caused by the temperature-dependent heat capacity that influences the heat flow between the two crucibles. Figure 3.15 displays also the melting behavior of the thermoplastic matrix. The phase transition begins at approximately 110°C and ends at 180°C.

Considering the measurements presented in Figure 3.15, the melting temperature of polypropylene is 180 °C. This means that the temperature of the incoming tape is below the melting temperature of the thermoplastic matrix for all the measurements shown in Figure 3.13 and Figure 3.14. According to those figures, the incoming tape temperature is however in the phase transition domain. This is also the case for all the experimental investigations presented in section 3.4.

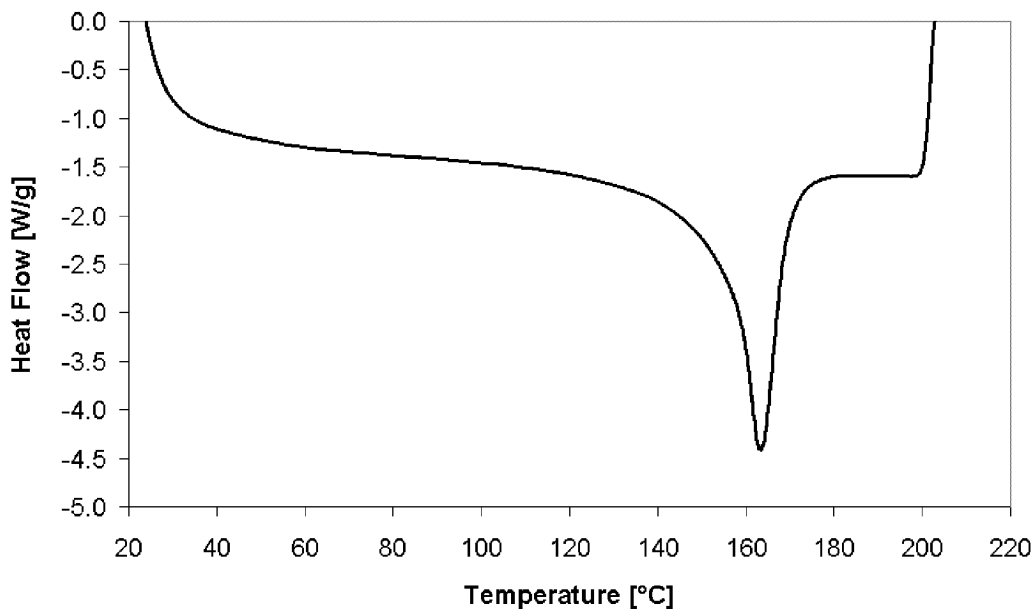


Figure 3.15: Differential scanning calorimeter measurement of the fiber reinforced polypropylene with an heating rate of 20 °C/min

Cho and Kardos ^[16] show that the strength of semi-crystalline PEEK specimens due to polymer chain diffusion develops when the specimen temperature is lower than the melting temperature of the thermoplastic matrix. Considering this observation, the results presented above can be considered as consistent. Further investigations should be performed to relate the degree of polymer chain diffusion with the temperature of the composite material during the process, in order to determine if the bond strength difference between the best wound specimens and the post-processed specimens is related with the polymer chain diffusion process.

3.5.2. Discussion on the polymer degradation

Figure 3.16 plots a thermogravimetric analysis measurement of the glass fiber reinforced polypropylene. The thermoplastic matrix is heated to the temperature (200°C) at which the weight loss is studied. The first cooling is the end of the weight loss study at 200°C. The measurements are finished with an enforced degradation of the polypropylene with a heating of the thermoplastic matrix. The released weight after the degradation is the weight of the fibers.

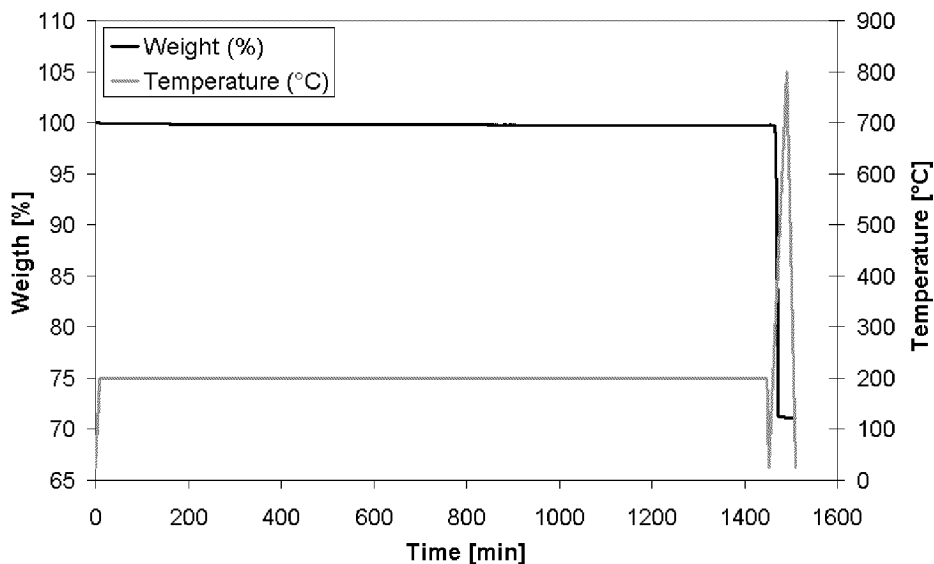


Figure 3.16: TGA measurement of the fiber reinforced polypropylene at 200 °C

The weight loss of the thermoplastic matrix is lower than 1% after 24 hours. Since the weight loss of the polypropylene at 200 °C can be neglected (see Figure 3.16) and the temperature of the incoming tape is lower than 200 °C (see Figure 3.13 and Figure 3.14), the degradation is assumed to be negligible on the surface measured by the pyrometer. Therefore, the 80% limit cannot be explained by a degradation of the thermoplastic matrix at this location.

3.6. Micrograph analysis

The last sections don't indicate reasons for the difference between the results of the short beam shear tests (SBS) for the best tape wound specimens and those for the post-consolidated specimens. The short beam shear method characterizes the entire structure of the samples and not directly the interlaminar properties of the samples. The objective of this section is therefore to control whether or not one of the reasons of this difference is related with the intralaminar structure.

This analysis doesn't study the fiber distribution, the fiber and matrix content, because the same tape is used for the tape wound and post-processed specimens. Only the void content (Table 3.5) and their locations are determined for some specimens : they are cut from the post-consolidated cylinder and from the cylinders presented in section 3.4.4 that have the best interlaminar shear strength.

Process	Nitrogen Flow Temperature	Winding Pitch	Number of Analyzed Pictures	Void Content	Error
	°C	mm		%	
Autoclave			56	0.46	0.08
Tape Winding	650	5.5	64	1.08	0.12
Tape Winding	700	5.7	64	1.48	0.10
Tape Winding	700	5.9	64	1.47	0.10

Table 3.5: Void contents

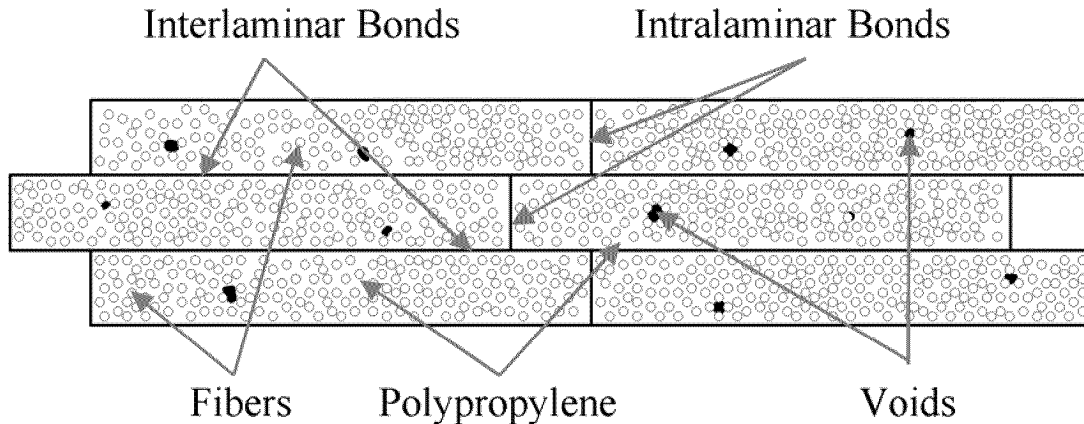


Figure 3.17: Different regions identified in a micrograph

Table 3.5 shows that the void content of the post-processed cylinder is lower than those of the tape wound cylinders. The cylinder wound at 650 °C has also a lower void content than the two other wound cylinders.

Considering that the bonding regions (black lines) and those originated from the tape (rest), the voids are located in the tapes (Figure 3.17). Since the tape temperature before the nip is lower than the melting temperature of the thermoplastic matrix during the tape winding process, it is assumed that the intralaminar voids are not caused by a deconsolidation of the incoming tape, because the polypropylene matrix is partly crystalline in the tape. It is further presumed that they are already present in the original tape.

Despite the voids are intralaminar, the different void contents could be one of the reasons for the 80% limit, because the voids influence the mechanical properties of laminates ^[24]. They are probably not the single cause, because the tape wound cylinders with the best interlaminar shear strength have different void contents, and because the latter is low.

Considering the high viscosity of the thermoplastic matrix and the very short dwell time at the nip, a better consolidation of the tape should be performed upwards of the nip to reduce or eliminate the intralaminar voids in the tape wound cylinders. This can be done on-line or prior to the tape winding process.

3.7. Conclusion

This work confirms that the compaction force applied to the nip, the heating power and the winding speed influence the interlaminar shear strength (ILSS). It shows also that the influence of the winding pitch should not be neglected.

This experimental work shows that the best ILSS determined with the short beam shear test for the tape wound cylinders is 80% of that of the post-processed cylinder. Different sets of process parameters lead to this limit.

The experimental investigations demonstrate that the cause of this difference isn't the degradation of the thermoplastic matrix on the incoming tape just before the nip.

The microstructure analysis shows that the void contents of the tape wound cylinders are higher than that of the post-processed cylinder. The voids are localized in the regions that are originally inside the tape. They are not process-induced. A better pre-consolidation of the tape should reduce or eliminate the voids in the tape wound cylinders, and improve the short beam shear results. This can be done on-line or prior to the automated tape winding process.

The incoming tape temperature measured by the pyrometer just before the nip is lower than the melting temperature of the polypropylene matrix. The highest measured temperatures are however in the phase transition domain. Further investigations need to be performed to determine whether or not the polymer chain diffusion through the interfaces is another cause of the limit.

In the next chapter, a numerical program will be presented. It simulates the temperature of the composite material during the automated tape winding process. Then a model will be added in the numerical program, to evaluate the degree of polymer chain diffusion. Simulations will be performed to define whether or not the polymer chain diffusion is a cause of the 80% limit.

CHAPTER 4

Thermal Phenomena in the Automated Tape Winding Process: Computational Simulations and Experimental Validations

4.1. Introduction

Filament winding with on-line impregnation of thermoset matrix and automated placement of thermoset pre-impregnated tapes are established processes. Their course is divided in two main steps. First, the composite material is laid down on a support and subsequently on the substrate until the latter forms the desired part. In the second step, the thermoset matrix is cured.

The use of the thermoset matrixes is the cause of various process drawbacks: slipping of rovings and tows limits the selection of the fiber orientations in the final part, the exothermic reaction of the thermoset matrix creates problems in case of thick laminates, and the curing of the thermoset increases manufacturing time and necessitates further tooling and ancillary materials.

These limitations do not occur when a pre-impregnated fiber reinforced thermoplastic tape is bonded on-line to the substrate. The bonding process of the incoming tape to the substrate begins to develop in the region closed to the nip line. It consists of two steps. First, compaction forces are applied to the nip to create an intimate contact between the joining surfaces. Second, the polymer chains diffuse through the contact areas.

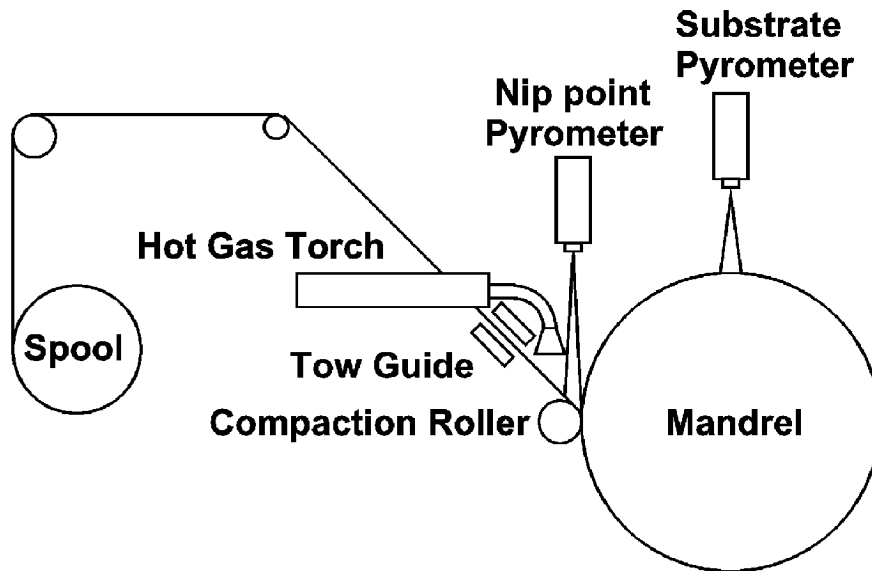


Figure 4.1: Sketch of the current tape winding setup

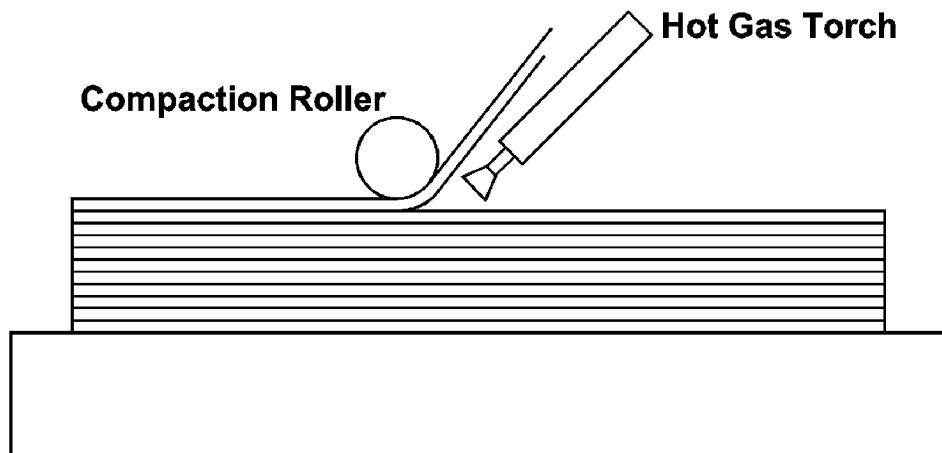


Figure 4.2: Sketch of a tape placement setup

On-line bonding can be applied to the automated tape winding (Figure 4.1) and the automated tape placement (Figure 4.2). Both manufacturing processes have the potential to widespread the use of composite materials and are very promising in terms of cost-effectiveness and implementation of tailored design solutions.

Motivated by the high potential of thermoplastics, several researchers investigated theoretically these processes. Models take into account intimate contact^[56], healing (autohesion, self-diffusion, polymer chain diffusion)^[56], melting and crystallization^[80], thermoplastic degradation^[70], void consolidation and growth^[69], process induced stresses^[29] and viscoelastic deformation of the material in the nip^[81].

As each of these phenomena are dependent on either the temperature, the temperature gradients or both, a simulation of those processes must use a thermodynamic model that describes reliably the temperature distributions. Thermal analyses^{[1]&[83]} are performed accounting for different types of heat sources. It is also necessary to compare the model predictions with measurements to assess its accuracy, otherwise the modeling effort is an intellectual enterprise. Earlier investigations consider steady-state thermal models or quasi-steady-state models. Grove^[34] presents a two-dimensional steady-state model. Argarwal et al.^[1] use the two-dimensional model developed by Beyeler and Güçeri^[11]. Their comparisons between the measurements and the computed temperatures suggest that only 20% of the laser energy is absorbed. Mantel et al.^[57] simulate the tape laying process considering an intimate contact model. Mantel et al.^[55] add a polymer chain diffusion model. James and Black^[42] validate a three-dimensional model with measurements made with an infrared camera. Kim et al.^[46] use a two-dimensional model for the tape-laying process. They found reasonable agreements between their numerical results and their experimental data given by thermocouples. Somnez and Hahn^[80] describe the tape placement process with a two-dimensional model including the crystallization and melting kinetics of the thermoplastic matrix. The two-dimensional model presented by Shih and Loos^{[77]&[78]} simulates the thermoplastic filament winding process, however the incoming tape is not integrated in the model. Tumkor et al.^[91] present an unsteady-state model for the tape laying process. They introduce a time-delay at the end of each layer to control the validity of their model with the measurements made by Kim et al.^[46].

James and Black^[42] mention that steady three-dimensional analysis cannot accurately model the frequent cycling of their infrared lamp in the axial direction, the conditions that exist in the manufacture of short filament wound or very thin parts. Yardimci et al.^[99] mention that the quasi-steady-state models neglect the effect of non-uniform heating and the effect of varying winding speed during the process. More generally, steady-state models and quasi-steady-state models cannot simulate processes when the boundary condition assumptions are not fulfilled. They are only valid when a representative control area or volume can be defined. Their usefulness is consequently limited to particular cases that are bounded by the types of boundary conditions.

Despite those limitations and the transient nature of those processes, there is to the author's knowledge no transient simulations validated with transient experiments.

The heat input of a hot gas torch (HGT) has not been thoroughly investigated. Charrier et al. ^[15] evaluate this coefficient to be 105 W/(m²K). Mantel et al. ^[57] use a value 11357 W/(m²K) for the coefficient of convection closed to the HGT with a heated length of 63.5 mm. The convection coefficient behind the compact roller is assumed to be 6814 W/(m²K). Kim et al. ^[46] assume a convection coefficient of 900 W/(m²K) between the gas and the substrate, and a coefficient of 250 W/(m²K) between the gas and the incoming tape. The heated areas on the substrate and the incoming tape are assumed to be 11 mm long. Somnez and Hahn ^[80] assume a coefficient of 2500 W/(m²K) on a heated length of 15 mm for their parametric study. Shih and Loos ^[78] determine the coefficient by comparing measurements and model predictions. They estimate it to have a value of 350 W/(m²K).

The objective of the present chapter is therefore threefold : 1) to develop a three-dimensional transient thermal model for the tape winding process, 2) to describe a method to determine separately the heat transfer between the hot gas from a HGT and the composite material, 3) to demonstrate the validity of the model by comparing the model predictions with temperature measurements.

4.2. Theory

In the present model, the heat transfer in the composite material is described by the heat diffusion equation for anisotropic materials. Cylindrical coordinates are appropriate for the substrate (Equation 4.1) and the Cartesian coordinates for the incoming tape (Equation 4.2). The incoming tape is assumed to be straight in the model.

$$\frac{K_r}{r} \left(r \frac{\partial^2 T}{\partial r^2} + \frac{\partial T}{\partial r} \right) + \frac{K_\phi}{r^2} \frac{\partial^2 T}{\partial \phi^2} + K_z \frac{\partial^2 T}{\partial z^2} = \rho C \frac{\partial T}{\partial t} \quad (4.1)$$

$$K_x \frac{\partial^2 T}{\partial x^2} + K_y \frac{\partial^2 T}{\partial y^2} + K_z \frac{\partial^2 T}{\partial z^2} = \rho C \frac{\partial T}{\partial t} \quad (4.2)$$

The progress of the tape winding process is simulated throughout the adaptation of the mesh : different meshes describe the material according to the elapsed process time.

The model does not consider heat generation/sink term in Equation 4.1 and Equation 4.2, because (Figure 4.3) :

$$\dot{H}_{me} \ll \dot{Q}_{HG} \quad (4.3)$$

$$\dot{H}_{cr} \ll \dot{Q}_E \quad (4.4)$$

Based on measurements made with a differential scanning calorimeter (DSC) with a heating rate of 0.3°C/s , the influence of dH_{me}/dt (dH_{cr}/dt) results in an overestimation of the temperature at the nip point by approximately 5°C . Since the heating rate is three orders of magnitude (at least 1000°C/s), this value is a maximum error.

To solve Equation 4.1 and Equation 4.2, the initial and the boundary conditions must be specified (see Figure 4.3).

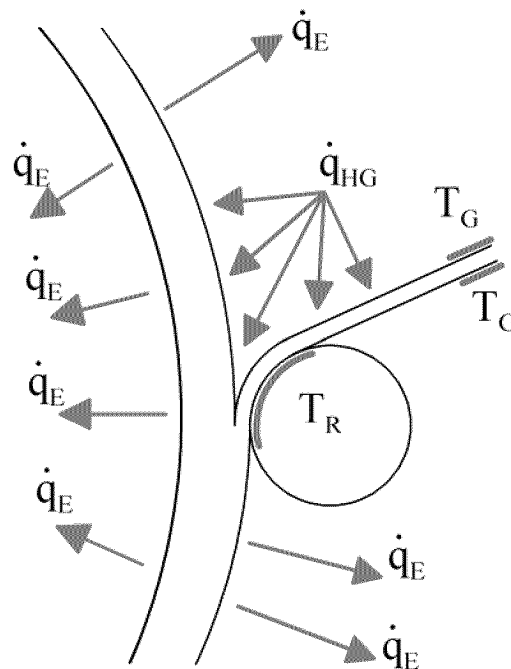


Figure 4.3: Location of the boundary conditions

Equation 4.5 and Equation 4.6 determine the initial temperature of the mandrel and of the incoming tape. Before the beginning of the process, the mandrel is kept enough time at room temperature so that thermal equilibrium with the environment is reached. The incoming tape originates from a spool whose temperature is only influenced by the room temperature.

$$T = T_{m_i} \quad (4.5)$$

$$T = T_{i_i} \quad (4.6)$$

Since the composite material is in contact with the guiding elements and the compaction roller, contact boundary conditions are introduced in the model at their respective locations with :

$$T = T_G \quad (4.7)$$

$$T = T_R \quad (4.8)$$

Convective heat transfer exists at the internal surface of the mandrel and at the external surface of the substrate :

$$\dot{q}_E = \alpha_E (T - T_E) \quad (4.9)$$

Two surfaces are subjected to the convection heat transfer of the hot gas torch, the incoming tape and the substrate :

$$\dot{q}_{HG} = \alpha_{HG} (T_{HG} - T_s) \quad (4.10)$$

Remark

The heat transfer is determined assuming a pure convection between the material and the environment. Radiation is not considered.

The influence of radiation terms (see Figure 4.4) on heat transfer is smaller than 6% in the considered temperature range (Equation 4.11) with $T_h=113$ °C, $T_c=30$ °C, $\alpha_E=21$ W/m²K and $\alpha'_E=11.58$ W/m²K.

$$error = \frac{\int_{T_c}^{T_h} \alpha_E (T_h - T_c) dT_h - \left(\int_{T_c}^{T_h} (\alpha'_E (T_h - T_c) + \varepsilon_0 (T_h^4 - T_c^4)) dT_h \right)}{\int_{T_c}^{T_h} (\alpha'_E (T_h - T_c) + \varepsilon_0 (T_h^4 - T_c^4)) dT_h} \quad (4.11)$$

where α'_E is the real convection coefficient

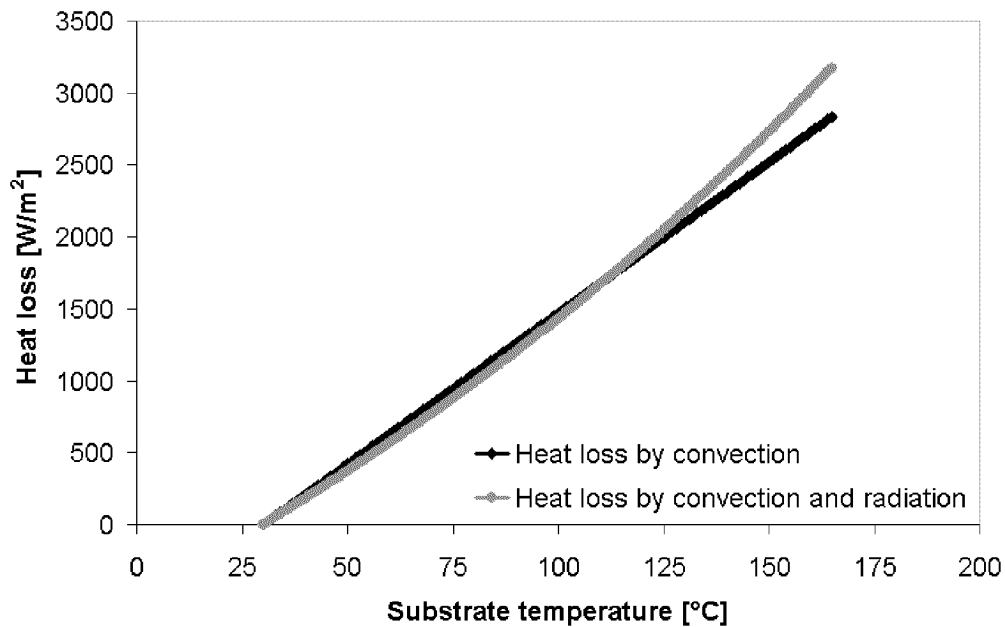


Figure 4.4: Comparison of the heat losses

4.3. Numerical simulation

4.3.1. Approach

A numerical simulation of the process has been performed using a commercial FE-program (ANSYS version 5.6 ^[5]). It considers that the laying location of the incoming tape is moving, that the locations of the boundary conditions are changing and that the mass of the substrate is increasing.

A critical issue in the development of the model is how to deal with computer time limitations. In the present study, three grids of different fineness were employed in different regions to circumvent the combination of a very large number of elements and time steps.

A grid generation process is meant to correspond to only a time step, because the regions with high and low temperature gradients vary during the simulation.

Since the grids generation requires a large CPU-time and the simulations use the same grids during a parametric study, the program consists of three stages (Figure 4.5): the creation of the basic mesh, the creation of the grids for each step, and the simulation of the process.

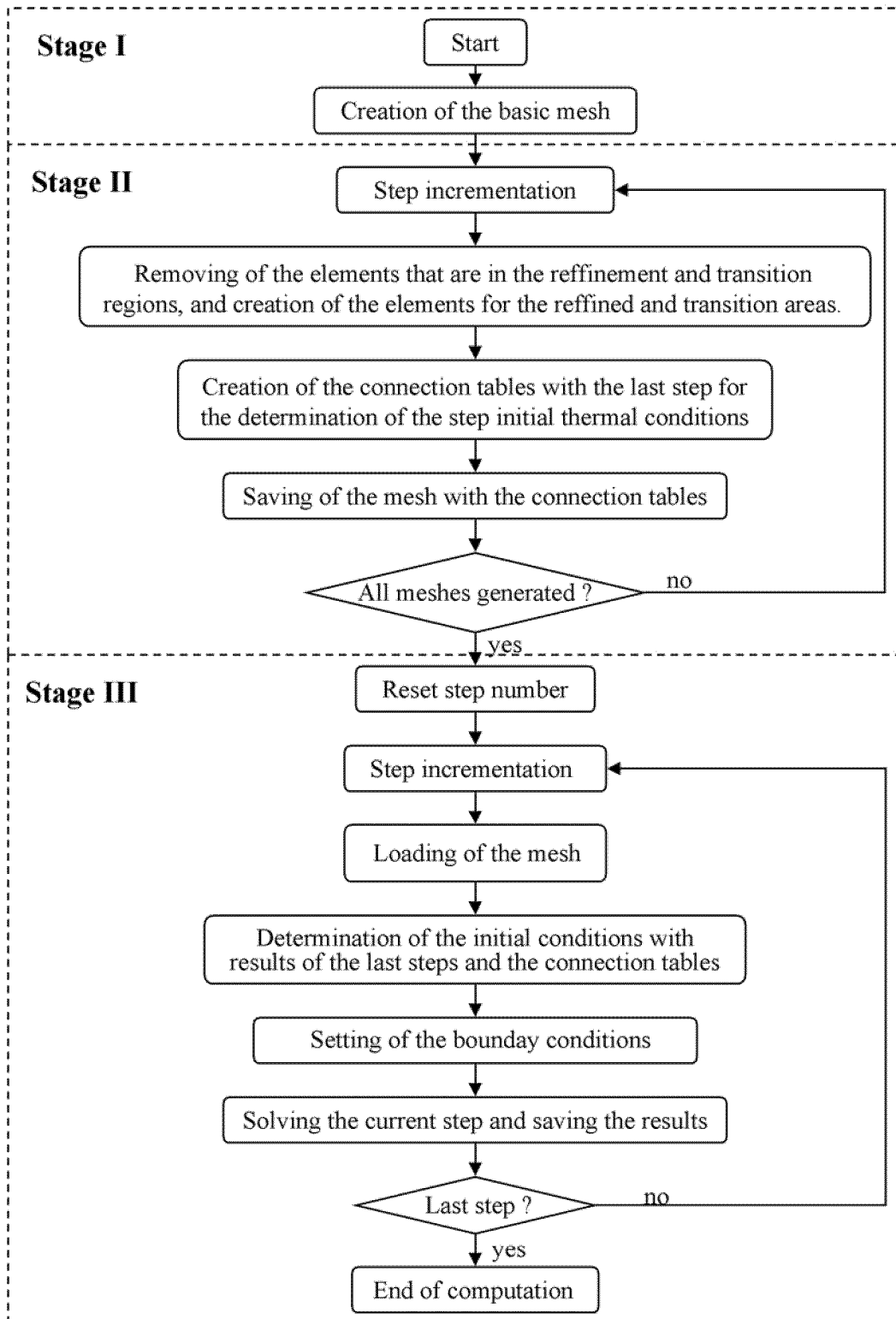


Figure 4.5: Flow chart of the program

4.3.2. Discretization and solution procedure

Stage I : Creation of the basic mesh

The first stage is to discretize the basic geometry (see Figure 4.6), i.e. the mandrel and the laid material at the end of the process. The mesh is coarse, because the temperature gradients are small in most regions. This mesh defines the winding path, the number of simulation steps and the amount of material laid during a simulation step.

The latter is given by the volume of one basic element. The width and the thickness are equal to the width and the thickness of the incoming tape after the compaction. The duration of a step can be determined by the length of the basic element divided by the process-speed in the tape motion direction.

$$\Delta t = \frac{l_{\varphi}}{v} \quad (4.12)$$



Figure 4.6: View of the basic mesh

Stage II : Creation of the mesh for each steps

The basic mesh is too coarse to accurately model regions where high temperature gradients are expected, i.e. the nip region and the incoming tape. In this context, a procedure to locally refine the mesh is presented in the following.

The second stage begins with the removing of the elements of the substrate that are not yet laid down in the current time step. Then, the elements of the basic geometry are taken off in the region of the nip point (Figure 4.7). The fine and transition meshes replace them. Finally, the elements representing the incoming tape are added to the grid (Figure 4.8).

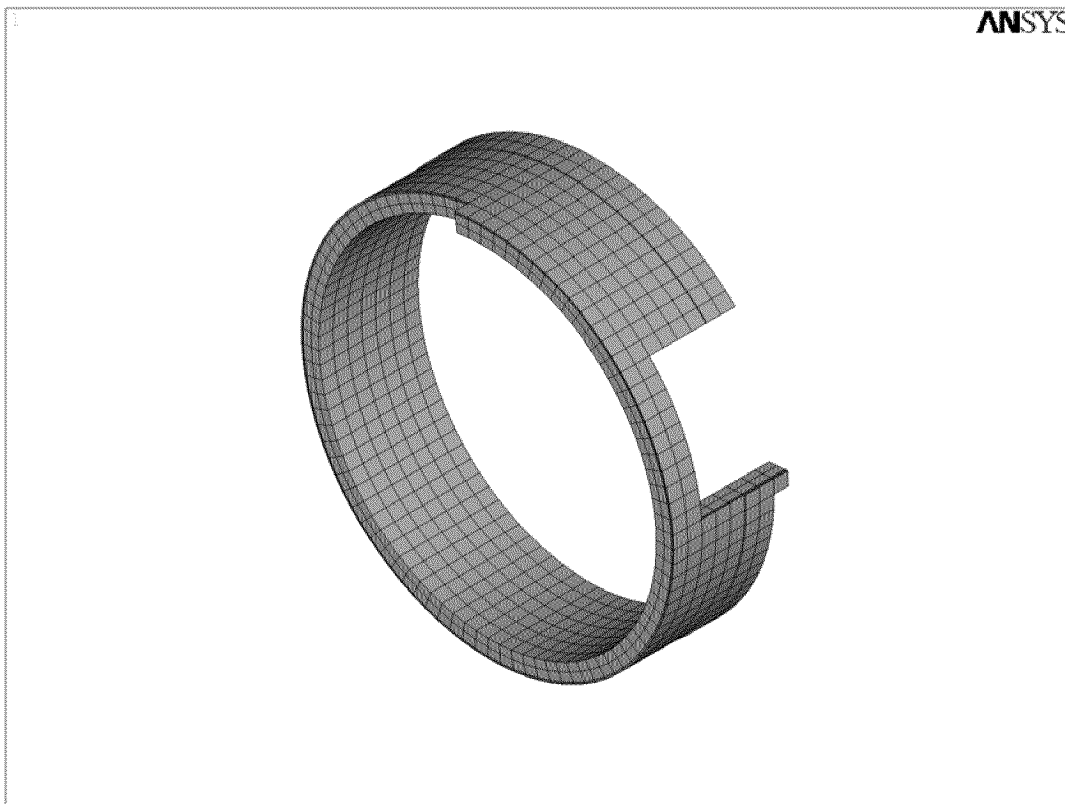


Figure 4.7: View of the geometry before the introduction of the fine and transition grids

The nodes are however kept during the removing session of the elements. They will be used in the determination of some initial conditions (see Stage III).



Figure 4.8: View of the nip region with one mesh refinement

Stage II is repeated for each time step. Figure 4.9 to Figure 4.12 show the grids for successive steps assuming a constant time step (constant process-speed).

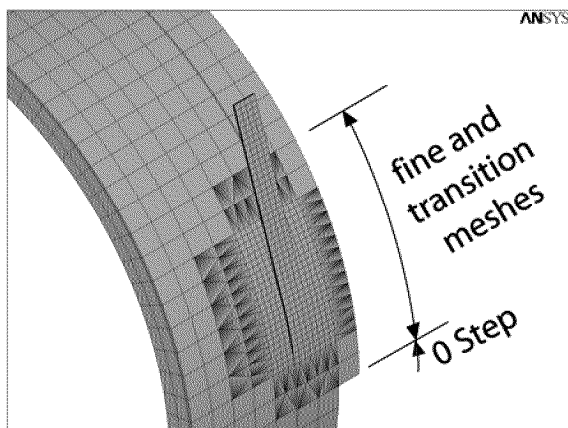


Figure 4.9: mesh at t_1

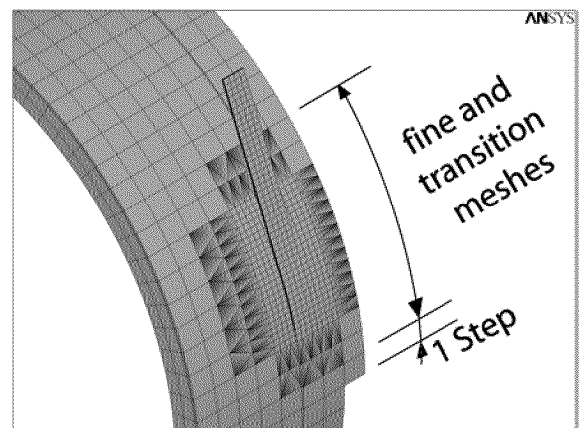


Figure 4.10: mesh at $t_2 = t_1 + \Delta t$

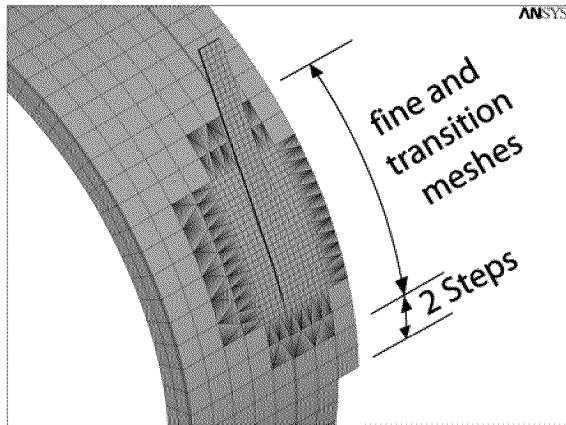


Figure 4.11: mesh at $t_3=t_2+\Delta t$

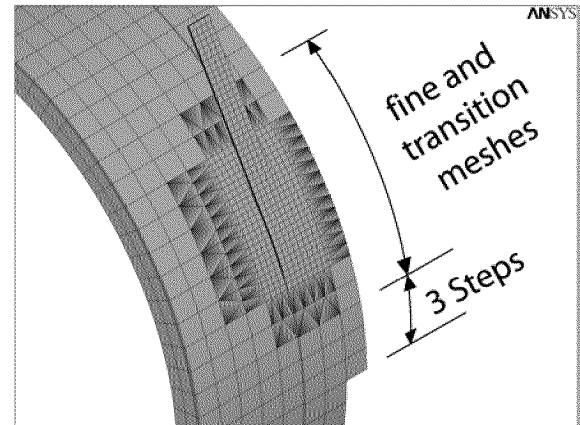


Figure 4.12: mesh at $t_4=t_3+\Delta t$

Stage III : Simulation of the process

The simulation of a step begins with the loading of the geometry. Since the nip line is moving (see Figure 4.9 to Figure 4.12), the boundary conditions are adapted in relation to its location. Generally, the initial conditions are equal to the final conditions of the preceding step. For the nodes corresponding to nip surface, the initial condition is the mean value of the final condition of the merging nodes. The initial conditions for the new generated nodes are determined considering the initial conditions of the surrounding nodes of the basic geometry. In this study, they are evaluated with linear shape functions according to the theory of finite elements ^[5].

Once the initial and the boundary conditions are determined, the program solves the problem for the step at hand and stores the results in a file. This operation is repeated until the solution of all steps is known.

The use of finite elements introduces one complication at the beginning and the end of the layers: each contact surface between two elements must be the same. The reason is that otherwise more than one shape function would exist between the same nodes. To avoid this problem, the lay down process is supposed to be terminated and restarted for each layer. The elements of the new layer are laid directly on the elements of the last layer and the winding direction is changed between two successive layers.

4.3.3. Material parameters

The material parameters are determined with standard measurement methods and are summarized in Table 4.1. During the simulations, the density is assumed to remain constant. The specific heat as a function of the temperature has been determined using a differential scanning calorimeter measurement system.

K_1 ^[33]	K_2 ^[33]	K_3 ^[33]	ρ ^[33]	C
W/(mK)	W/(mK)	W/(mK)	kg/m ³	J/(kg K)
0.55	0.41	0.41	1640	$969.32+5.0244 T - 0.0097944 T^2$

Table 4.1: Material parameters

4.3.4. Results

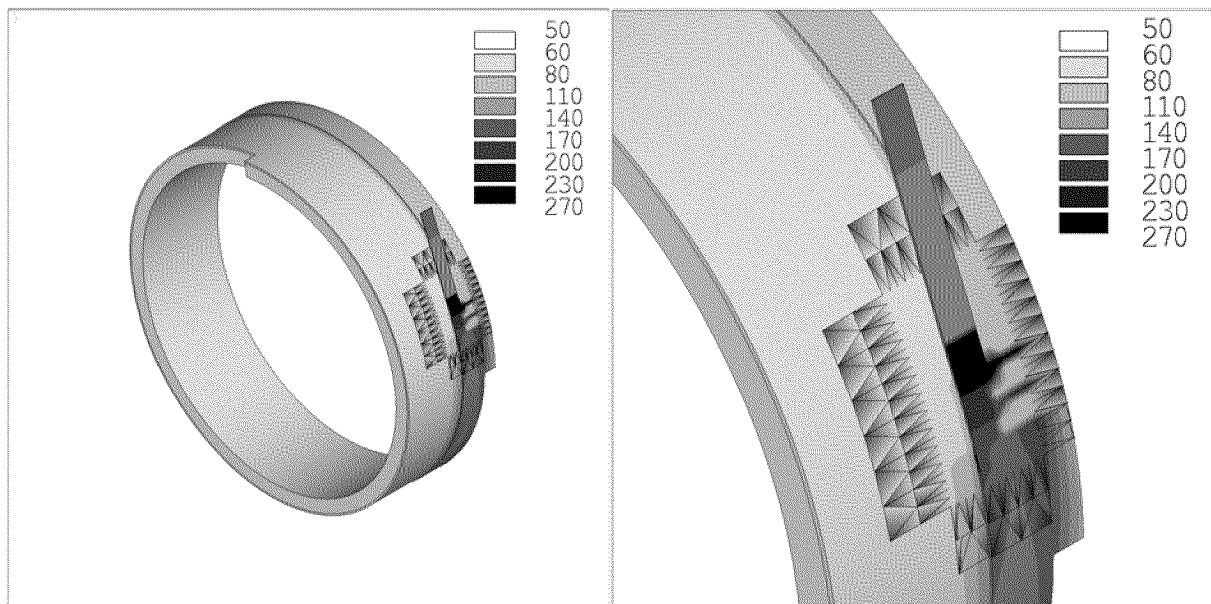


Figure 4.13: Views of an example of a result for a time's step

The result of a simulation step is given by the temperature history at each node. Since there are several nodes, they are stored in an array. The sum of all the arrays forms the complete result of a simulation.

A temperature plot example is shown in Figure 4.13. The heavy black lines define some of the element borders. The transition mesh can be easily recognized. It helps to determine the location of the nip line. The black area corresponds to the contact areas between the composite material and the compaction roller. The latter touches the composite at three locations: the incoming tape, the compaction area and the substrate on the side of the nip line. The last location is a line, because it is assumed that the composite material is only compacted in the nip region. The reason of the dark narrow region behind this line is that the heat does not have sufficient time to diffuse into the composite material. There is also a border effect over the transition mesh. It is due to the slow cold flow penetration between the downstream substrate and the upstream substrate. Comparison between simulations and experiments are presented and discussed after the section describing the experimental results.

4.4. Experimental determination of the heat transfer in the vicinity of the gas torch

Since the literature provides extremely different values for the convective heat transfer coefficient of the hot gas torch (α_{HG}) and the external stream temperature (T_{HG}) in Equation 4.10, this chapter aims to determine them experimentally.

The first question arising is if the flow is laminar or turbulent for the selected process parameters (see Table 4.2). According to Incropera and DeWitt ^[39], the critical Reynolds number corresponding to the onset of turbulence is 2300 in a fully developed flow.

$$\text{Re} = \frac{v_T(T) d}{\nu(T)} \quad (4.13)$$

SET	T	dV_{RT}/dt	$\rho_{RT}^{[94]}$	$\rho^{[94]}$	v_T	$v^{[94]}$	Re
--	°C	m ³ /h	kg/m ³	kg/m ³	m/s	10 ⁻⁷ m ² /s	--
1	500	2.81	1.15	0.44	52.45	805	4627
2	650	2.81	1.15	0.36	62.61	1081	4112

Table 4.2: Reynolds number for the two sets of process parameters

Knowing the volumetric flow of the torch at room temperature, the temperature dependent flow velocity can be calculated using Equation 4.14 and Equation 4.15:

$$v_T(T) = \frac{\dot{V}_T(T)}{A} \quad (4.14)$$

$$\dot{V}_T(T) = \frac{\rho_{RT}}{\rho_T(T)} \dot{V}_{RT} \quad (4.15)$$

Results are summarized in Table 4.2. They indicate that the flow in the vicinity of the torch is not laminar. Therefore, the measurement system must smooth its turbulent variations, or be fast enough to capture these fluctuations. The first option is chosen herein.

4.4.1. Setup

A still setup was used for those measurements to avoid process-induced vibrations that would false the measurements. This simplification doesn't introduce large errors, because the velocity of the hot gas is two orders of magnitude higher than the velocity of the incoming tape.

The temperature distribution of the hot gas in the nip region is measured with an infrared camera. Since bolometers cannot determine directly the temperature of a gas, a special sheet made from a low conductivity material^[4] is introduced at the center of the gas flow. The sheet has a thickness of 0.2 mm to minimize the conduction heat transfer, the influence on the hot gas flow, and subsequently measurement errors.

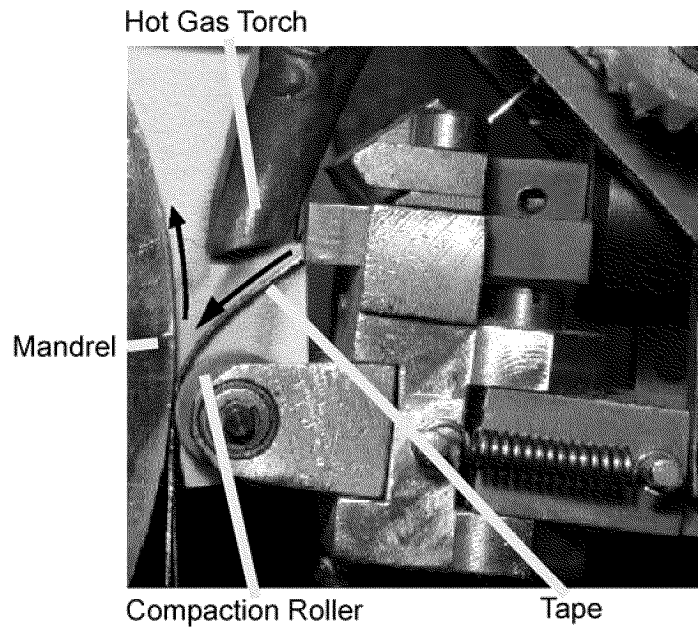


Figure 4.14: View from the infrared camera

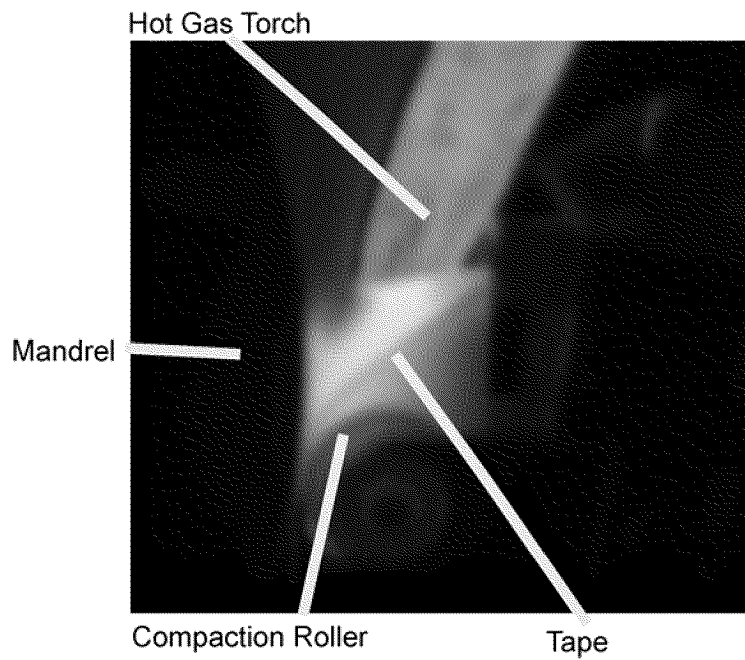


Figure 4.15: Example of an infrared picture

Figure 4.14 shows the setup as it is viewed from the infrared camera location. In this setup, an iron band replaces the incoming thermoplastic tape on each side of the low conductivity sheet, to avoid matrix degradation effects. The roller is also divided in two equal parts. In this configuration, the rollers and the iron tapes act as a holder for the sheet. The latter is also fixed on the mandrel and is lightly stretched to prevent any displacements.

4.4.2. Measurement and evaluation method

Once the setup is mounted, the hot gas torch is turned on. After an equilibration time, infrared pictures are recorded. Different temperature scales were used for each combination of parameters, to capture precisely the high temperature gradients.

Figure 4.15 shows an example of an infrared picture. Since the temperature scales are chosen to determine the temperature field of the hot gas flow in the nip region, only few other elements can be seen on the picture. The incoming tape, the compaction roller, the mandrel, the hot gas torch and the isolation sheet can be recognized, because they are continuously heated by the hot gas flow.

The gray-scale format is chosen to facilitate the determination of the temperature field on the isolation sheet. For each pixel, the gray level corresponds to a defined temperature. The dimensions of the pixels are estimated with the dimension of the elements that are seen on the infrared picture.

The temperature and geometric information are then compiled to piece together the temperature field. Along the incoming tape and along the substrate, the temperature outside the boundary layers is then directly read from the above process.

In order to calculate the convective heat transfer coefficient, the temperature variation along the normal direction to the heated surface is determined. Figure 4.16 shows a sketch to support the explanation of the method used. The squares represent the pixels of an infrared picture. The black areas correspond to surface elements. The white elements belong to the area heated by the hot gas. The gray line is the slope of the surface, and the one with an arrow represents the normal to it. This latter line goes through the center of the first white pixel away from the element surface. Its origin "O" is at the intersection between the white and black region. It is divided in segments. They correspond to the intersections between the pixels and the normal. The middle of each segment is denoted with

a “S”. There are 18 such locations in the present example. The last one (S_{18}) is the top of the perpendicular line.

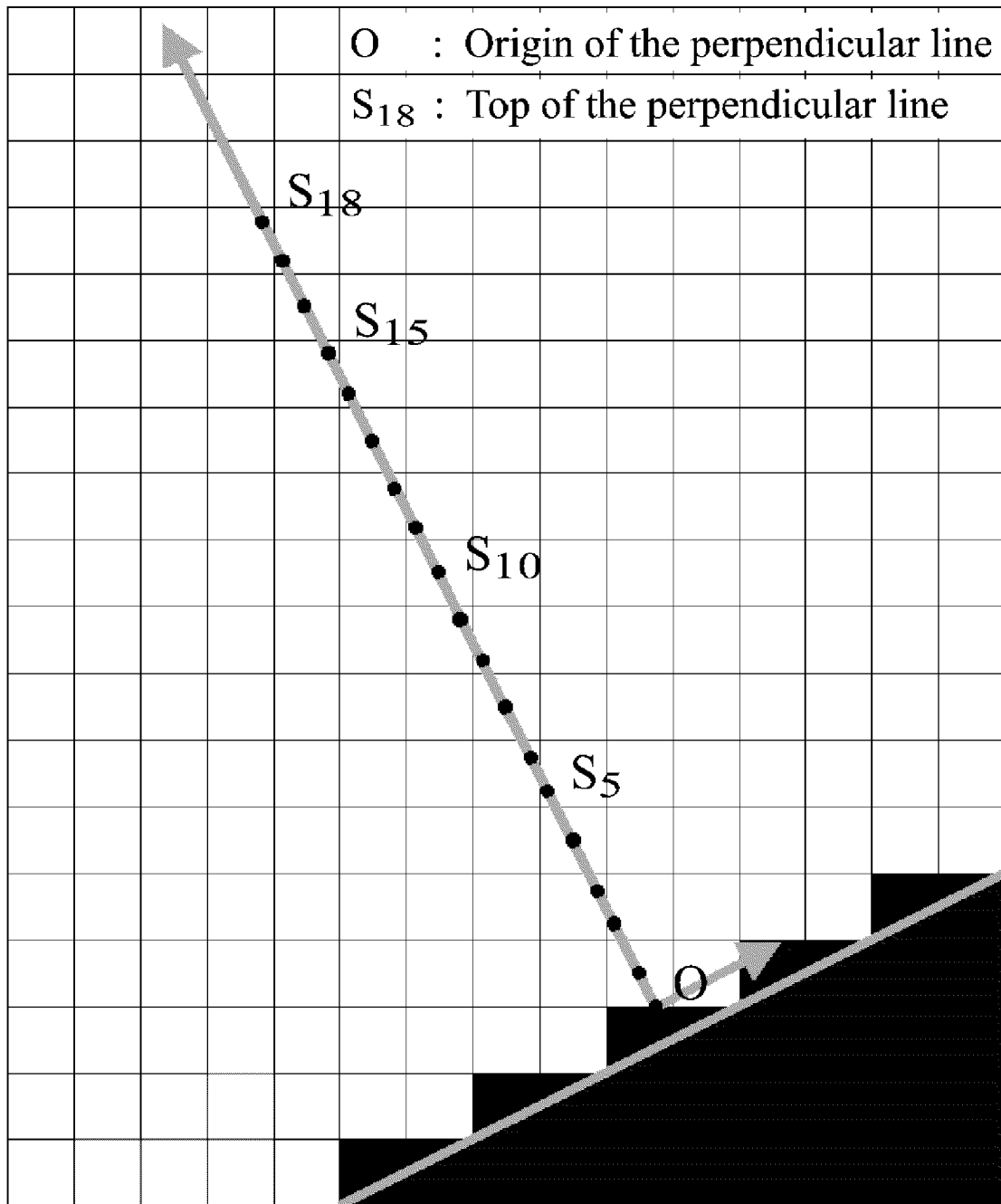


Figure 4.16: Principle of the determination of the temperature variation through a boundary layer

The temperature at each location S is reported on a diagram. Figure 4.17 shows an example of the temperature variation through such a boundary layer. The distances between the point on the abscissa are not constant, because the lengths of the segments are not constant.

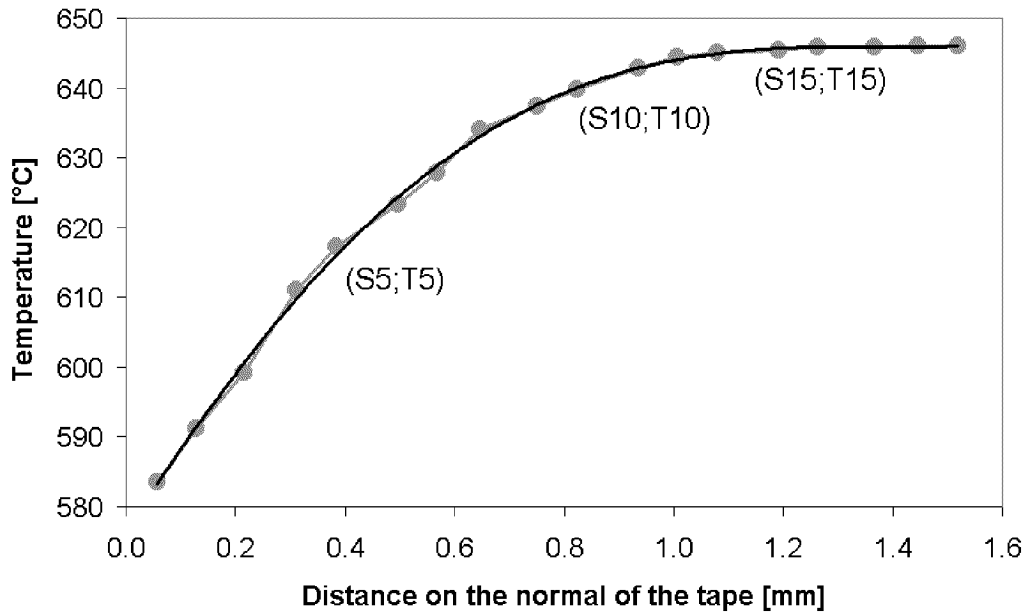


Figure 4.17: Temperature through a boundary layer created by the hot gas torch

The convective heat transfer coefficient is calculated with the temperature curve through the boundary layer, Equation 4.16 and the thermal conductivity of the hot gas. Appendix A describes the well-known development that leads to Equation 4.16.

$$\alpha_{HG} = \frac{-K}{(T_{HG} - T_S)} \left(\frac{\partial T}{\partial y} \right)_{y=0} \quad (4.16)$$

As shown in Figure 4.17, the temperature distribution in the vicinity of the tape can be assumed to be linear. Therefore Equation 4.16 can be approximated as follow :

$$\alpha_{HG} = \frac{-K}{(T_{\max} - T_{S_1})} \left(\frac{T_{S_2} - T_{S_1}}{S_2 - S_1} \right) \quad (4.17)$$

The previous method is repeated for each pixel along the incoming tape and the substrate.

4.4.3. Results

Figure 4.18 and Figure 4.19 show the temperature outside the boundary layers.

To limit the noise due to the approximation made with the pixels in the evaluation of the convective coefficient, the average of 10 coefficients is calculated. Figure 4.20 and Figure 4.21 display the convective coefficient on the incoming tape and on the substrate.

The values on the ordinates of Figure 4.18 and Figure 4.20 and those on the ordinates of Figure 4.19 and Figure 4.21 correspond to the same parts of the boundary layers.

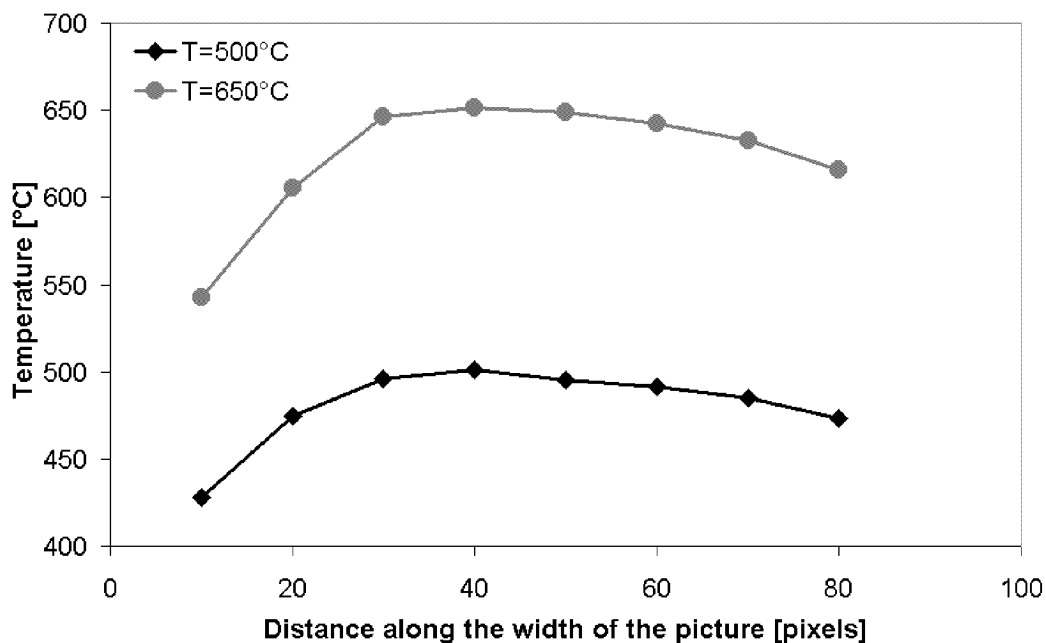


Figure 4.18: Temperature outside the boundary layer between the incoming tape and the hot nitrogen flow

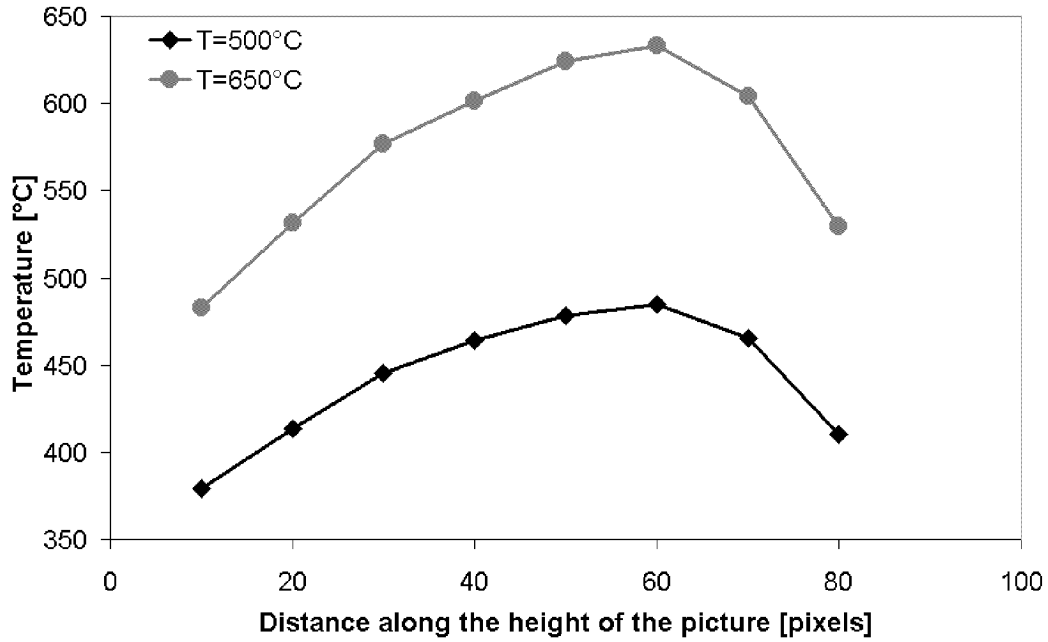


Figure 4.19: Temperature outside the boundary layer between the substrate and the hot nitrogen flow

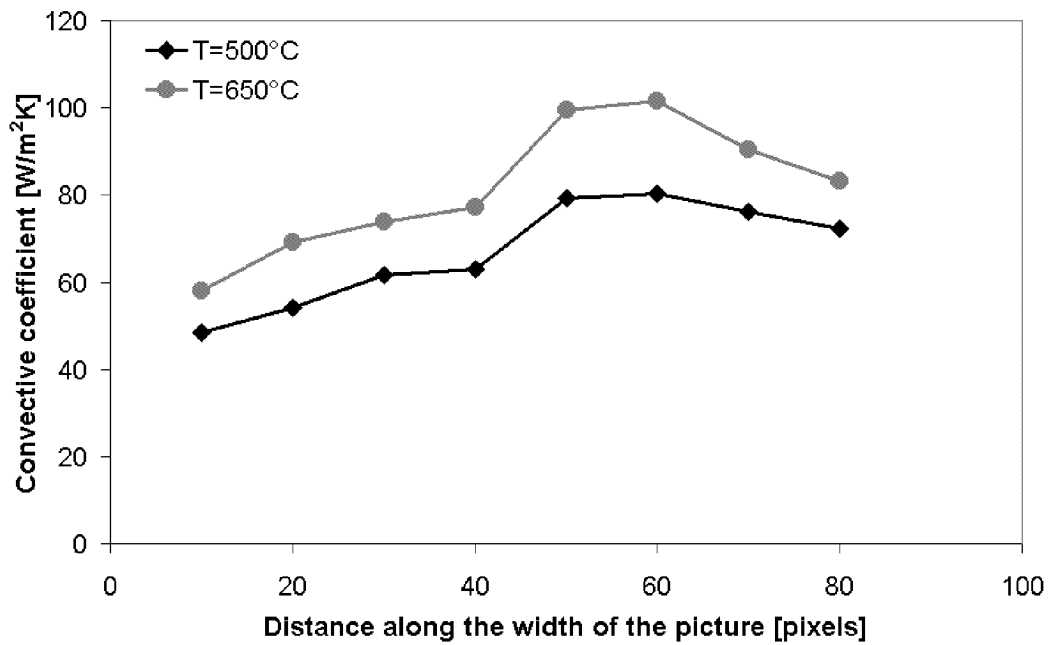


Figure 4.20: Convective coefficient between the incoming tape and the hot nitrogen flow

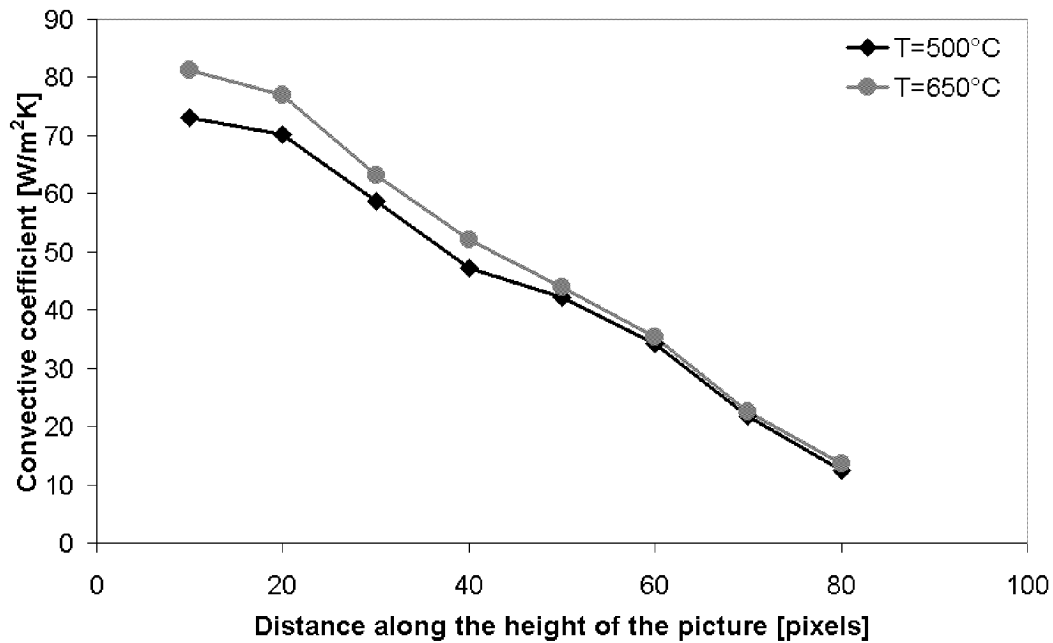


Figure 4.21: Convective coefficient between the substrate and the hot nitrogen flow

In Figure 4.18, the location between 0 and 10 are upstream of the hot gas torch, and the nitrogen temperature is lower than that at the hot gas torch outlet. In the rest of the locations, the nitrogen temperature is approximately equal to the temperature at the outlet of the torch. The location of their measurements is in the main flow direction.

The locations between 0 and 20 in Figure 4.20 are upstream of the torch. On this part, the convective coefficients increase slowly. The presence of convective coefficients means that there is a part of the nitrogen that flows in the opposite direction to the nip (back flow). Elements of the setup prevent further measurements in that direction (Figure 4.14).

The locations between 30 and 75 in Figure 4.20 are directly under the hot gas and the torch. The middle of the flow has the highest convective coefficient. It is assumed that the different flow conditions between its center and its border cause this difference. The flow profiles inside a tube are not constant. They show generally a maximum in their center. Therefore the nitrogen speed is higher under the center of the hot gas torch than under its borders.

As the surface of the incoming tape is not perpendicular to the nitrogen flow, the lateral position of the origin and the top of the perpendicular line serving to the determination of a local convective coefficient are not the same (Figure 4.16).

As a consequence, the maximum of the curves of Figure 4.18 and Figure 4.20 are not on the same perpendicular of the incoming tape.

Measurements are not possible over the location 80 in Figure 4.18 and Figure 4.20. This can be explained by vortexes that are due to the closed nip region. They stop the hot nitrogen flowing up in the nip and therefore the convection.

The presence of a convective heat transfer on the substrate could confirm the existence of vortexes that deviate the nitrogen flow. Figure 4.21 shows the convective coefficients. Their maximum values are the closest to the nip. They are approximately equal to the last one before the vortexes on the incoming tape. The convective coefficient decreases approximately linearly with the distance to the nip.

Figure 4.19 shows that the temperature increases and decreases relatively fast. It rises, because the location of the maximum temperature on the perpendicular to the substrate surface becomes closer to the torch outlet. It diminishes when it moves away.

4.5. Experiments for the validation of the simulation

4.5.1. Setup

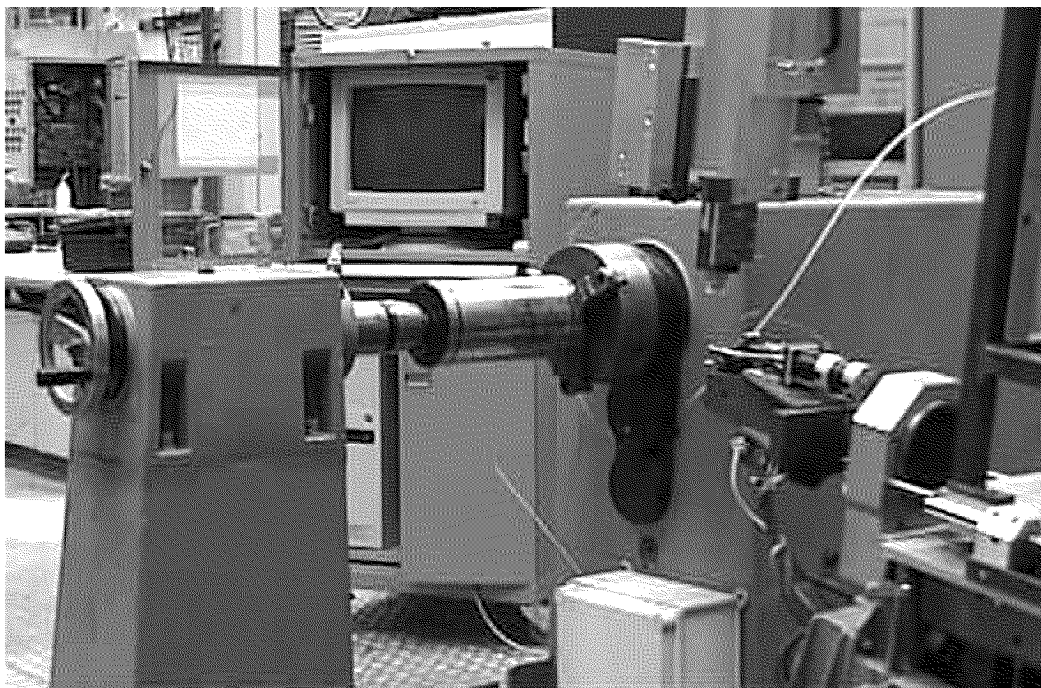


Figure 4.22: Tape winding setup at the ETH

The setup for the experimental validation is shown in Figure 4.22. It consists of a Baer WSE-II winding machine with a Baer TCS-84 control system and an ADC compaction assembly.

A program controls the winding process (it determines the constant processing speed and the winding paths). The process is continuous and uses a small winding angle (hoop winding). Equation 4.18 gives the geometrical relation that defines the winding angle:

$$\gamma = \pm \arctan \frac{2\pi R_{m_o}}{w} \quad (4.18)$$

The plus minus sign in Equation 4.18 denotes that the winding angle changes alternately between the even and uneven layers.

The ADC control cabinet fixes the parameters of the hot gas torch that is the nitrogen flow and the temperature at the outlet of the hot gas torch.

A pressure regulator (Festo MPPE-3-010B) and two pyrometers (Heimann KT19.82 and KT15.82) are connected to a PC that runs Labview to visualize and store the pressure and temperature data during the experiments. The pressure regulator serves to set the pressure of the compaction roller.

Figure 4.1 shows the location of the pyrometer spots. Both pyrometers move laterally with the compaction assembly. The nip point pyrometer measures the temperature of the incoming tape just before the nip line. This is to avoid measurement errors resulting from mixed values between the substrate temperature, the nip temperature and the incoming tape temperature. The knowledge of the incoming tape temperature just before the nip line is essential, because the phenomena at the nip line are directly dependent on this temperature. It enables to control the validity of the heat input upstream from the nip line.

In comparison to the nip point location, the substrate pyrometer is shifted 12.5 mm along the axial direction of the mandrel to avoid any mixed measurements between the layer that was previously laid and the current one. The substrate pyrometer enables to determine the variation of the substrate temperature during the process in an area without high temperature gradients, because such gradients twist the measurements and introduce uncertainty. It enables to verify the influence of the time on the process.

4.5.2. Experiments

SET	T	P	v	γ
--	°C	N	m/s	°
1	500	276	0.1	89.3
2	650	276	0.1	89.3

Table 4.3: Experimental parameters

All processing parameters are chosen according to prior experimental studies ^[90]. The research is focusing on the influence of the processing parameters on the laminate quality of the final part. Two sets of parameters have been selected considering parts with low and high interlaminar shear strength values. Both sets of parameters (see Table 4.3) use the same winding speed and winding angle. To avoid long computation time, the length of the cylinders is reduced in comparison to the experimental study. It is however long enough to obtain a stabilized temperature with the nip point pyrometer.

4.5.3. Results

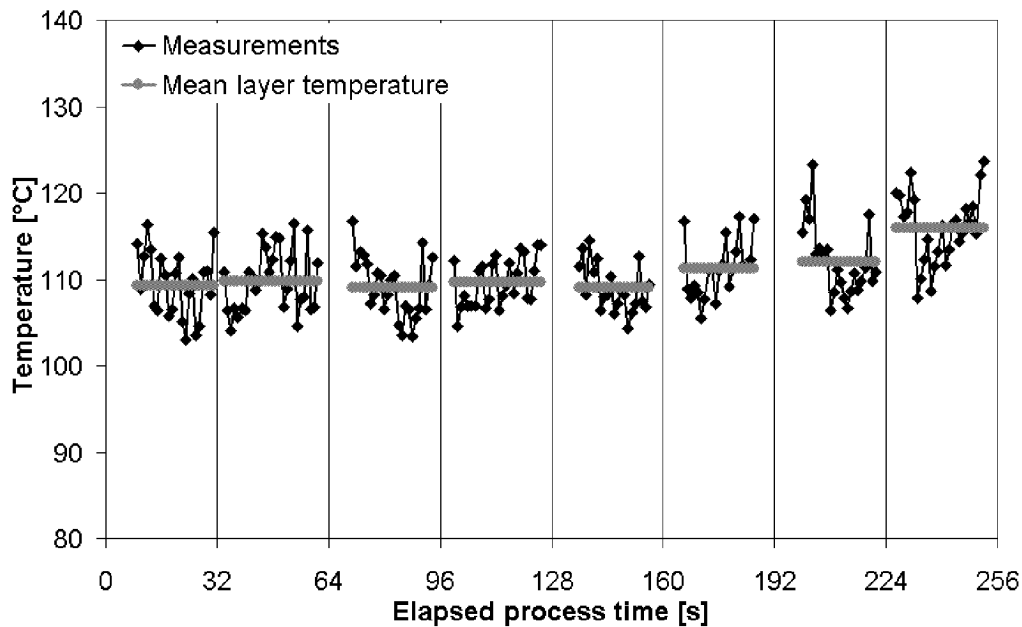


Figure 4.23: Experimental measurements of the nip point pyrometer with the first set of parameters

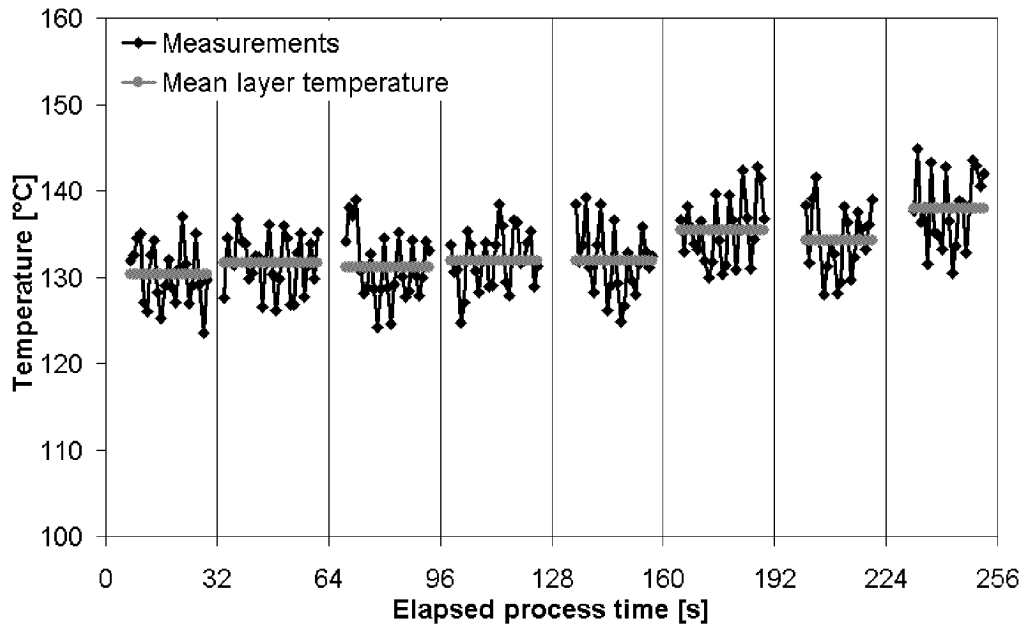


Figure 4.24: Experimental measurements of the nip point pyrometer with the second set of parameters

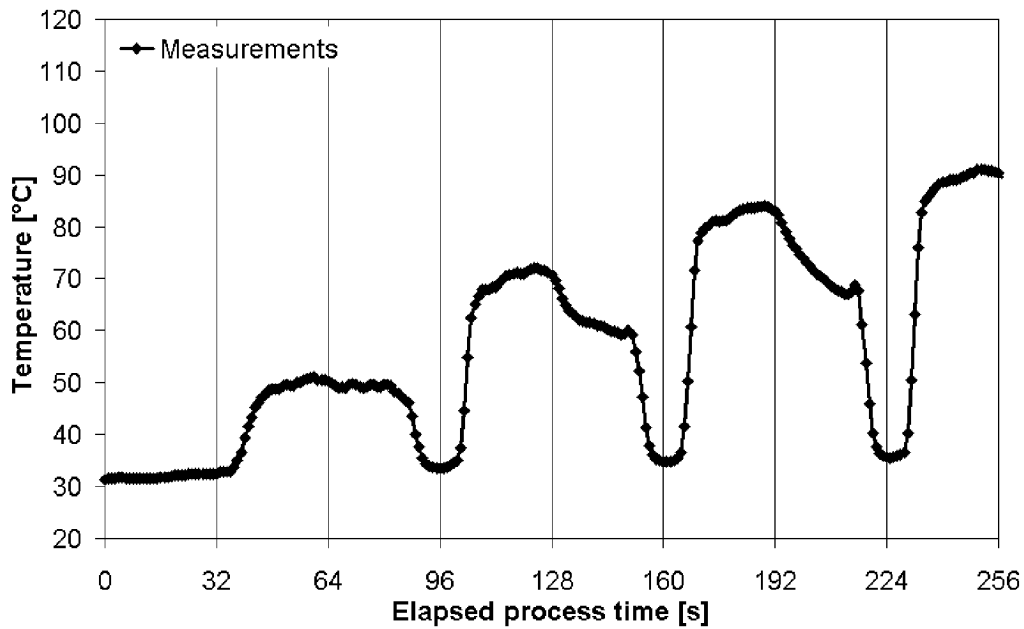


Figure 4.25: Experimental measurements of the substrate pyrometer with the first set of parameters

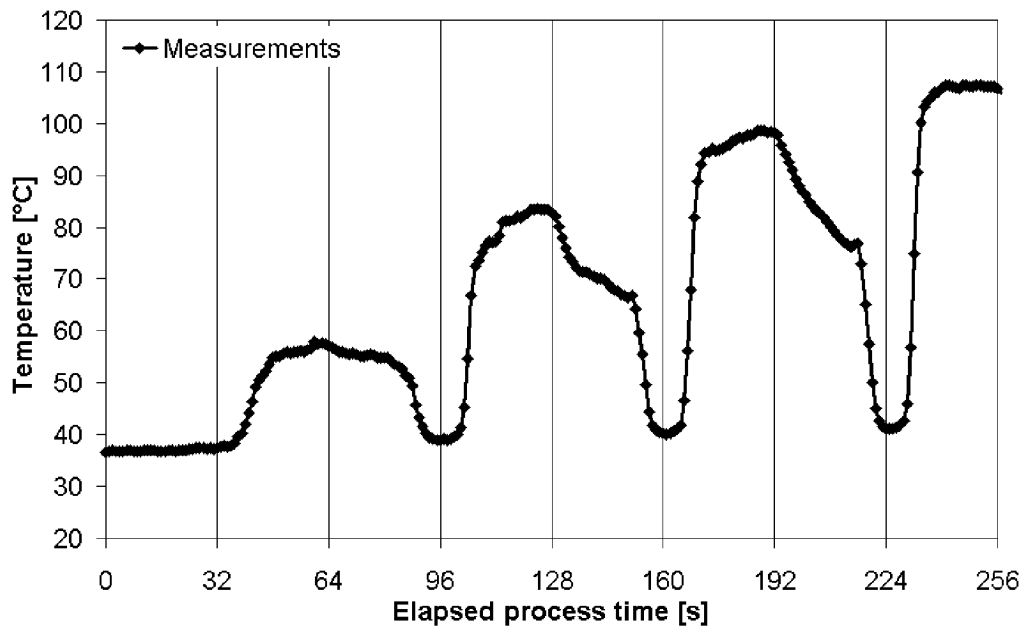


Figure 4.26: Experimental measurements of the substrate pyrometer with the second set of parameters

Figure 4.23 and Figure 4.24 show the temperatures measured by the nip point pyrometer for the two sets of parameters. The eight suites of temperature correspond to the measurements for the eight layers. The duration of the lay down of a layer was 32 s. The diagram does not exhibit the temperatures at the beginning and the end of the layers, because the measurements are meaningless. The temperature variation is due to the vibrations that are transmitted from the setup to the pyrometer holder. They change the physical location of the pyrometer spot on the incoming tape, and thus the temperature that is measured by the pyrometer. With the exception of two values, all the measurements of a suite are however inside $\pm 7\%$ of the mean value of the temperature of a layer. As expected, the mean temperature of the incoming tape remains almost constant during the winding process. The small mean temperature increase is probably due to the temperature increase of the elements that are heated during the whole process by the hot gas flow and are in contact with the incoming tape.

Figure 4.25 and Figure 4.26 display the measurements of the substrate pyrometer. In contrast to the measurements shown in Figure 4.23 and Figure 4.24, the vibrations of the pyrometer holder have no visible influence on the temperature, because the spot is focused on very low temperature gradient areas.

Due to the shifted location of the spot in comparison to the nip point, the measurements of the uneven layer are made on the one that was previously laid, and those of the even layer on the one that is currently laid. This explains the different trends between the even and uneven layer measurements. There is a very low increase on the even layer, and a strong temperature decrease on the uneven layer from the fifth layer. The temperature increases are low, because the elapsed time between the heating and the measurement is constant on the even layer. The decreases become visible when the substrate temperature is high and the heat losses through convection and radiation with the surrounding air influence sufficiently the substrate temperature.

From the third layer, strong decreases and increases can be recognized between the end of the uneven layer and the beginning of the even one. This is due to the shifted position of the pyrometer that measures cold areas at the end of each uneven lay-down step.

The comparison of the measurements of the even layers shows the general trend of the temperature of the substrate. It rises with the number of the laid layers. This increase is however not linear, but decreases with the number of layers. This phenomenon is a consequence of the increase of the heat losses through convection with the surrounding air when the substrate temperature rises.

4.6. Comparison between experiments and simulations

To discuss the validity of the numerical model, two runs were performed to simulate the experiments presented above. The parameters for the boundary conditions are listed in Table 4.4 and Table 4.5. The convective coefficient between the environment and the substrate, the guiding and roller temperatures have been experimentally determined (Figure 4.3).

T_G	T_R	α_E
$^{\circ}\text{C}$	$^{\circ}\text{C}$	$\text{W}/(\text{m}^2\text{K})$
135	233	21

Table 4.4: First set of simulation parameters

T_G	T_R	α_E
$^{\circ}\text{C}$	$^{\circ}\text{C}$	$\text{W}/(\text{m}^2\text{K})$
162	262	21

Table 4.5: Second set of simulation parameters

Figure 4.27 and Figure 4.28 display the temperatures measured with the nip point pyrometer and the results of the simulation. The latter are the mean temperature of the nodes that are included in the ellipse that corresponds to the pyrometer spot in the model. The maximum error is 7.6 %. The curves show that the error decreases with the number of layers. The reason is that the temperature of the guiding element (T_G) is chosen constant during the simulation, and that its value is not determined considering transient effects. Agreement between experiments and simulations is good, thus confirming the validity of the model and of the assumptions. In particular, we deduce that the influence of melting and crystallization energy can be neglected.

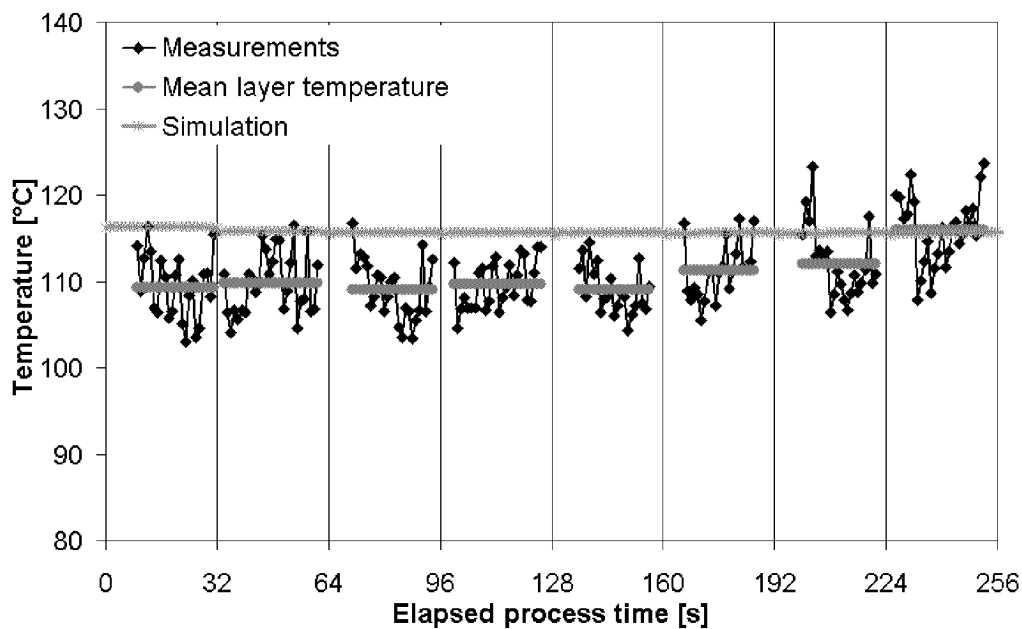


Figure 4.27: Validation with the measurements of the nip point pyrometer with the first set of parameters

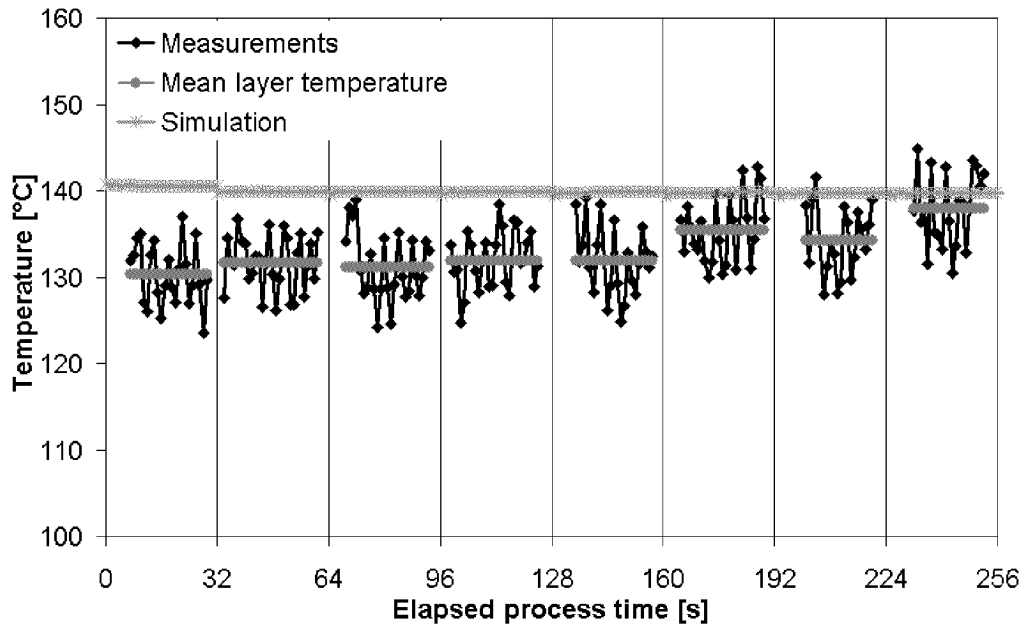


Figure 4.28: Validation with the measurements of the nip point pyrometer with the second set of parameters

Figure 4.29 and Figure 4.30 show the comparison of the simulation results with the measurements of the substrate pyrometer. The peaks at the times 64, 128 and 193 s in the simulated temperature curves have no physical reason. They result from the way the winding process has been modeled to simulate the transition between two layers : the termination and the restart of each layer takes place on the same location. This causes locally two successive heatings in a much shorter time than in reality.

Around the times 32, 96, 160 and 224 s, the substrate pyrometer spot is measuring the cold area beside the substrate which is not considered by the numerical analysis.

The comparison of the experiments with the simulations in the region covered by the substrate pyrometer shows again that they are in agreement with each other. Not considering the inaccuracy in conjunction with the inversion of the compaction assembly moving speed parallel to the mandrel, the difference between measured and simulated temperature is below 10%.

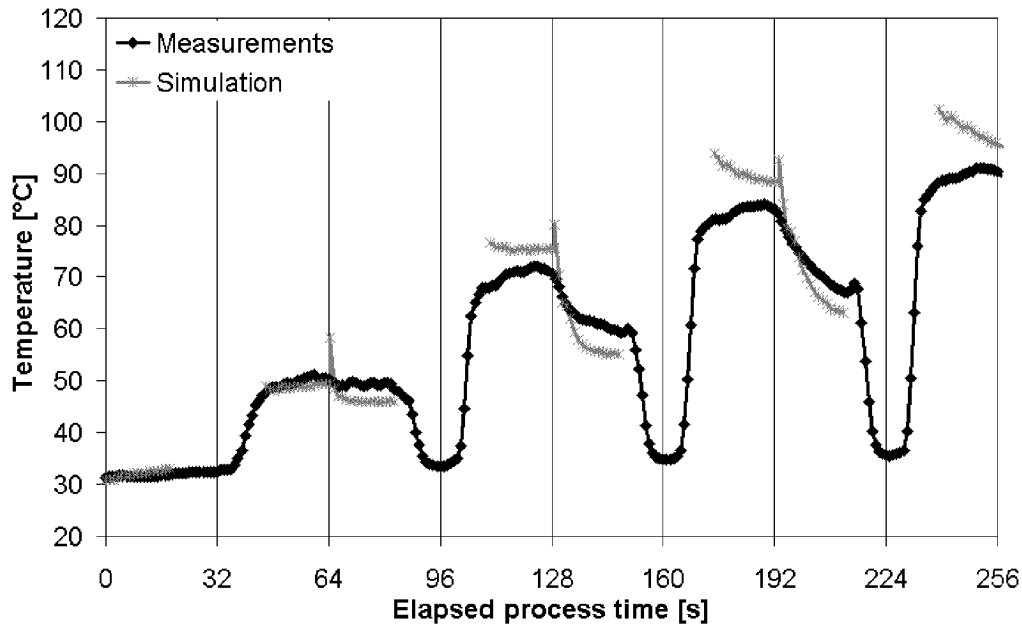


Figure 4.29: Validation with the measurements of the substrate pyrometer with the first set of parameters

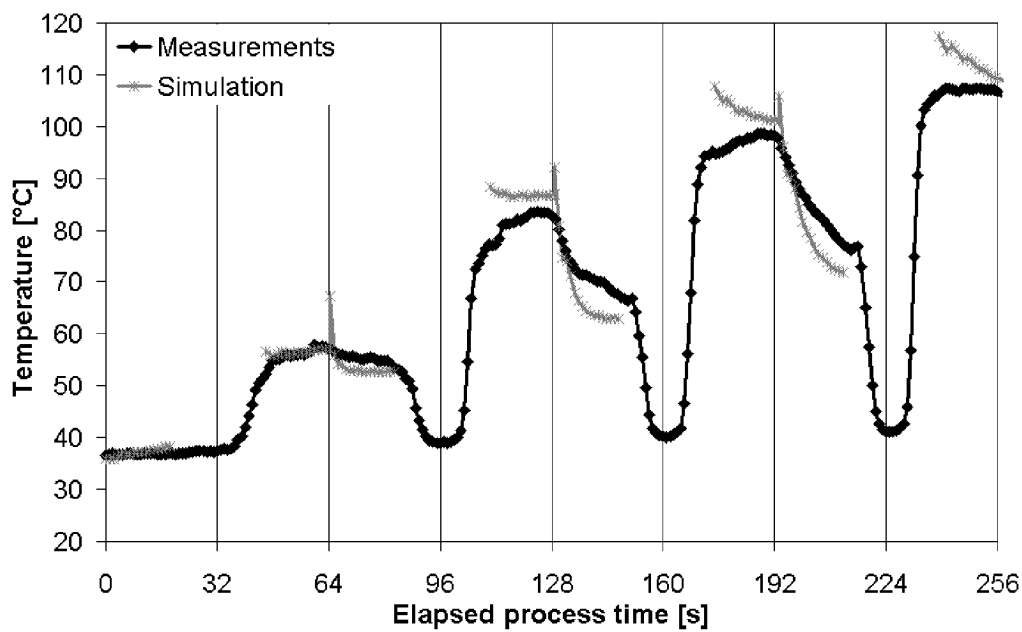


Figure 4.30: Validation with the measurements of the substrate pyrometer with the second set of parameters

4.7. Conclusion and outlook

This study presents a numerical model to simulate the fiber reinforced thermoplastic tape winding process. Unlike models used in other researches, it considers transient three-dimensional effects. In order to provide accurate input values for the model, a method to evaluate the heat flow parameters of the hot gas torch (i.e. the outside flow temperature and the convective heat transfer coefficient) is also developed. Concurrently to the numerical simulations, a comprehensive experimental program is carried out to provide the data that serve to validate the numerical simulations. The comparison of experimental measurements and simulation predictions shows good agreements for the two sets of parameters. As a next step, the developed model will be used in conjunction with an adequate polymer chain diffusion model to predict the quality of the bond strength with regard to different process parameters.

4.8. Nomenclature

α	convective heat transfer coefficient
ϵ_0	constant of Stefan-Boltzmann ($5.67 \cdot 10^{-8} \text{ W/m}^2\text{K}^4$)
γ	winding angle
φ	circumferential coordinate
ρ	density
ν	cinematic viscosity
A	cross-section
C	specific heat
d	diameter
H	enthalpy
K	thermal conductivity
l	length
P	pressure
q	heat transfer through a unit surface
Q	heat transfer through a surface
r	radial coordinate
R	radius
Re	Reynolds number
S	location on the perpendicular to the surfaces for the measurement of the heat transfer due to convection
t	time
T	temperature

v	winding speed
v	flow velocity
V	volume
w	expected width of the incoming tape after compaction
x, y	Cartesian coordinates
z	axial coordinate

Subscript

φ	circumferential coordinate
c	cold
cr	crystallization
E	environment
G	guiding element
h	hot
HG	hot gas
i	initial
m	mandrel
me	melting
max	maximum
o	outside
r	radial coordinate
R	roller
RT	room temperature
S	surface
t	tape
T	tube
x, y	Cartesian coordinates
z	axial coordinate
1	in the fiber direction
2, 3	perpendicular to the fiber direction

CHAPTER 5

Heating Strategies for the Automated Tape Winding (ATW) Process

5.1. Introduction

The automated tape winding and the automated tape placement processes are promising techniques for manufacturing fiber reinforced thermoplastic structures. Intrinsic advantages of those processes are the high reproducibility of the manufactured parts, the reduced labor work and the enhanced safety for the personal. Furthermore they provide high flexibility during manufacturing, because the composite material can be bound on-line, post-processed and/or reprocessed. The thickness of the final product is not limited, because the on-line consolidation prevents the introduction of large process-induced stresses.

In the past, various researches have studied the influence of process parameters on the phenomena that occur during those processes. Grove^[34] models the automated tape placement process. He studies the dependence of the temperature history and temperature at some locations on the process speed, the laser intensity, the angle of incidence, the laser beam and the surface reflectance of the composite material. Mantel et al.^[55] investigate the influence of the applied compaction pressure during the tape laying process. They determine the degree of bond strength for experiments and simulations. Mantel et al.^[57] describe the automated tape placement process with a thermal two-dimensional model including the development of the degree of intimate contact. They compare various simulation and experimental results. They study the influence of process speed, applied compaction force, temperature of the nitrogen and number

passes. Ghasemi Nejjhad ^[30] analyzes the thermal phenomena during the automated tape placement and the automated tape winding processes. He investigates the influence of the processing speed, heat flux, heater width, compaction roller temperature, substrate preheating and incoming tape preheating. He shows that the processing windows are closed windows bounded by insufficient melting at the bottom, degradation limitations at the top, minimum practical processing speed at the left and converging point of the upper and lower bounds as the maximum viable processing speed at the right of the window. Don et al. ^[23] study the automated tape placement process. They take into account the degradation of the thermoplastic matrix, the void consolidation, the development of intimate contact and polymer chain diffusion. They vary the process speed, the heating settings and the compaction forces to investigate their influence on the above-mentioned phenomena. Irwin and Güçeri ^[40] simulate the thermal phenomena occurring during the automated tape winding process with a laser heating. They study the effect of laser power, process speed, laser beam's width and beam offset. They use the temperature to determine processing windows. The lower and upper limits are the melting and the degradation temperatures of the thermoplastic matrix. James and Black ^[41] determine process windows for the fiber reinforced thermoplastic filament winding process. They use two-dimensional steady-state simulations. The lower and upper limits are the degree of polymer chain diffusion and the degradation of the thermoplastic matrix. They investigate the influence of the process speed and heat intensity. Pitchumani et al. ^[67] investigate the automated tape placement process considering various phenomena: thermal, polymer degradation, intimate contact, polymer chain diffusion and void consolidation. They show the influence of the number of plies, compaction forces and process speed on those different phenomena. Pitchumani et al. ^[68] study the automated tape placement process considering a void consolidation model and a void growth model. They examine the effect of heating temperature, compaction forces and process speed on the final void content and tow thickness. They demonstrate that the void growth contributes significantly to the final void content and that an estimation of the void content accounting for the consolidation process alone will lead to considerably lower estimate the composite void fraction. Pitchumani et al. ^[69] perform analyses of the automated tape placement process. They carry out parametric studies to investigate the effects of the process speed, compaction force, torch temperatures and placement head configuration on the consolidation process. Pitchumani et al. ^[70] present a methodology for determining process windows and optimum operating conditions for the automated tape placement process. They use various models (heat transfer, degree of bond strength, degree of compaction, degradation kinetics, void growth and consolidation) and constraints (degradation, void content and dimensional changes). Somnez and Hahn ^[80] model the heat transfer and the crystallization kinetics during the automated tape placement process. They investigate the effect of roller velocity,

preheating, heated length and heated length ratio. Somnez and Hahn ^[81] simulate the automated tape placement process. They analyze the effect of the preheating temperature, heated length, roller radius and heated length ratio (ratio of the heated area on the substrate to that on the tape) on process windows and/or the optimization of the process speed considering different constraints (e.g. the degree of bond strength).

So far, transient models have not been used to simulate the thermal phenomena during those manufacturing processes. Considering the good agreements between the simulation and experimental results (Chapter 4), the main objective of this chapter is to discuss different heating strategies with respect to the achievable laminate quality. A model evaluating the degree of polymer chain diffusion is added to the thermal simulation program that is presented in Chapter 4. The use of those models enables also to answer the question whether or not the polymer chain diffusion is a cause of the difference between the interlaminar shear strength of the best tape wound specimens and that of the post-processed specimens.

5.2. Process

Figure 5.1 shows a schematic illustration of the automated tape winding process considered in this study. During the process, the spool supplies the composite material. The latter is warmed up in the tow guide, by the hot gas and by the compaction roller. The incoming tape is compacted with the compaction roller at the nip. The deposited and consolidated material composes the substrate. Its quantity increases as the process is going on. The process is terminated, when the desired quantity of composite material is laid on the planned locations.

An ADC control cabinet fixes the parameters of the hot gas torch, i.e. the nitrogen flow and the temperature at the outlet of the hot gas torch. A pressure regulator and two pyrometers are connected to a PC that runs Labview to visualize and store the pressure and temperature data during the experiments. The pressure regulator serves to set the pressure of the compaction roller.

Figure 5.1 shows the location of the pyrometer spots. Both pyrometers move laterally together with the compaction assembly. The nip point pyrometer measures the temperature of the incoming tape just before the nip line. It enables to control the validity of the heat input upstream from the nip line. In comparison to the nip point location, the substrate pyrometer is shifted 12.5 mm along the axial direction of the mandrel to avoid any mixed

measurements between the layer that was previously laid and the current one. It enables to verify the influence of the elapsed time on the process.

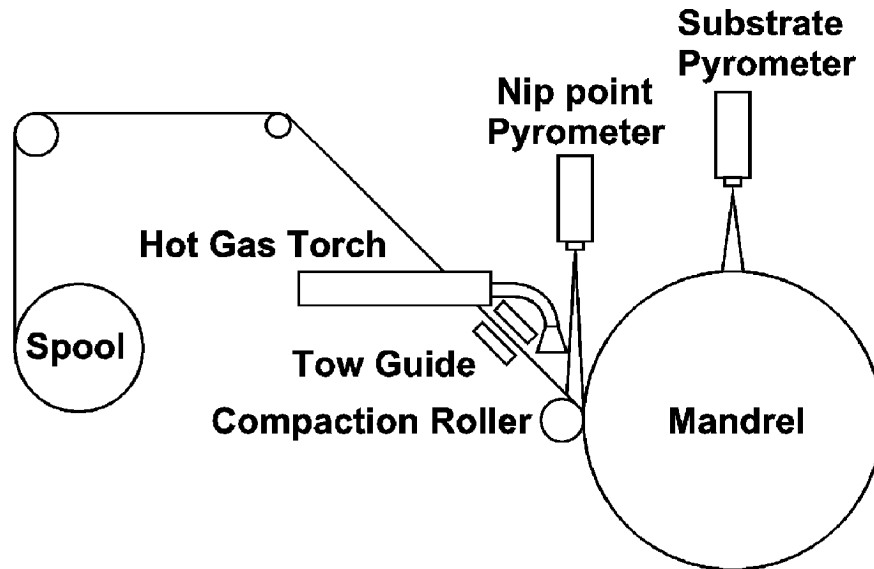


Figure 5.1: Sketch of the automated tape-winding setup at the ETH

5.3. Theory

5.3.1. Heat transfer

The current investigations employ the transient thermal model developed in Chapter 4. Figure 5.2 reviews the heat transfers in the nip region. In the composite material, it is described by the heat diffusion equation for anisotropic materials. There are two convective heat transfers (dq_E/dt and dq_{HG}/dt) and two contact boundary conditions (T_G and T_R).

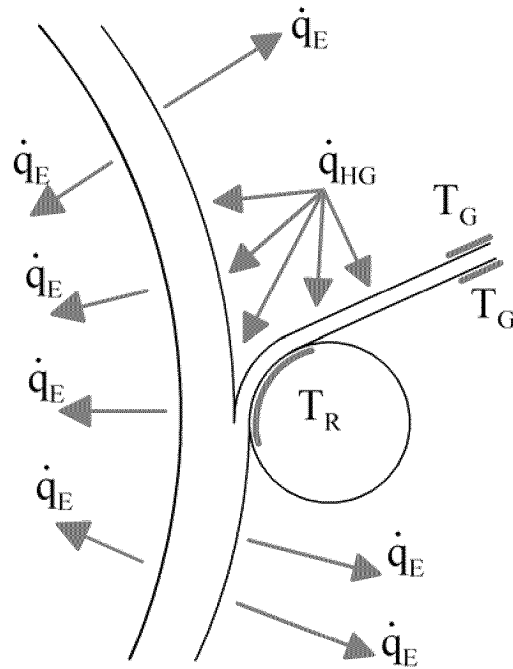


Figure 5.2: Location of the boundary conditions

5.3.2. Degree of polymer chain diffusion

The degree of polymer chain diffusion describes the ratio between the current interlaminar shear strength and the maximum reachable interlaminar shear strength (Equations 5.1 and 5.2). The model origin, the determination of its parameter and the numerical integration are described in Appendix B.

$$D_{pcd} = \frac{\sigma(t)}{\sigma_{\infty}} = 0.9 \left(\frac{t}{t_{mech}} \right)^{1/4} \quad (5.1)$$

where

$$t_{mech}(T) = C \exp\left(\frac{T_A}{T - T_V}\right) \quad (5.2)$$

where $C=8.9574 \cdot 10^{-3}$ s, $T_A=836$ K and $T_V=282$ K

5.4. Model

A program simulates the thermal phenomena and the development of the degree of polymer chain diffusion. Each numerical simulation is based on an explicit time integration scheme and covers the duration of the process.

Figure 5.3 to Figure 5.6 show examples of the mesh adaptations that model the progress of the automated tape winding process.

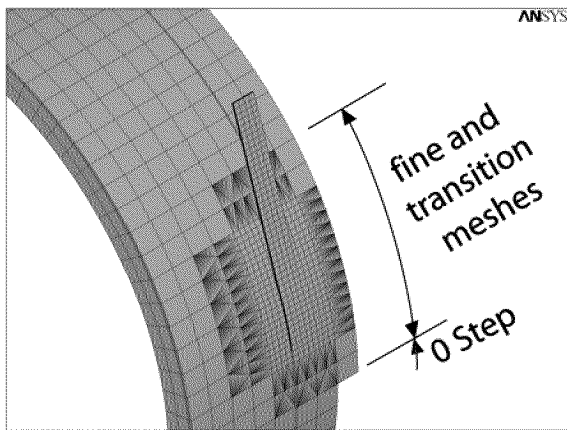


Figure 5.3: mesh at t_1

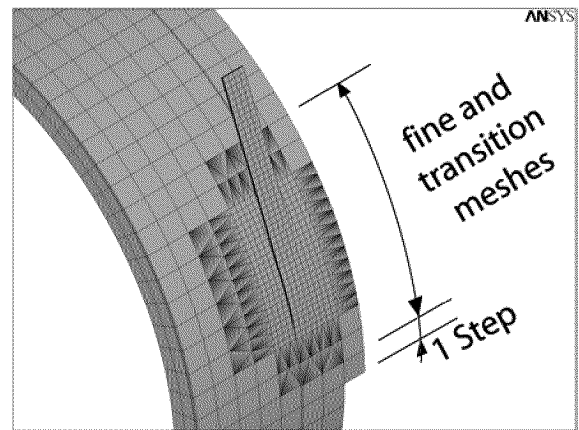


Figure 5.4: mesh at $t_2=t_1+\Delta t$

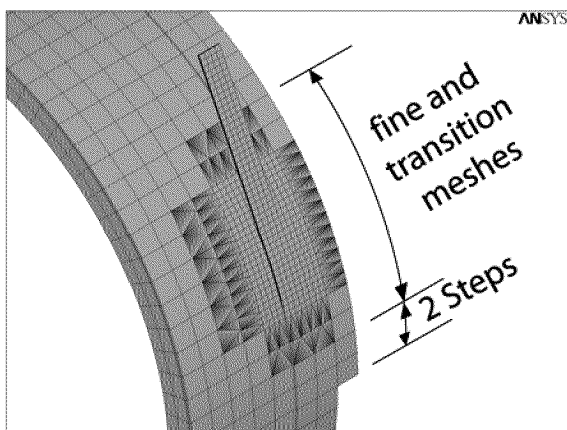


Figure 5.5: mesh at $t_3=t_2+\Delta t$

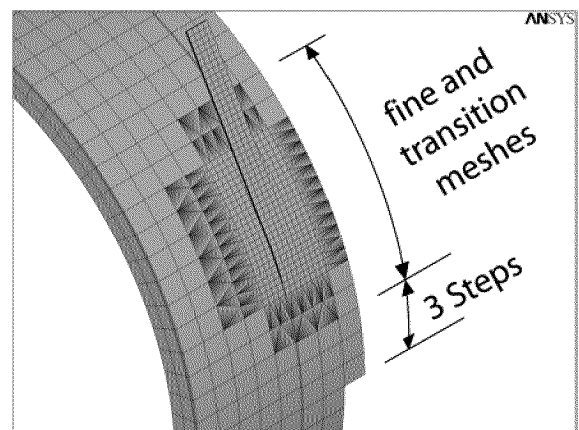


Figure 5.6: mesh at $t_4=t_3+\Delta t$

The simulation within each time step begins with the determination of the temperature at each node. The latter is performed with a thermal steady-state model. The calculation of the progress of the degree of polymer chain diffusion ends the simulation of each step. It is carried out for the nodes that correspond to the interlaminar surfaces.

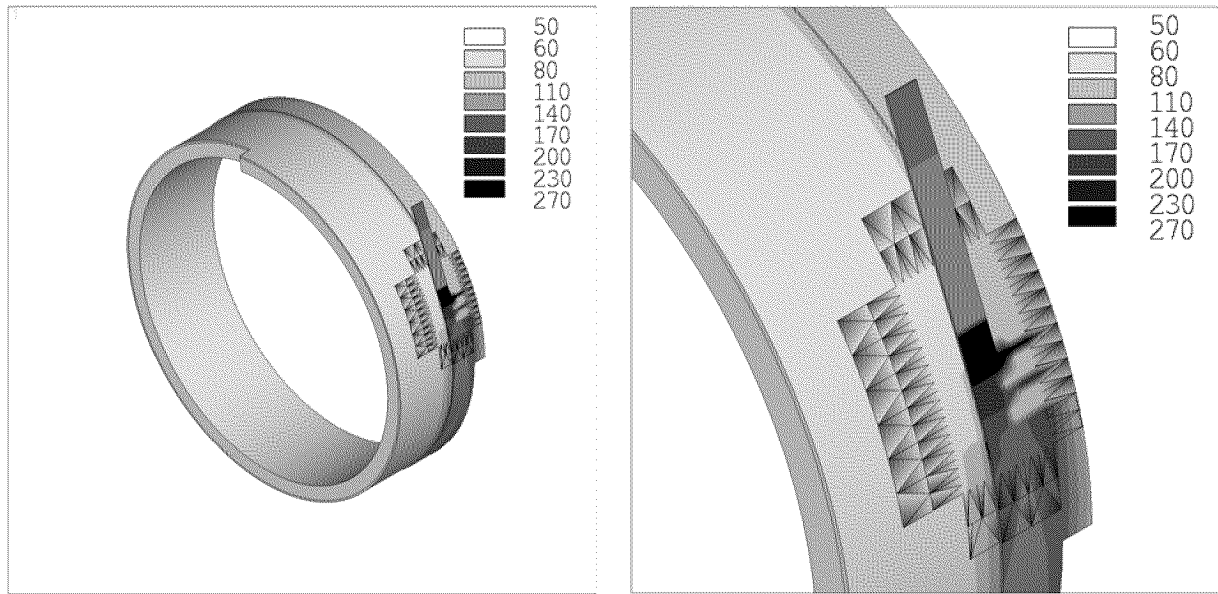


Figure 5.7: Views of a temperature plot of a result for a time's step

A temperature plot example is shown in Figure 5.7. The black lines define some of the element borders. The black area corresponds to the contact area between the composite material and the compaction roller. The latter touches the composite at three locations: the incoming tape, the compaction area and the substrate on the side of the nip line. The last location is a line, because it is assumed that the composite material is only compacted in the nip region. The reason of the dark narrow region behind this line is that the heat does not have sufficient time to diffuse into the composite material.

5.5. Validation

In order to validate the model, the degree of polymer chain diffusion is compared to the degree of bond strength (Equation 5.3) for the two sets of process parameters used in Chapter 4. According to the experimental studies presented in Chapter 3, both sets have been selected considering parts with low and high interlaminar shear strengths.

$$D_b = \frac{ILSS_{tape\ winding}}{ILSS_{autoclave}} \quad (5.3)$$

Table 5.1 resumes the process parameters and the parameters of the boundary conditions. Symbols are explained in section 5.8. The initial temperature of the mandrel and composite material (spool) is the room temperature. To avoid long computation time, the length of the cylinders in the simulation is reduced in comparison to the experiments.

SET	T_{N_2}	P	v	γ	T_G	T_R	α_{HG}	α_E
--	°C	N	m/s	°	°C	°C	W/(m ² K)	W/(m ² K)
1	500	276	0.1	89.3	135	233	69	21
2	650	276	0.1	89.3	162	262	86	21

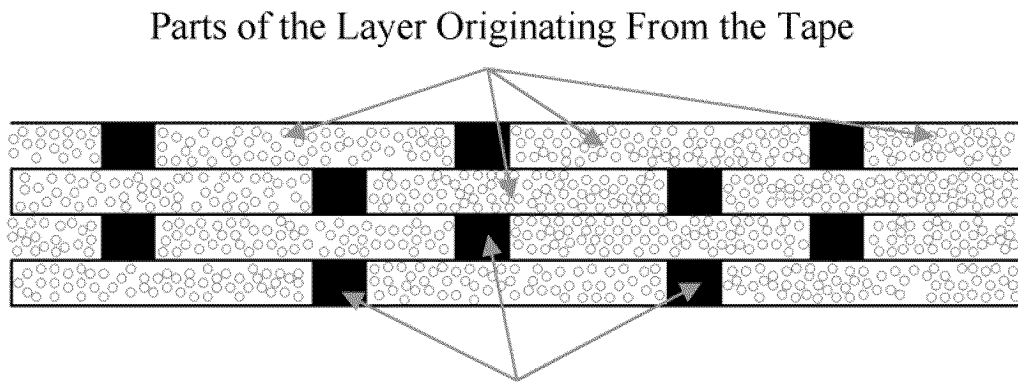
Table 5.1: Experimental and boundary condition parameters

Table 5.2 lists the degree of bond strength and the degree of polymer chain diffusion for both sets of process parameters. The averages of 10 interlaminar shear strength (ILSS) measurements are used in Equation 5.3 to determine the values of the degree of bond strength. The magnitudes of the degree of polymer chain diffusion are the average of all interlaminar nodes in the cylinder.

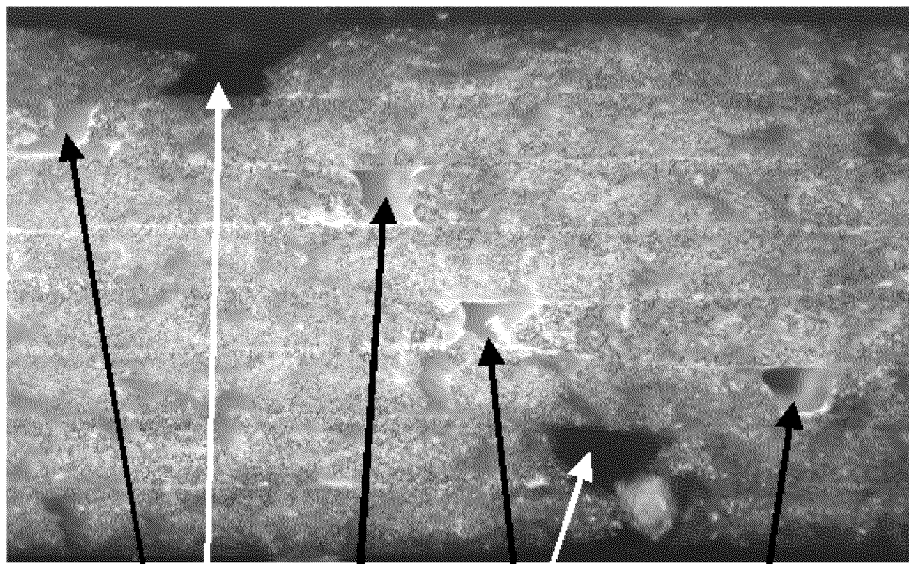
SET	D_b	D_{pcd}
--	%	%
1	23.6	56.4
2	79.3	81.5

Table 5.2: Comparison between experiment and simulation results

Considering the degree of bond strength as reference, Table 5.2 shows that the degree of polymer chain diffusion is too high for the first set of process parameters and that it agrees well to the reference value for the second set of process parameters.



Voids between the Parts of the Layer Originating From the Tape



Voids between the Parts of the Layer Originating from the Tape

Figure 5.8: Voids due to a too large winding pitch (a: sketch, b: example)

For the first set of process parameters, the large overestimation can be explained by the low deformation of the tape at the nip:

- When the tape deformation at the nip is insufficient and lower than the winding pitch, intralaminar voids are formed between the tapes during the process (Figure 5.8). They weaken the laminates.
- Since only small deformations of the tape occur, it is assumed that insufficient microscopic deformations take place in the nip during the process and that the intimate contact is incomplete.

The good agreement between the degree of bond strength and the degree of polymer chain diffusion for the second set of process parameter signifies:

- The intimate contact is complete for this set of process parameters.
- The lower interlaminar properties of the tape wound cylinder are due to insufficient polymer chain diffusion.

Considering the experimental results (section 3.4.4), a complete intimate contact for the second set of process parameters is not surprising, because macroscopic deformations occur at the nip: in this case, the width of the tape after compaction is 10% higher than its original width.

5.6. Heating strategies

5.6.1. Convection heat input of the torch

During the process examples that are mentioned in section 5.5 and detailed in Chapter 4, large temperature differences exist between the incoming tape and the hot nitrogen temperature: between 380°C and 390°C for the first set of process parameters and between 510°C and 520°C for the second set of process parameters. Considering the room temperature and the temperature measured by the nip point pyrometer, those differences are approximately four times larger than the temperature increases in the composite material. Besides the large waste of energy, this heating method includes the risk to degrade the incoming tape when it stays a too long time under the torch, because the nitrogen flow temperature is much higher than the melting temperature of the polypropylene matrix (180°C and Table 5.1). The objective of this section is therefore to investigate the influence of the convection heat transfer of the hot nitrogen on the temperature of the incoming tape, that of the substrate and the degree of polymer chain diffusion.

Table 5.3 lists the parameters of the boundary conditions. The set #2 is the previous set of process parameters (Table 5.1). The set #3 has the same process parameters than the set #2 except for the convective coefficient of the hot gas torch that is zero. That signifies that the dq_{HG}/dt is zero in Figure 5.2 and that there is an adiabatic boundary condition at this location.

SET	T_G	T_R	α_{HG}	α_E
--	$^{\circ}\text{C}$	$^{\circ}\text{C}$	$\text{W}/(\text{m}^2\text{K})$	$\text{W}/(\text{m}^2\text{K})$
2	162	262	86	21
3	162	262	0	21

Table 5.3: Sets of simulation parameters

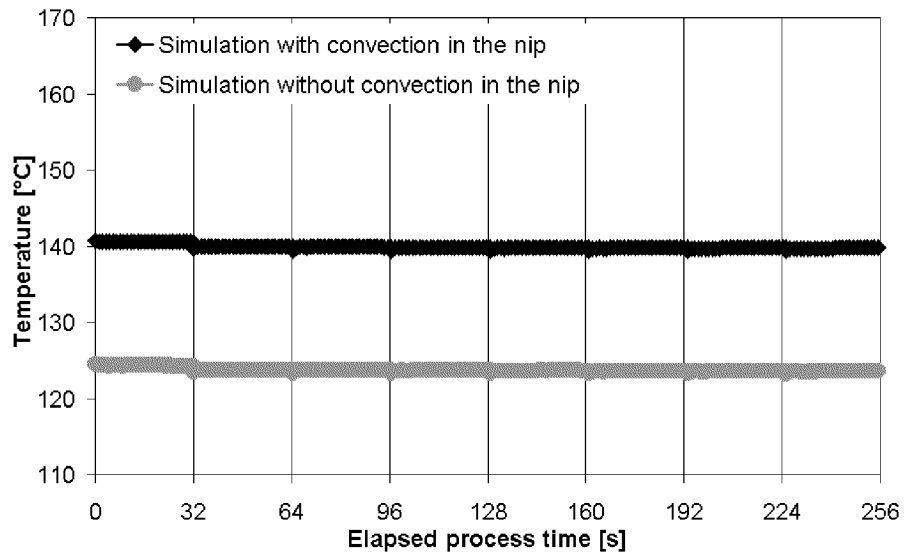


Figure 5.9: Influence of the convection in the nip (incoming tape)

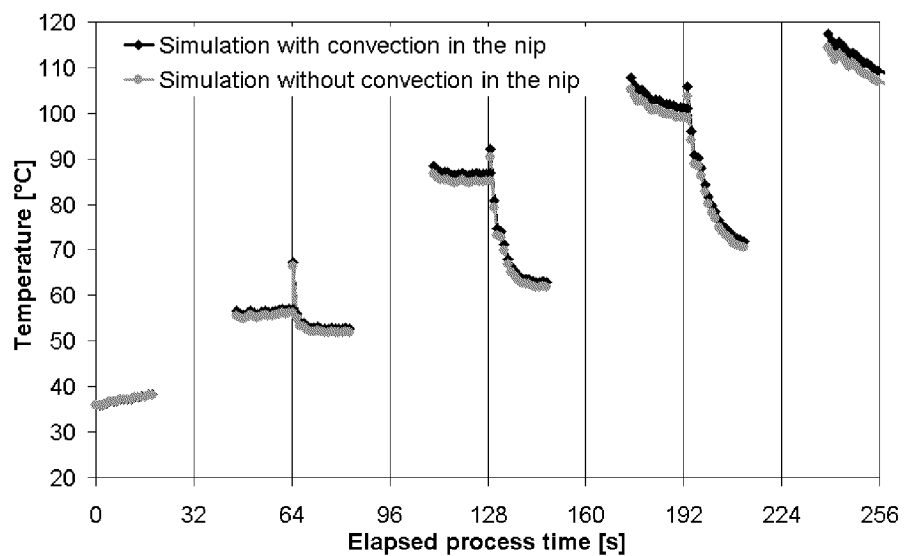


Figure 5.10: Influence of the convection in the nip (mandrel)

Figure 5.9 and Figure 5.10 plots simulation results. The curves are the average temperature of the nodes that are included in the ellipses that correspond to the pyrometer spots in the model. The eight suites of temperature correspond to the deposition of the eight layers. The duration of the lay down of a layer is 32 s.

Considering the temperatures shown in Figure 5.9, approximately 85% of the heat needed to warm-up the composite material is not coming from the convection heat transfer between the hot nitrogen and the incoming tape. This signifies that the contact boundary conditions (tow guide and compaction roller) have a much larger influence on the process conditions than the convection caused by the hot gas torch.

The peaks at the times 64, 128 and 193 s in Figure 5.10 have no physical reason. They result from the way the winding process has been modeled to simulate the transition between two layers: the termination and the restart of each layer takes place on the same location. This causes locally two successive heatings in a much shorter time than in reality. Around the times 32, 96, 160 and 224 s, the temperature magnitude can not be determined, because the location of the substrate pyrometer spot is measuring the cold area beside the substrate which is not considered by the numerical analysis.

Due to the shifted location of the pyrometer spot in comparison to the nip point, the simulation results that correspond to the measurements of the uneven layer are made on the one that was previously laid, and those of the even layer on the one that is currently laid. This explains the different trends between the even and uneven layer simulation results.

The maximum difference between the temperature magnitudes displayed in Figure 5.10 is lower than 2.6 %. It can be therefore considered that the heating introduced by the convection heat transfer between the hot nitrogen and the composite material has practically no influence on the substrate temperature.

SET	D_{pcd}
--	%
2	81.5
3	76.7

Table 5.4: Degree of polymer chain diffusion for the simulation with the two sets mentioned in Table 5.3

Table 5.4 lists the degree of polymer chain diffusion for both simulations. Their magnitudes confirm that the influence of the convection heat transfer caused by the hot gas torch is low: the difference between the two values is approximately 6%.

The simulation results show that the convection heat transfer between the hot nitrogen and the composite material in the nip has only a small influence on the process temperature and the degree of polymer chain diffusion.

Since the temperature of the hot nitrogen is much higher than the temperature of the composite material in the nip region during the process, it is assumed that the latter is dependent on the dwell time under the hot nitrogen flow. Large process speed variations or abrupt process stops could therefore lead to a deconsolidation of the incoming tape or to a degradation of the thermoplastic matrix. In order to reduce those risks, a new heating strategy can be envisaged: only the contact heat inputs (tow guide and roller) should warm the composite material. Since the hot gas and the torch heat indirectly the metallic components in the nip region (including the compaction roller and the tow guide) through convection and radiation, other heat inputs like resistance heating should replace them.

5.6.2. Influence of the initial mandrel temperature

The objective of this section is to find sets of process parameters that can produce cylinders with a complete degree of polymer chain diffusion. In order to consider the same experimental setup, only the initial mandrel temperature (T_{m_i}) is systematically varied.

SET	T_G	T_R	α_{HG}	α_E
--	°C	°C	W/(m ² K)	W/(m ² K)
1	135	233	69	21
2	162	262	86	21

Table 5.5: Sets of constant boundary condition parameters for this section (Table 5.1)

Table 5.5 resumes the boundary conditions that are constant during the simulations. They are the same as in section 5.5.

Since the initial mandrel temperature influences mainly the substrate temperature, the incoming tape temperature is not considered in this section. Figure 5.11 and Figure 5.12 plots simulation results. The curves are the average temperature of the nodes that are included in the ellipses that correspond to the substrate pyrometer spot in the model.

Figure 5.11 and Figure 5.12 confirm that the initial mandrel temperature has a large impact on the substrate temperature. Its influence decreases however with the progress of the process.

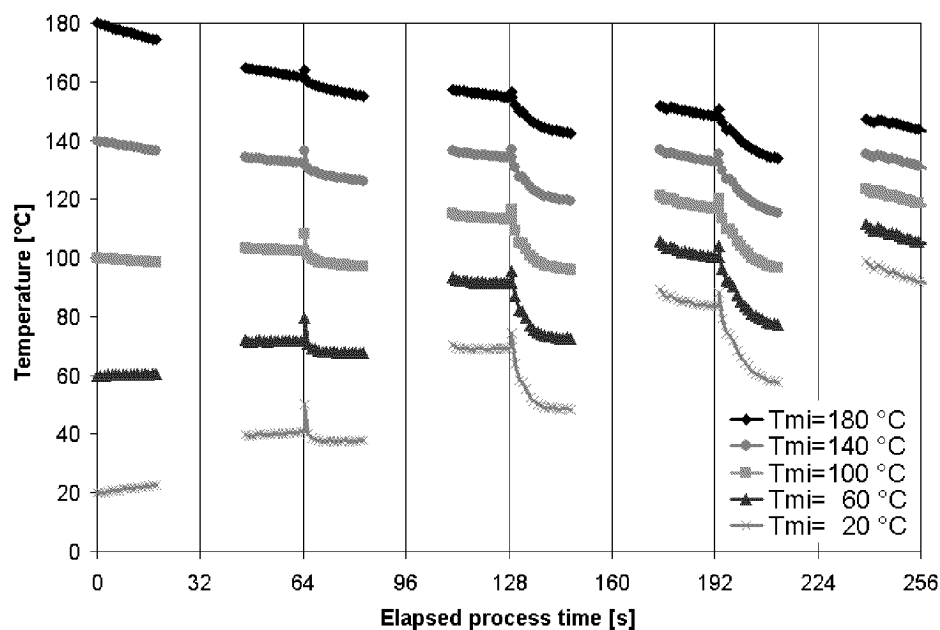


Figure 5.11: Influence of the initial mandrel temperature on the substrate temperature (first set of process parameters)

Considering the curves for an initial mandrel temperature of 100°C, the substrate temperature becomes approximately cyclic from the fourth layer (elapsed process time of 96 s). It is supposed that the mandrel and substrate heat capacities absorb the majority of the cyclic variation during the deposition of the three first layers.

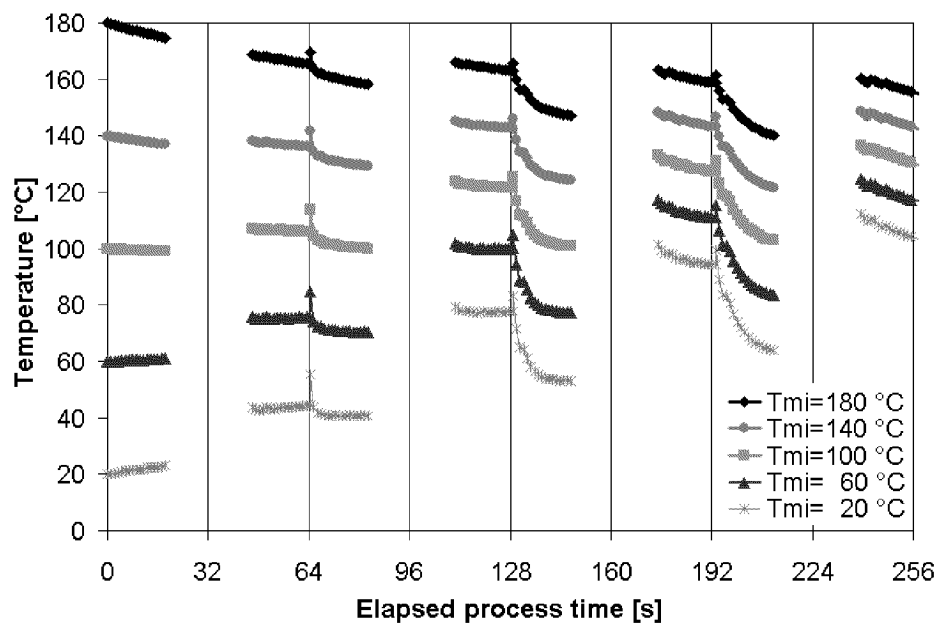


Figure 5.12: Influence of the initial mandrel temperature on the substrate temperature (second set of process parameters)

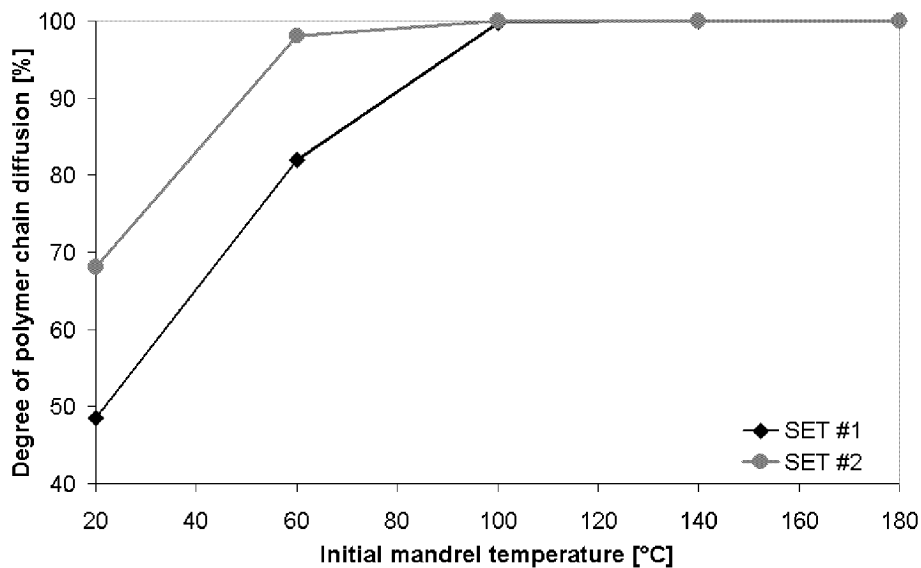


Figure 5.13: Influence of the initial mandrel temperature on the degree of polymer chain diffusion

The origin of the cyclic temperature is related with the cyclic lay down of the incoming tape: all even layers are placed with a winding angle of $-\gamma$, and all uneven layers are deposited with a winding angle of $+\gamma$.

It should be also noted that the cyclic substrate surface temperature appears only when the heat losses and heat inputs are equal on a period of time. For the current examples, this is only the case for an initial mandrel temperature of 100°C.

Figure 5.13 plots the degree of polymer chain diffusion as function of the initial mandrel temperature. Each magnitude corresponds to the average of all interlaminar nodes. Figure 5.13 shows that a maximum degree of polymer chain diffusion can be reached for the two sets of process parameters that are mentioned in Table 5.5.

Since the degree of intimate contact is maximum with the second set of process parameters (section 5.5), and since the degree of bond strength depends on the degree of intimate contact and the degree of polymer chain diffusion, it is better to choose the second set of process parameters with an initial mandrel temperature equal to 100°C in order to manufacture cylinders with the maximum interlaminar shear strength. Higher initial mandrel temperature are not recommended, because they would prolong the cooling time. Very high initial mandrel temperature (over 180°C) should not be considered, because the polypropylene matrix would be fluid during the deposition of the first layer(s). This could imply high deformations of the composite material.

5.7. Conclusion

Transient thermal simulations are performed with a model that determine the development of the degree of polymer chain diffusion.

Two sets of process parameters are used to validate the models. For each set, the value of the degree of bond strength is compared with that of the degree of polymer chain diffusion. The degree of bond strength is evaluated from interlaminar shear strength measurements. The degree of polymer chain diffusion is calculated from the simulations.

The validation shows that the degree of bond strength and the degree of polymer chain diffusion are different for the first set and that they agree well for the second one.

For the first set, an insufficient intimate contact and voids inside the laminate are assumed to cause the discrepancy. The intimate contact can be considered as maximum for the second set, because both degrees agree well.

Considering the results of the comparison between the simulations with and without a convection heat transfer between the hot gas and the composite material, a new heating strategy for the automated tape winding process can be to use exclusively hot elements to warm the composite material through contact boundary conditions. This strategy disregards the localized heating of the nip.

The initial mandrel temperature investigations show that the optimum polymer chain diffusion can be reached with the automated tape winding process. For the present setup, an initial mandrel temperature of 100°C should be chosen.

The study also demonstrates that cyclic surface substrate temperature can be attained when the deposition of the incoming tape is cyclic, and when the heat inputs and the heat losses are equal on the cyclic period.

5.8. Nomenclature

α	convective heat transfer coefficient
γ	winding angle
σ	strength
D	degree
ILSS	interlaminar shear strength
P	pressure
q	heat transfer through a unit surface
t	time
T	temperature
v	speed

Subscript

b	bond strength
E	environment
G	guiding element
HG	hot gas
i	initial
m	mandrel
mech	mechanical relaxation
N ₂	nitrogen
pcd	polymer chain diffusion
R	roller

CHAPTER 6

Development of a New Compaction Tool for the Fabrication of Reinforcement Frames of a Railway Coach

6.1. Introduction

The processes for fiber reinforced thermoplastic composite materials require fabrication of parts with complex geometries and complex fiber orientations, in order to take advantages from the material intrinsic anisotropic properties. Theoretically, the automated tape winding process offers the possibility to lay down tapes on complex paths and surfaces.

Experimental investigations confirm the potential of this process. Hümmler et al. ^[38] investigate the thermoplastic robotic filament winding process for complex part geometries. They wind on cylinder/cone sections and on a cylindrical mandrel with two concave sections. They also process cylinders with different winding angle using non-geodesic paths. The advantages of thermoplastic filament winding appear in particular during the manufacture of parts with non-geodesic fiber paths and concave mandrel sections. Mazumdar and Hoa ^[59] study the fabrication of non-axisymmetric thermoplastic composite parts by the tape winding technique. They suggest that the maintenance of constant tape speed during the fabrication of non-circular shapes is desired for uniform bond quality. Therefore, they present a generalized formula to determine the mandrel speed for obtaining a constant tape speed during the manufacture of non-axisymmetric composite parts. They verify their method by performing experiments on a mandrel with an elliptical cross-section. Romagna ^[71] investigates the thermoplastic filament winding. He winds frames on a train coach mandrel.

Those experimental works utilize either a tape-tension unit ^[71] and/or a solid compaction tool (shoe ^[38] or roller ^{[38]& [59]}) to apply the compaction force at the nip. When tension is used, the support shape must be convex and the compaction force is dependent on the curvature radius. It varies when the latter changes. Inherently, the use of tension introduces the risk of leaving residual stresses in the manufactured products. The shape of solid compaction tool is a limiting factor, because it is adapted to one type of nip geometry. It can be replaced during the manufacturing process when the nip geometry does not vary continuously. This increases however the duration of the process, because it must be stopped and restarted.

Since a uniform compaction force is necessary, whatever the type of surface that is encountered, one of the main process limitations is related with the application of a uniform compaction force on the full width of the incoming tape.

In order to extend the potential of the automated tape winding process, the aims of this investigation are to develop a new compaction tool that allows to wind an incoming tape on various support shapes and to verify its application potential with an example.

6.2. Test geometry

The processing of reinforcement frames for train coaches is following discussed. The uniform cross-section of the train coach geometry is displayed in Figure 6.1. It is divided in 14 segments. Most of them are arcs of circle. Table 6.1 lists the coordinates of their centers (x_c and y_c) and radii (r_c). The location of the two vertical segments is determined with their x-coordinate. The intersections between the segments are not given, but they can be easily reconstructed from their basic geometries.

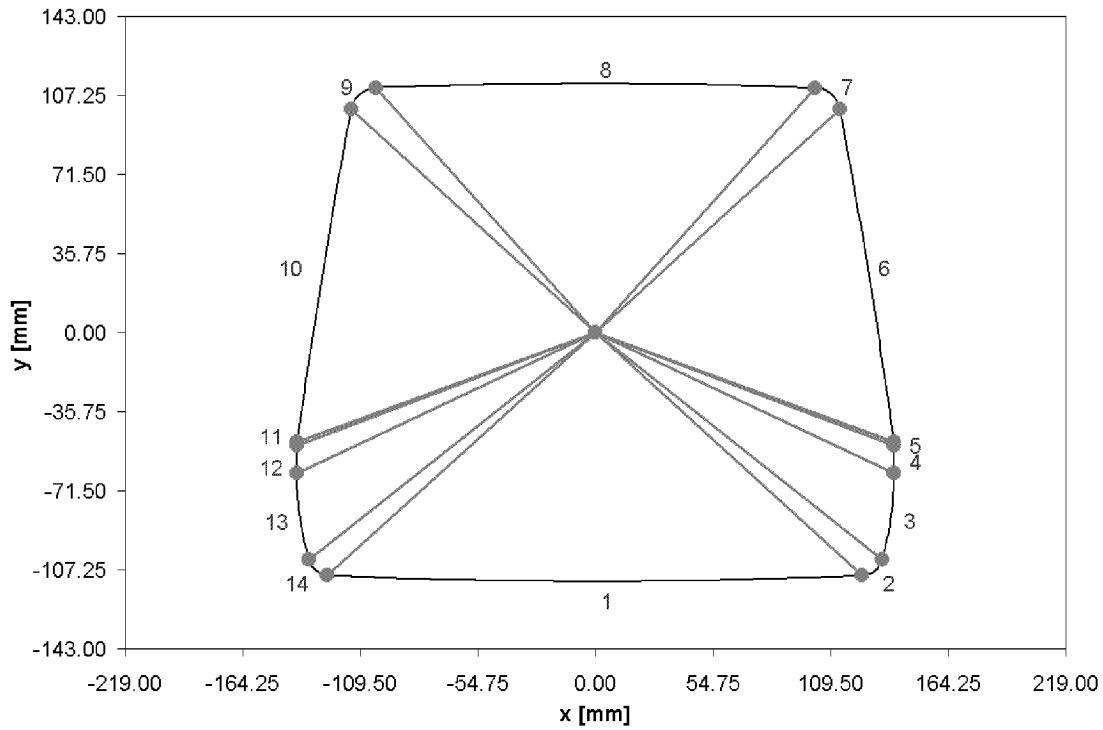


Figure 6.1: Cross-section of the railway coach

Segment	Type	x_c mm	y_c mm	r_c mm	x mm
1	arc of a circle	0.0000	2887.5000	3000	
2	arc of a circle	123.7468	-99.9382	10	
3	arc of a circle	0.0000	-63.5000	139	
4	vertical segment				139
5	arc of a circle	129.0000	-50.9832	10	
6	arc of a circle	-2831.8200	-467.6900	3000	
7	arc of a circle	101.9966	98.7586	12	
8	arc of a circle	0.0000	-2887.5000	3000	
9	arc of a circle	-101.9970	98.7586	12	
10	arc of a circle	2831.8200	-467.6900	3000	
11	arc of a circle	-129.0000	-50.9832	10	
12	vertical segment				-139
13	arc of a circle	0.0000	-63.5000	139	
14	arc of a circle	-123.7470	-99.9382	10	

Table 6.1: Geometry of the railway coach cross-section

6.3. Tape compaction concepts

Prior to the development of the new compaction tool, possible concepts are reviewed and discussed in this section. This strategy enables to evaluate various concept and to identify the most appropriate one.

6.3.1. Utilization of a tape-tension system

Tension is widely used during the filament winding process with thermoset resins. Funck ^[26] uses this technique for the fabrication of high-pressure tanks to introduce process-induced residual stresses in the laminates.

Figure 6.2 shows that a compaction pressure can be applied on the entire width of the nip. Standard tape-tension systems are available: e.g. brake and tension unit.

This compaction technique has various drawbacks. First, changes in the winding angle create shear stresses that can generate localized delaminations. Substrate delaminations destroy the intimate contact, prevent the polymer chain diffusion and then the bond development. In this case, additional processing steps are necessary in order to remove the delaminations and create the bond at the delaminated locations.

The use of a tape-tension system can introduce residual stresses in the laminates. However pre-loading of the structure is generally not desired. Investigations must be carried out in order to prevent the development of residual stresses during the process using this compaction technique.

Figure 6.3 displays the forces resulting from the tape tension. Friction forces are neglected. Considering that the compaction pressure plotted in Figure 6.3 is constant and that the forces must be in equilibrium, it results that:

$$p = \frac{T}{w r} \quad (6.1)$$

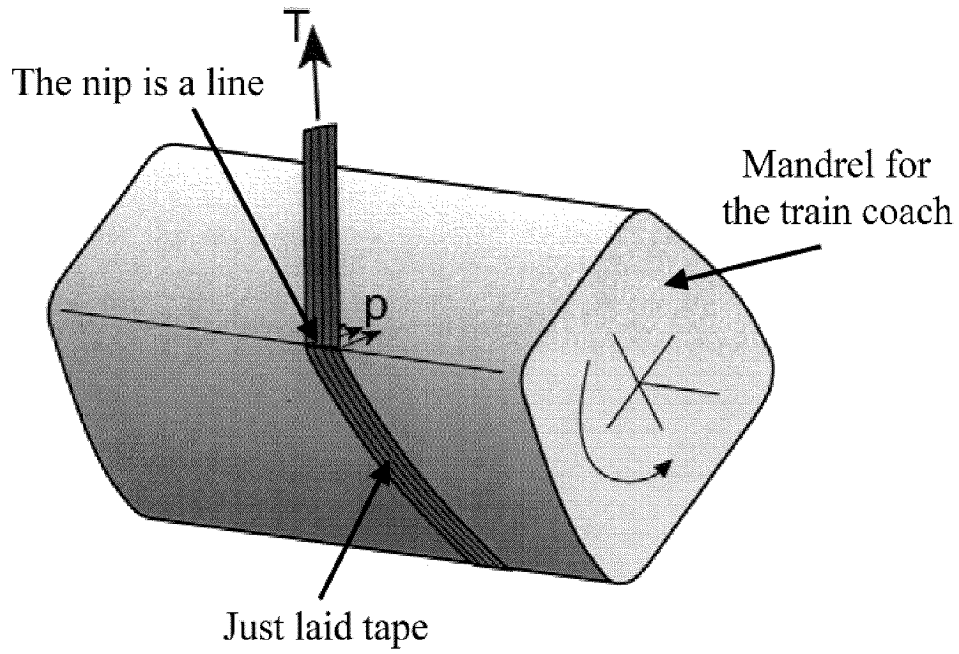


Figure 6.2: Use of tension in the incoming tape

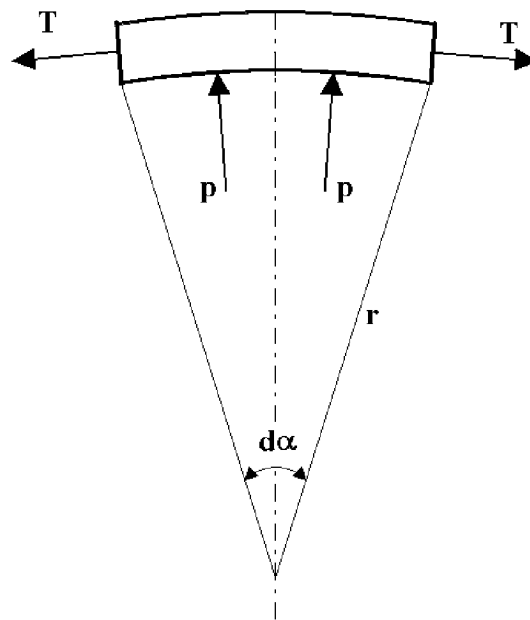


Figure 6.3: Forces and pressures during the process with tension in the incoming tape

Equation 6.1 shows that the compaction force is inversely proportional to the radius of curvature “ r ”. When the latter changes, the tension should be varied in order to minimize the variations of the compaction pressure. This is the most appropriate strategy to prevent fluctuations of the degree of intimate contact and of the bond quality.

Considering Equation 6.1 and the geometry of the train coach (Table 6.1), the variations of the tension force should be very large. Since no compaction pressure could be applied on the flat segments of the train coach mandrel, no bonding can occur on those locations during the automated tape winding process.

6.3.2. Utilization of a solid compaction roller

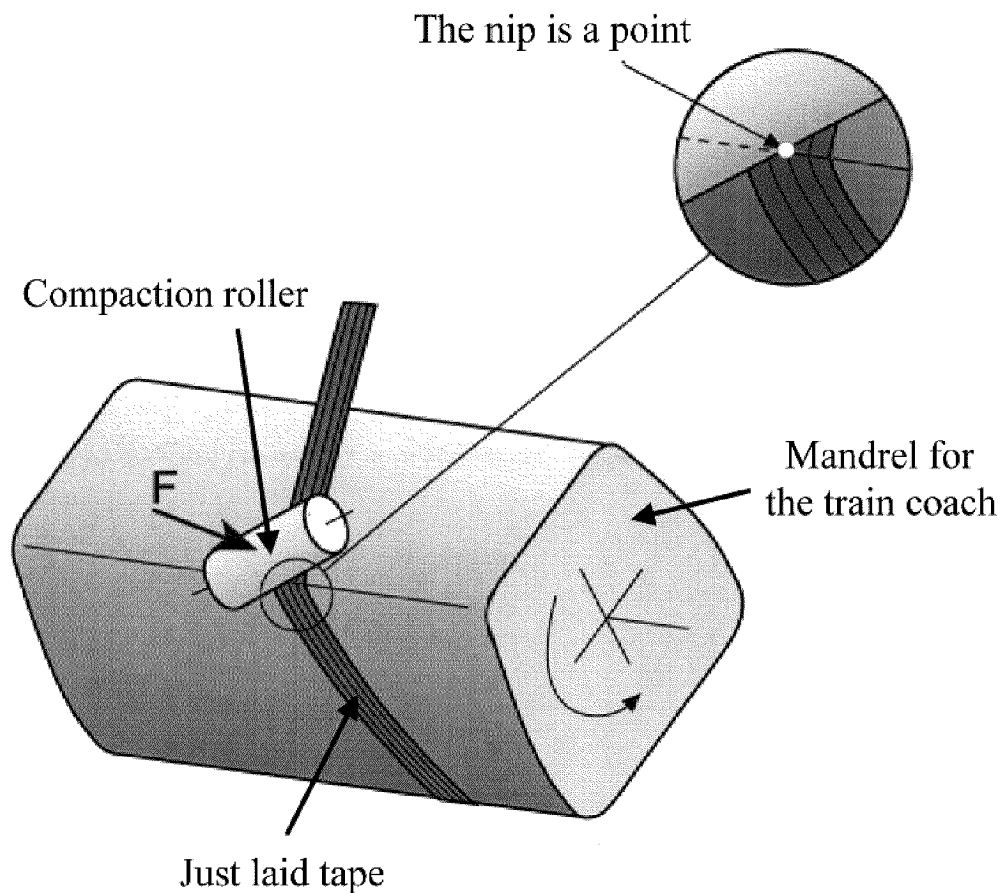


Figure 6.4: Utilization of a compaction roller during the winding process

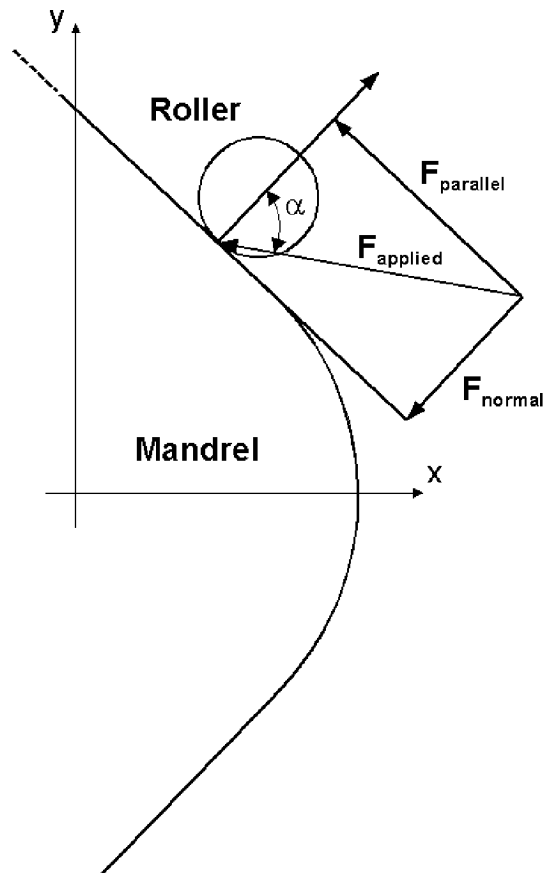


Figure 6.5: Forces during the utilization of a compaction roller

Compaction rollers are standard tools for the automated tape winding and the automated tape placement processes. Figure 6.4 visualizes the largest problem related to this technique: the roller presses the composite material on a point. This occurs when the form of the nip changes.

In the present example, the form of the nip varies when the axial axis of the roller is not parallel to the axial axis of the mandrel. The solution is to keep those axes parallel to each other. That requires to separate the guiding system from the compaction roller, because the orientation of the guiding system needs to vary when the winding angle changes.

Considering the current setup, the direction of the applied compaction force F_{applied} is constant (Figure 6.5). The angle α between the local surface normal of the train coach mandrel and the compaction assembly axis will therefore change during the process. As a consequence, the compaction force F_{normal} will vary between 0 and F_{applied} . Since the intimate contact and the bond strength cannot develop when the compaction force is zero, the implementation of this solution requires the development of a special assembly and an additional axis.

6.3.3. Utilization of a deformable compaction roller

A deformable compaction roller can be another solution (Figure 6.6), because its shape takes automatically the form of the nip. The compaction force is applied on the full width of the incoming tape during the process of the reinforcement frames.

In comparison with the preceding concept, the guiding system does not need to move relatively to the compaction roller. Both can be mounted on the same assembly in order to lay the incoming tape with various winding angles.

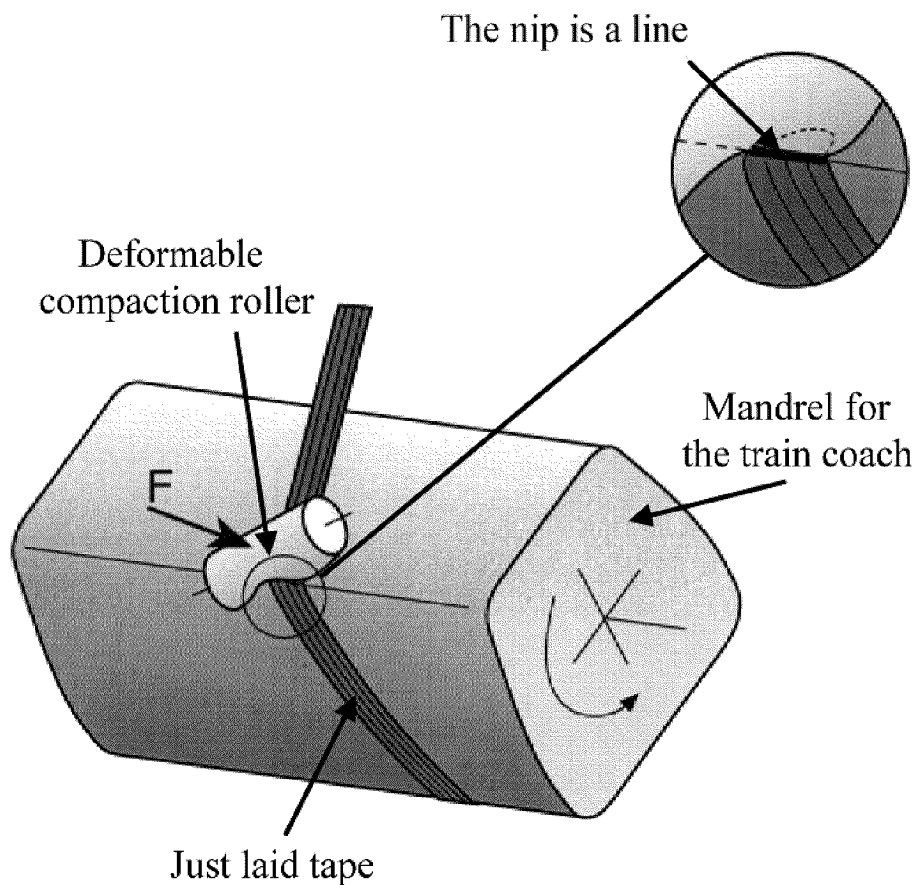


Figure 6.6: Utilization of a deformable compaction roller during the winding process

6.3.4. Utilization of a compaction shoe

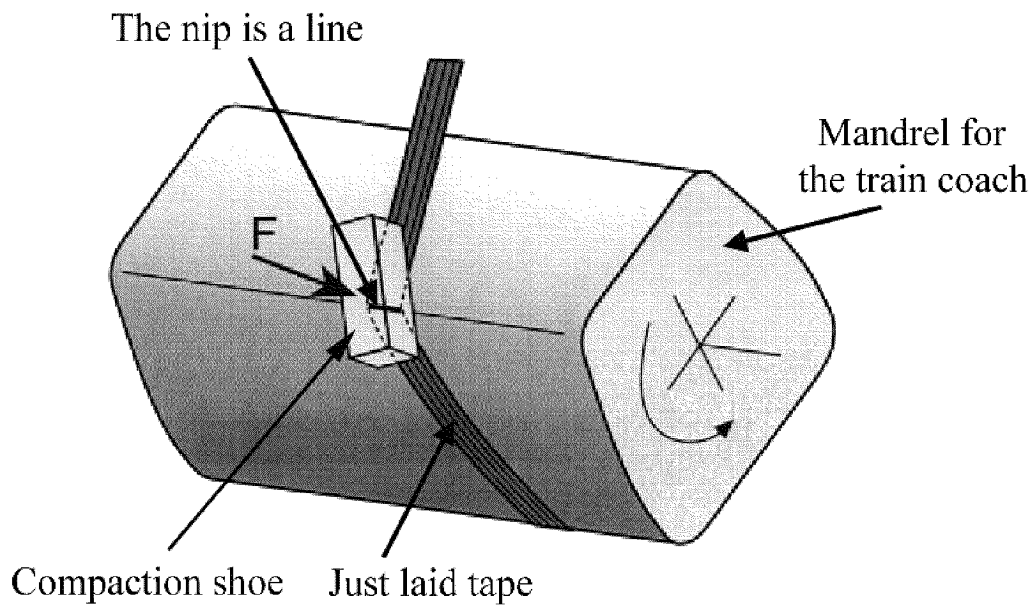


Figure 6.7: Utilization of a compaction shoe during the winding process

A compaction shoe (Figure 6.7) is a well-known compaction technique for the automated tape winding process. The main characteristic of this compaction unit is that the incoming tape glides on the surface of the tool. In order to prevent this slipping, compaction shoes are often combined with flexible tapes (Figure 6.8).

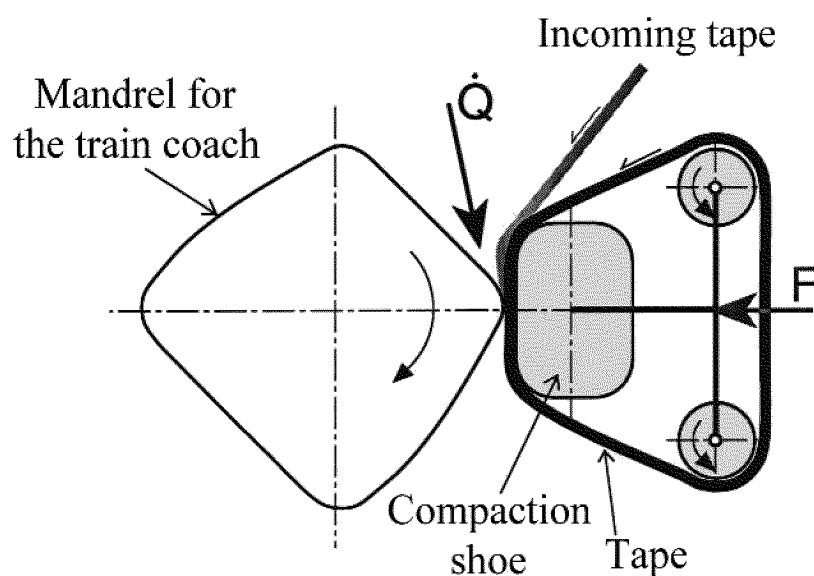


Figure 6.8: Combination of a flexible tape and a compaction shoe

Compaction shoes can be used when the form of the nip does not change. In the current example, this is the case. Since the railway coach has always the same cross-section, the nip form can stay constant when a flat compaction shoe is used (Figure 6.7).

6.3.5. Utilization of a deformable band

Section 6.3.1 shows that the incoming tape can alone fit the nip geometry for the current test geometry. In order to employ this advantage without the drawbacks related with the use of tape-tension systems, a band could be utilized to compact the incoming tape on the substrate (Figure 6.9).

The main characteristic of this concept is that the incoming tape and a band fit the same range of geometries.

The band will exert a compaction force as a reaction, when it is stretched and deformed. It needs therefore to be held. It can be either fixed on a support or mounted on a special assembly (Figure 6.10). In the first case, the incoming tape has to glide on the band, because the latter is fixed. The second technique prevents the slipping of the incoming tape relatively to the band, because both can move together.

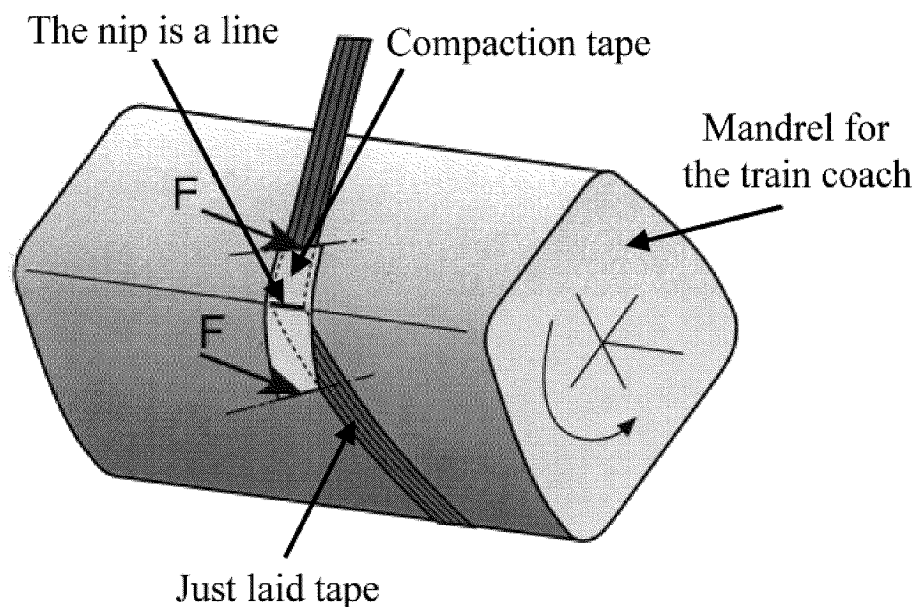


Figure 6.9: Utilization of a band during the winding process with an angle

Both methods can be used to apply a compaction pressure on the entire circumference of the train coach during the process.

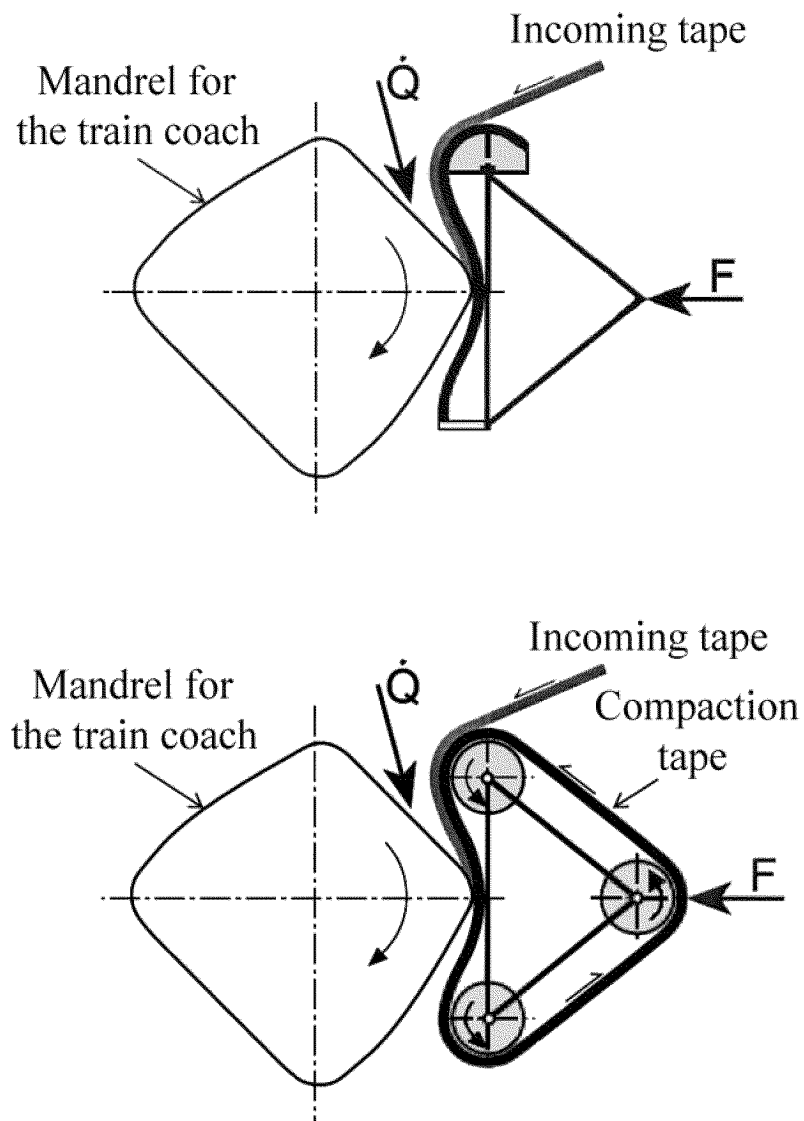


Figure 6.10: Two methods to use a band

6.3.6. Evaluation of the different compaction concepts

Some of the above-mentioned concepts can be used to compact the incoming tape on the railway coach mandrel. In order to determine the best solution, they are therefore evaluated with the following criteria:

- the magnitude of the compaction force,
- the risk of damage of the incoming tape,
- the adaptation of the hot gas torch to the new setup,
- the adaptation of the new compaction assembly to the current setup,
- the complexity of the fabrication of the new assembly,
- the simplicity of the maintenance,
- the lifetime
- and the flexibility.

Table 6.2 evaluates the different concepts. It uses the following scale: 1 sufficient, 2 medium, 3 good and 4 very good. It shows that the best solution is the utilization of a band.

Criteria	Weight factors	Concepts					
		Compaction shoe		Deformable roller		Band	
		Note	Evaluation	Note	Evaluation	Note	Evaluation
Compaction force	1.00	2.0	2.00	2.0	2.00	1.5	1.50
Damage on the tape	1.00	3.5	3.50	3.0	3.00	3.5	3.50
Hot gas torch	0.81	3.0	2.43	3.0	2.43	3.0	2.43
Adaptation	0.68	1.5	1.02	1.5	1.02	1.5	1.02
Fabrication	0.55	2.0	1.10	2.0	1.10	2.5	1.38
Maintenance	0.34	2.0	0.68	1.5	0.51	3.0	1.02
Lifetime	0.34	1.0	0.34	3.0	1.02	3.0	1.02
Flexibility	0.68	1.0	0.68	3.0	2.04	4.0	2.72
Sums			11.75		13.12		14.59

Table 6.2: Evaluation of the concepts ^[13]

Since the utilization of tape-tension systems will not permit to apply a compaction force on the vertical segments of the train coach mandrel during the process, this technique is not retained for the evaluation. In order to prevent tape damage caused by friction forces, the concepts implying slip of the tape are not evaluated. Solutions with solid compaction rollers are also not considered, because they will need resources that are not available.

6.4. Development of the new compaction head

Cerini and Beretta ^[13] describe in detail the development of the new compaction assembly in their diploma thesis. Since there are various solutions during the development of a new tool, this section reviews the choices of the main components of the new compaction assembly.

6.4.1. Choice of the band

The choice of the material for the band is restricted to metals, because the band can be heated up to elevated temperatures: the highest compaction roller temperature for the simulations is 262°C (Table 4.5). A commercial type of band is selected in order to avoid special investigations. It is made of spring iron (Ck101, material number 1.1274 according to DIN 17007, tensile stiffness 2000 N/mm²).

6.4.2. Number of rollers guiding the band

Figure 6.10 shows a sketch of the construction that is to be developed. It is composed of three rollers that change the direction of the band. Considering that the tape wear decreases when the roller radii increase, the principle of the new compaction assembly is slightly modified. It consists of two rollers (Figure 6.12).

6.4.3. Rotation of the compaction assembly

The section 6.3.2 shows that rollers must not apply the compaction pressure. The compaction assembly is therefore free to rotate such that the band always stays in contact with the train coach mandrel (Figure 6.12, Figure 6.13 and Figure 6.14). Its angular position is adapted automatically due to the compaction force.

6.4.4. Description of the new setup

Most of the elements of the original setup are shown in Figure 6.11. It consists of a Baer WSE-II winding machine with a Baer TCS-84 control system and an ADC compaction assembly.

The Baer control system determines the processing speed and the winding paths. The ADC control cabinet fixes the parameters of the hot gas torch that are the nitrogen flow and its temperature at the outlet of the hot gas torch.

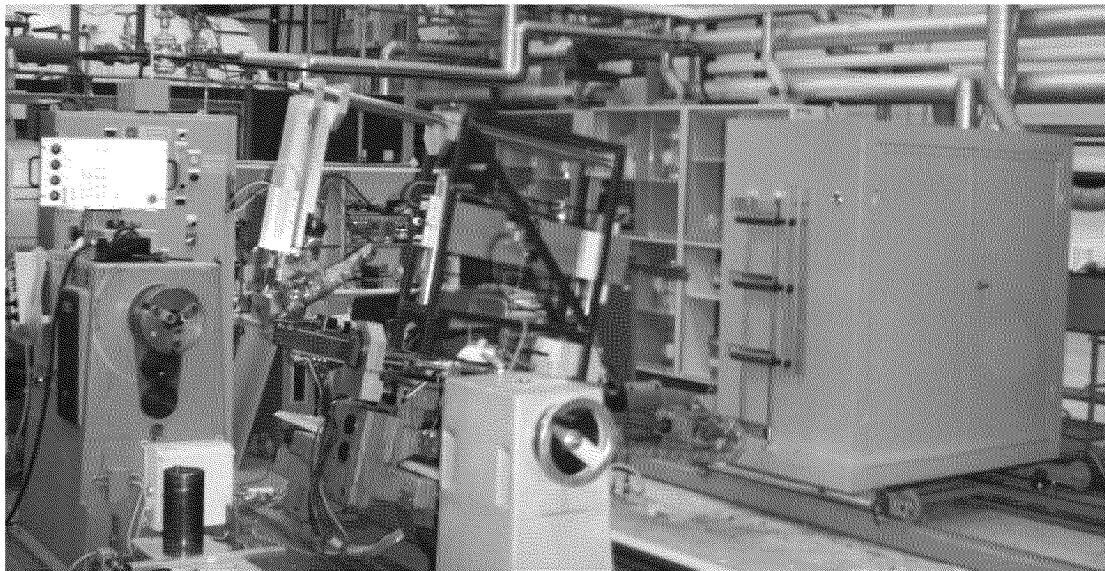


Figure 6.11: View of the original automated tape winding setup

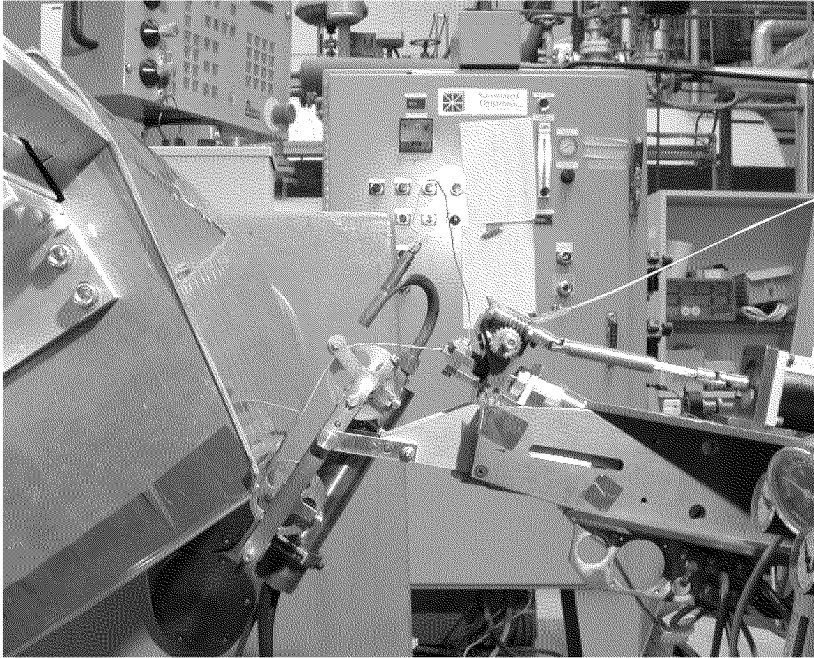


Figure 6.12: View of the new compaction assembly #1

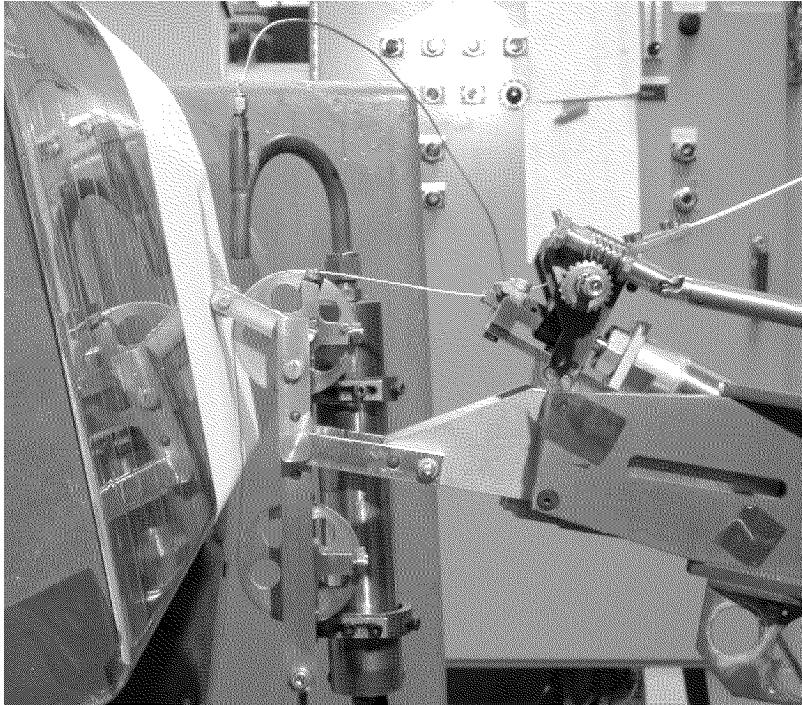


Figure 6.13: View of the new compaction assembly #2

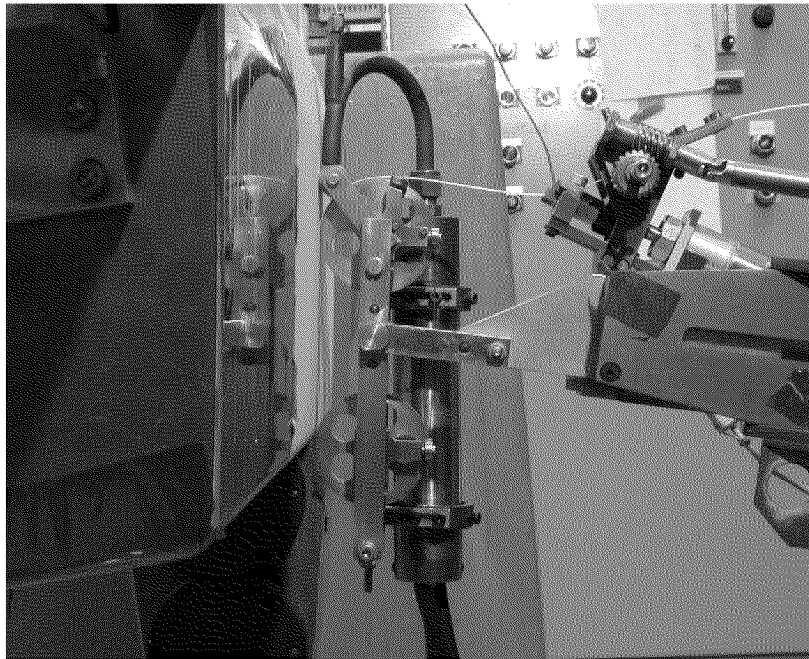


Figure 6.14: View of the new compaction assembly #3

The original compaction assembly and heat torch holder are modified. Prior to its utilization, the new tool is tested. Figure 6.12, Figure 6.13 and Figure 6.14 show the new assembly with three different positions of the mandrel. A white sheet of paper is added to prevent reflections on the mandrel (Figure 6.13 and Figure 6.14).

6.5. Fabrication of reinforcement frames for a railway coach

Reinforcing frames are wound using the train coach mandrel to verify the quality of parts delivered by the compaction assembly described in section 6.4.

Following the methodology used in chapter 3, a reference frame is fabricated. It is first cold wound on the train coach mandrel. Then it is post-processed under vacuum in an autoclave using the cycle shown in Figure 6.15.

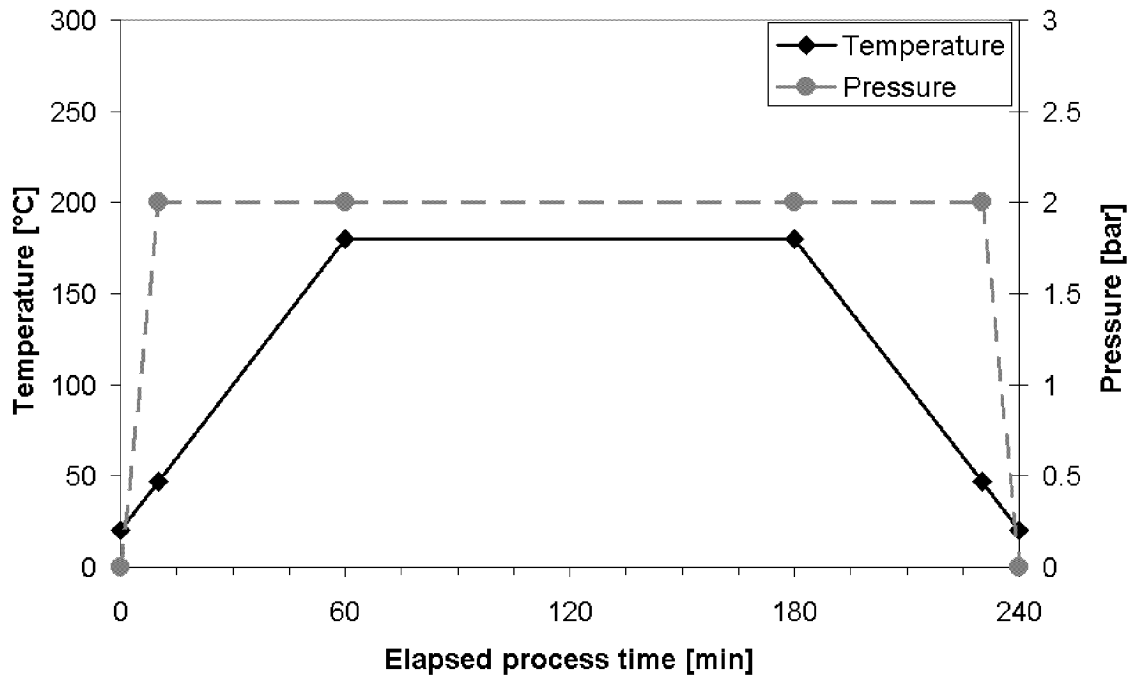


Figure 6.15: Autoclave parameters

Specimen number	Temperature	Speed	Compaction Force #1	Compaction Force #2
	°C	rad/s	N	N
1	600	0.07100	69	69
2	600	0.07100	207	207
3	575	0.14199	69	69
4	600	0.14199	207	69
5	575	0.14199	345	69
6	525	0.07100	207	69
7	525	0.07100	69	69
8	525	0.07100	207	207

Table 6.3: Process parameters for the automated tape winding process

Table 6.3 lists the process parameters used to manufacture various frames. Since the contact surface between the band and the substrate varies during the process, two compaction forces are used during a rotation of the mandrel. Compaction force #1 is applied for straight surfaces (segments 1, 3, 4, 5, 6, 8, 10, 11, 12 and 13 of Figure 6.1), while compaction force #2 is used for the edges (segments 2, 7, 9 and 14 of Figure 6.1).

6.6. Results

6.6.1. Preparation of the specimens for the mechanical tests

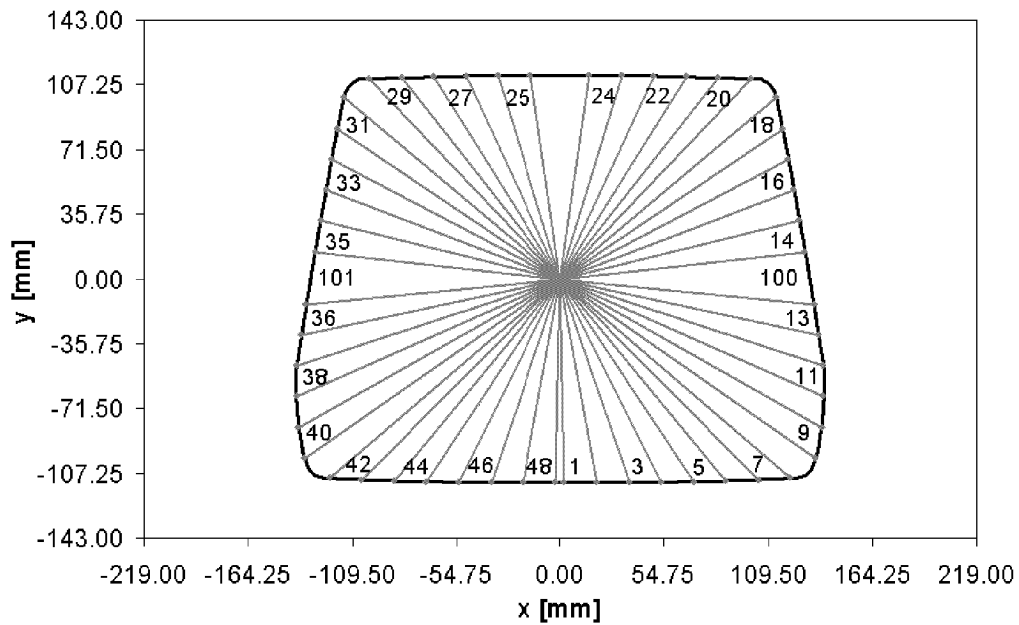


Figure 6.16: Short beam shear specimens

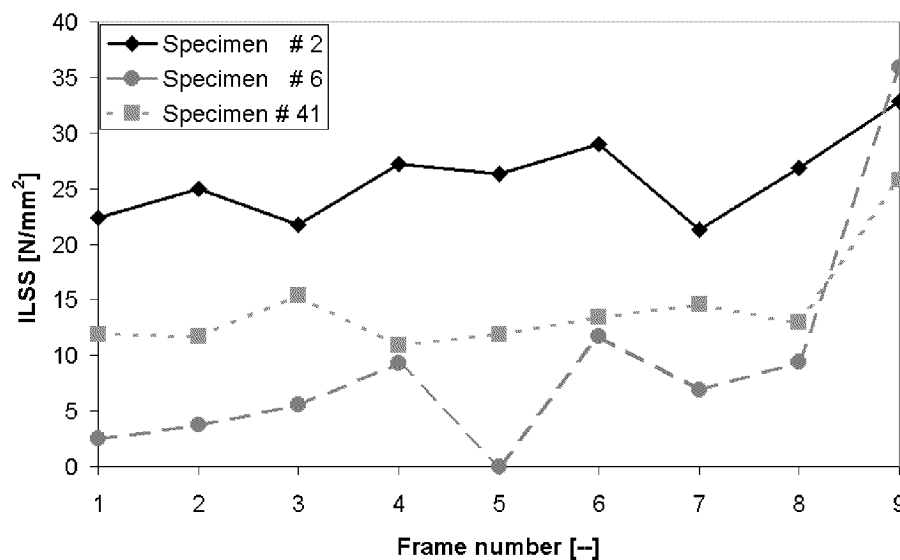


Figure 6.17: Interlaminar shear strength of the automated tape wound specimens (#1 to #8) and of the reference (#9)

Specimens for the short beam shear test (chapter 3) are sawn from the frame. Figure 6.16 shows the locations from where the specimens originate. Since they do not have the same geometries, only the interlaminar shear strength (ILSS) of specimens coming from the same location can be compared.

6.6.2. Evaluation of some specimens for each frames

The test of all specimens for each frame would be a large labor work. Therefore, the ILSS of three specimens (#2, #6 and #41) for each frame is measured in order to determine the frame with the best ILSS. Figure 6.1 shows that the location #2 is on a segment of the frame that has a high radius of curvature, that the location #6 is placed just after an edge and that the location #41 corresponds to an edge.

Figure 6.17 plots the ILSS of the different specimens. As expected, the ILSS of the reference frame varies in function of the location. It is assumed that the variation originates from the different geometries of the specimens.

The figure shows that the process parameters have the highest influence on the ILSS at location #6. Low degree of bond strength can be reached for this location: the maximum one is equal to 33%. No ILSS can be observed for the set #5 of process parameters. At location #2, the ILSS of the specimen made with the automated tape winding process are closer to that of the post-consolidated specimen. The best degree of bond strength is 88%. This result is better than those presented in chapter 3. The ILSS of the automated tape wound specimens originating from location #41 are in between.

6.6.3. Evaluation of the best frame

The best frame is determined with the results presented in the section 6.6.2. The ILSS at the three locations (#2, #6 and #41) are summed for each frame. The frame processed with the set of parameters #6 (Table 6.3) has the best sum of ILSS. It is therefore considered as the wound frame with the best ILSS.

Figure 6.18 allows to visualize the differences between the degree of bond strength of frame #6. There are four series of locations where it is small (#4-#8, #15-#19, #26-#30 and #36-#41). Considering the process, the locations of those series are on the edges or placed just after the lay down of the incoming tape over the latter. Since the contact surface between the band and the mandrel

is lower on the mandrel edges than on the segments with a high radius of curvature (Figure 6.12 and Figure 6.13), since the applied compaction pressure is inversely proportional to the compaction surface, it is assumed that the low degree of bond strength is not related to the applied compaction pressure. It is presumed that it is caused by the heat input limitations of the current setup.

The degree of bond strength on the other locations of the frame #6 is between 68% and 88%. Considering that the ILSS of automated tape wound specimens in chapter 3 are lower than 80% of that of their reference, those results are acceptable.

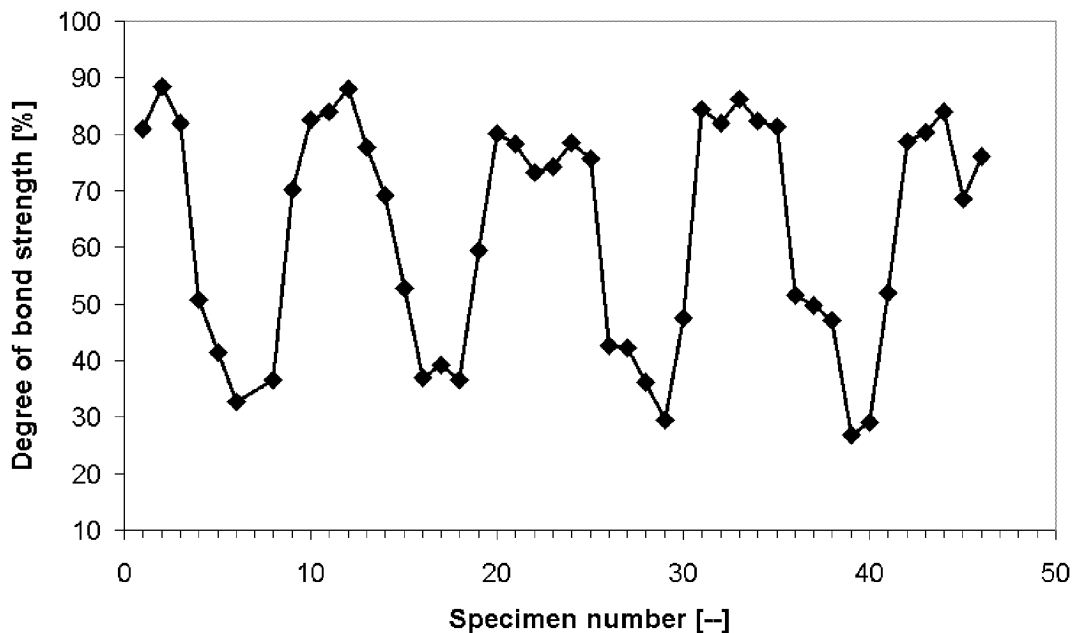


Figure 6.18: Degree of bond strength of the best automated tape wound frame

6.7. Conclusion

The aims of the current chapter are to develop a new compaction tool that allows to wind an incoming tape on various support shapes and to verify its application potential with an example.

First, various concepts are presented, discussed and evaluated with respect to the test geometry. Considering the best concept, a new compaction assembly is developed and adapted to the current setup.

Reinforcement frames are wound on a train coach mandrel and a reference frame is processed in an autoclave. In order to demonstrate the potential of the new compaction assembly, the interlaminar shear strength of the wound frames is compared to that of the reference frame. The results of the best wound frame show that the degree of bond strength exhibits large variations.

Since the cause of the low degree of bond strength is related with the heat input limitations, the new compaction tool can be used for the automated tape winding process. Further investigations should be however performed in order to define appropriate heating strategies for the current setup and to process highly consolidated frames.

6.8. Nomenclature

α	angle
F	force
p	pressure
Q	energy
r	radius
T	tension
w	width
x,y	Cartesian coordinates

CHAPTER 7

Conclusions and Outlook

7.1. Conclusions

The objectives of this Ph.D. thesis were:

- to investigate scientifically the automated tape winding process in order to process products with optimized interlaminar shear strength and to ameliorate its economic efficiency,
- to facilitate the laying of the tape on more complex geometries.

The study began with the development of an experimental setup and the related measurement system. The best value for the interlaminar shear strength of the tape wound cylinders was 80% of that of a reference cylinder that has been post-processed in an autoclave. Various sets of process parameters lead to this limit.

On-line measurements of the incoming tape temperature just before the nip have shown that the temperature is lower than the melting temperature of the polypropylene matrix. Considering measurements made with a differential scanning calorimeter, the temperature of the incoming tape just before the nip was however in the phase transition domain (solid-liquid) during the process of the cylinders that possess the best interlaminar shear strength. The measurements have also pointed out that the substrate temperature varies continuously during the process.

The experimental study did not permit to determine process conditions that lead to optimize interlaminar shear strength of the tape wound cylinders. It did not enable to localize the main cause of the interlaminar shear strength difference between the best tape wound and reference specimens. Therefore further investigations have been performed in order to determine whether or not the polymer chain diffusion through the interfaces was the main cause of the limit.

First, a numerical program has been developed. Unlike programs used in other researches, it simulates the three-dimensional transient thermal phenomena during the entire automated tape winding process. In order to provide accurate input values for the program, a method to evaluate the heat flow parameters of the hot gas torch (i.e. the outside flow temperature and the convective heat transfer coefficient) has been also developed. The program has been successfully validated with two sets of process parameters: small discrepancies have been observed between simulation results and experimental measurements.

Second, a model calculating the degree of polymer chain diffusion has been adapted to the non-isothermal calculations of the simulation program and integrated in its code. Its validation has shown that the incomplete degree of bond strength of the experimental specimens is caused by an incomplete degree of polymer chain diffusion.

A parametric study varying the initial mandrel temperature has been performed in order to find process conditions that enable to fabricate cylinders with a complete degree of polymer chain diffusion and a complete degree of bond strength. For the sets of process parameters that have been chosen, this investigation showed that the initial mandrel temperature should be 100°C in order reach the above-mentioned objective.

The variation of the initial temperature enables to lay down the incoming tape effectively according to the interlaminar shear strength and economical considerations. All cost related with weight will be reduced during the life of the products, when its weight can be optimized. The variation of the initial mandrel temperature can be performed with low cost solutions like resistance heating.

Further simulations show that the heat input caused by the hot gas torch has a small influence on the substrate temperature and the degree of polymer chain diffusion. They pointed out that the contact boundary conditions bring the most part of the heat in the composite material. Therefore a heating strategy disregarding the hot gas torch was proposed. It will reduce the process costs, because the price of the hot gas torch is elevated and its life relatively short.

In order to facilitate the laying of the tape on more complex geometries, a new compaction assembly for the automated tape winding process has been developed. It enables to process various geometries with the same setup. Therefore it increases the flexibility of this manufacturing technique. The use of such tools enables also to reduce the process costs, because the process does not need to be stopped and restarted for each variation of the nip form.

7.2. Outlook

One of the largest drawbacks of this technology was the lack of knowledge of its transient process conditions. The current works showed that transient simulations could be performed during the entire duration of the automated tape winding process.

The increase of the computing power will enable in the next years to simulate accurately the process conditions for a larger range of products. In order to realize this progress, further simulation programs need to be developed. They should:

- employ user-friendly interfaces,
- consider the deposition of the layers with various fiber orientations on various geometries,
- use the available basic models that describe all the phenomena occurring during this process.

The above-mentioned simulation programs with databases containing the material properties will help the engineers to determine in which cases (for which products), the automated tape winding process is appropriate. They will also provide all the information that is necessary to implement this technology in an industrial environment.

In order to make the automated tape winding process more attractive (cost-effective), the price of the used material must be reduced. A solution will be to employ more usual preforms: bundles and/or yarns. Investigations need to be performed in order to:

- determine the setup modifications that are required to use those preforms,
- define the process parameters for the new setup components.

APPENDIX A

Heat Transfer in the Vicinity of the Hot Gas Torch

A.1. Development for the determination of the convective heat transfer coefficient

Equation 4.10 contains the temperature of the hot gas outside the boundary layer, the temperature of the material surface and the convective heat transfer coefficient. Since the latter cannot be directly measured, this section aims to describe the theory related to a method to estimate it.

The technique assumes that temperature measurements are performed to determine the temperature field closed to nip region. It uses a still setup, because the winding machine vibrates during the process, and because the hot gas velocity is more than two orders of magnitude higher than the one of the incoming tape.

To support the theoretical overview, a sketch is shown in Figure A.1. In the flow, the energy equation describes the heat exchanges. Since the velocities vanish on still surfaces ($y=0$) and the variation of the mean temperature in the cross direction of the flow can be neglected, it becomes:

$$\rho \frac{\partial e}{\partial t} + \frac{\partial}{\partial x} \left(K \frac{\partial T}{\partial x} \right)_{y=0} + \frac{\partial}{\partial y} \left(K \frac{\partial T}{\partial y} \right)_{y=0} = 0 \quad (\text{A1})$$

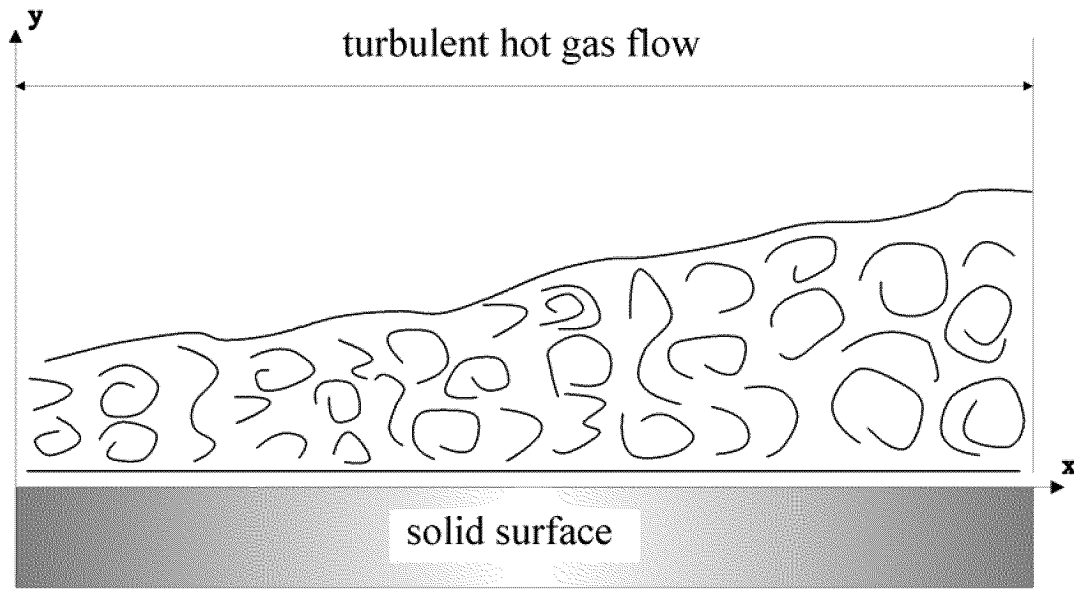


Figure A.1: Two-dimensional turbulent flow over a flat surface

The variation of the internal energy over time can be neglected, when the flow is stationary:

$$\frac{\partial}{\partial x} \left(K \frac{\partial T}{\partial x} \right)_{y=0} + \frac{\partial}{\partial y} \left(K \frac{\partial T}{\partial y} \right)_{y=0} = 0 \quad (\text{A2})$$

In most cases, the temperature gradient is assumed to be principally in the y-direction. The temperature gradient in the x-direction is negligible by comparison (i.e. 120°C/mm in the y-direction vis. 10°C/mm in the x-direction). Equation A2 reduces to :

$$\frac{\partial}{\partial y} \left(K \frac{\partial T}{\partial y} \right)_{y=0} = 0 \quad (\text{A3})$$

The definition of the convective heat transfer coefficient now reads:

$$\alpha_{HG} = \frac{-K}{(T_{HG} - T_s)} \left(\frac{\partial T}{\partial y} \right)_{y=0} \quad (\text{A4})$$

A.2. Nomenclature

α	convective heat transfer coefficient
ρ	density
e	internal energy
K	thermal conductivity
t	time
T	temperature
x, y	Cartesian coordinates

Subscript

HG	hot gas
S	surface

APPENDIX B

Development of the model of the degree of polymer chain diffusion

B.1. Degree of polymer chain diffusion

The degree of polymer chain diffusion describes the ratio between the current interlaminar shear strength and the maximum reachable interlaminar shear strength. Equation B1^[9] describes its development in the isothermal case.

$$D_{pcd} = \frac{\sigma(t)}{\sigma_{\infty}} = \left(\frac{t}{t_{rep}} \right)^{1/4} \quad (\text{B1})$$

This model requires the knowledge of the reptation time as function of the temperature. Butler et al.^[12] mentioned the research of Wool^[97] who relates the reptation time to the mechanical relaxation time:

$$t_{rep} = t_{mech} \left[1 - \sqrt{\frac{M_c}{M}} \right]^{-2} \quad (\text{B2})$$

The critical molecular weight M_c , the molecular weight M and the mechanical relaxation time t_{mech} are physical properties of the thermoplastic matrix. Wool^[97] determines M_c experimentally (7000 g/mol) and theoretically (7600 g/mol).

B.2. Determination of the mechanical relaxation time of the polypropylene matrix

In the present investigations, the mechanical relaxation time of the polypropylene matrix is determined experimentally with rheological measurements. The latter are performed on a PHYSICA UDS 200 viscometer (Figure B.1).

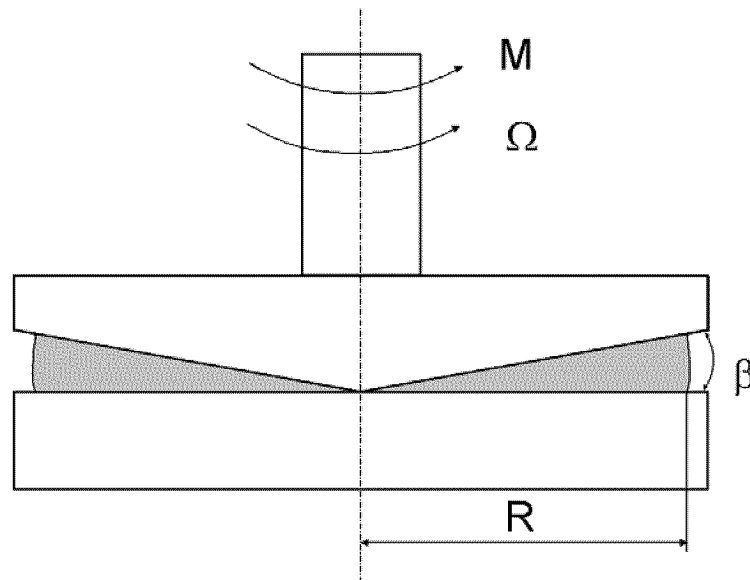


Figure B.1: Sketch of the PHYSICA UDS 200 viscometer

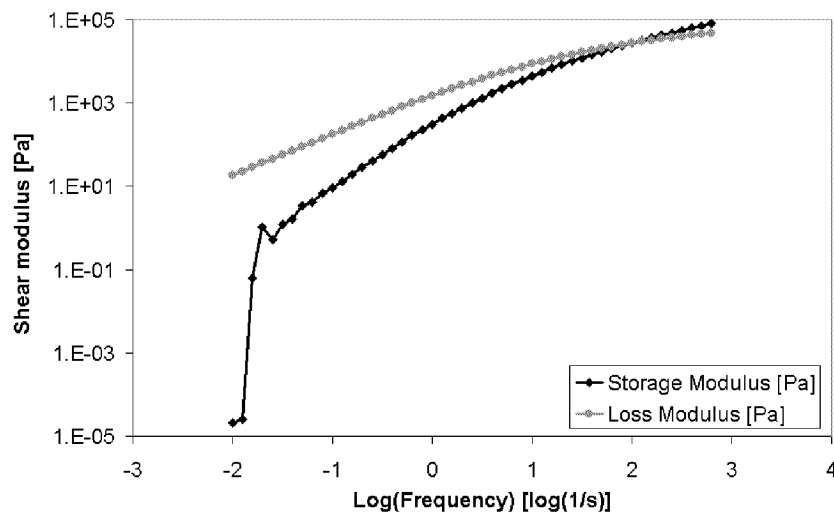


Figure B.2: Measured shear modulus at 200°C

Frequency sweep measurements are performed to determine the storage and loss modulus of the matrix as function of the frequency. In example, Figure B.2 plots the measured modulus at a constant temperature of 200°C. The large variations of the storage modulus at very low frequencies (below 0.0629 s⁻¹) are due to unstable measurements, and have therefore no physical meanings.

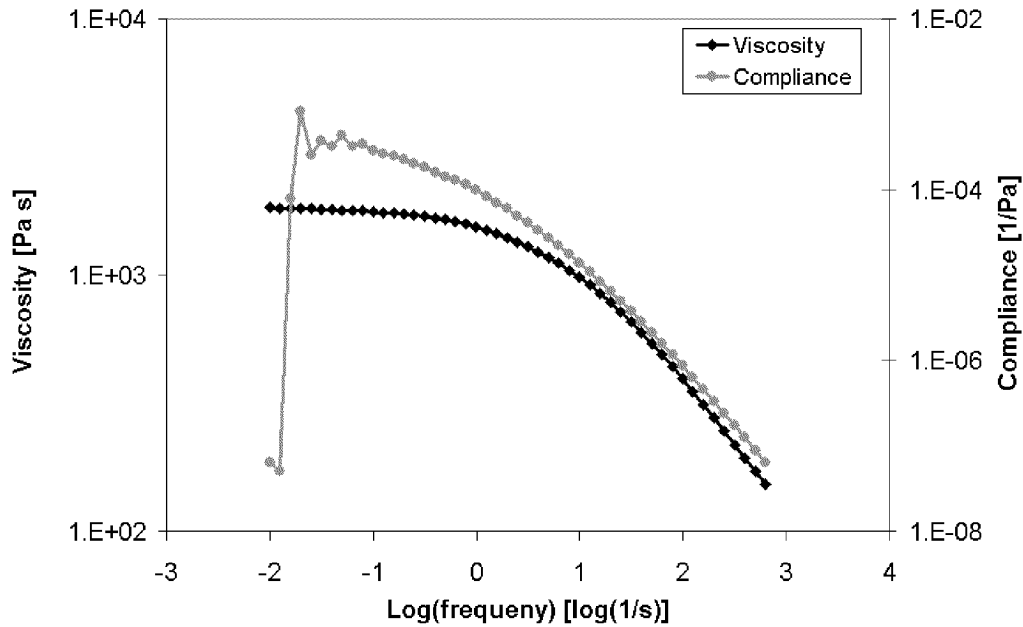


Figure B.3: Viscosity and shear compliance at 200°C

According to the theory presented by Strobl^[84] for the properties of polymer melts at low frequencies, Equations B3 to B5 gives the relations between the measurements and physical properties of the polypropylene matrix:

$$\eta_0 = \frac{G''(w \rightarrow 0)}{\omega} \quad (\text{B3})$$

$$J_e^0 = \frac{G'(w \rightarrow 0)}{\eta_0^2 \omega^2} \quad (\text{B4})$$

$$t_{mech} = J_e^0 \eta_0 \quad (\text{B5})$$

Figure B.3 displays the estimated value of the viscosity and shear compliance. According to Equations B3 and B4, they have a physical meaning only for the low frequencies. The magnitude of the viscosity is approximately constant for frequencies between 10^{-2} and 1 s^{-1} . It corresponds to the zero shear rate viscosity. The compliance magnitude is unstable for the very low frequencies (below 0.0629 s^{-1}), because it depends directly on the storage modulus measurements that are unstable in this domain.

Frequency sweep measurements are performed at various temperature to determine the temperature dependence of the viscosity and shear compliance.

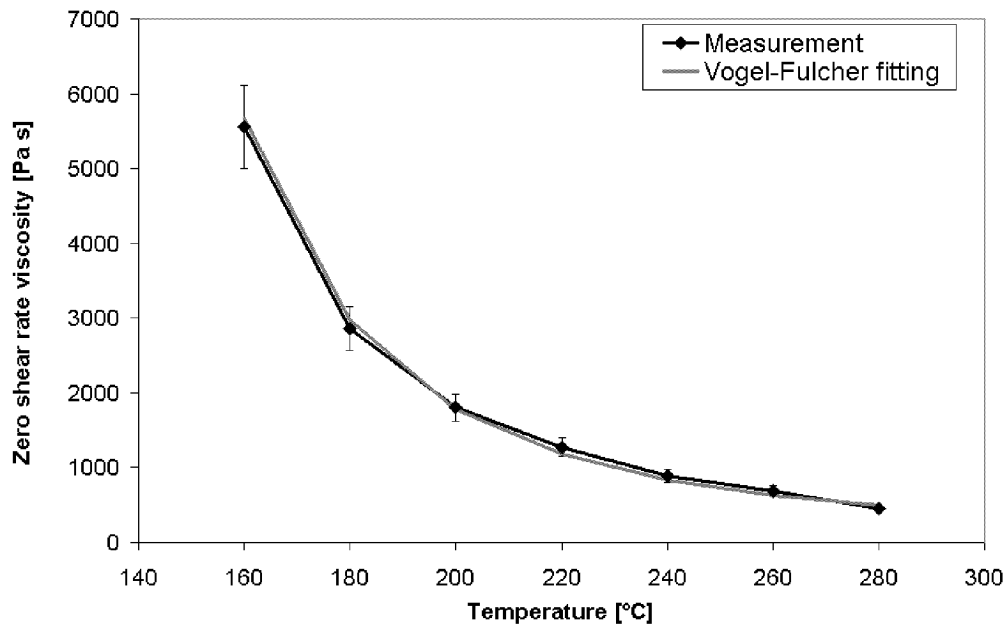


Figure B.4: Viscosity versus temperature

Figure B.4 resumes the results for the zero shear rate viscosity. In order to facilitate the calculations in the simulation program, the measurements are fitted with a Vogel-Fulcher function:

$$\eta_0(T) = B \exp\left(\frac{T_A}{T - T_V}\right) \quad (\text{B6})$$

where $B=22.5 \text{ Pa s}$, $T_A=836 \text{ K}$ and $T_V=282 \text{ K}$

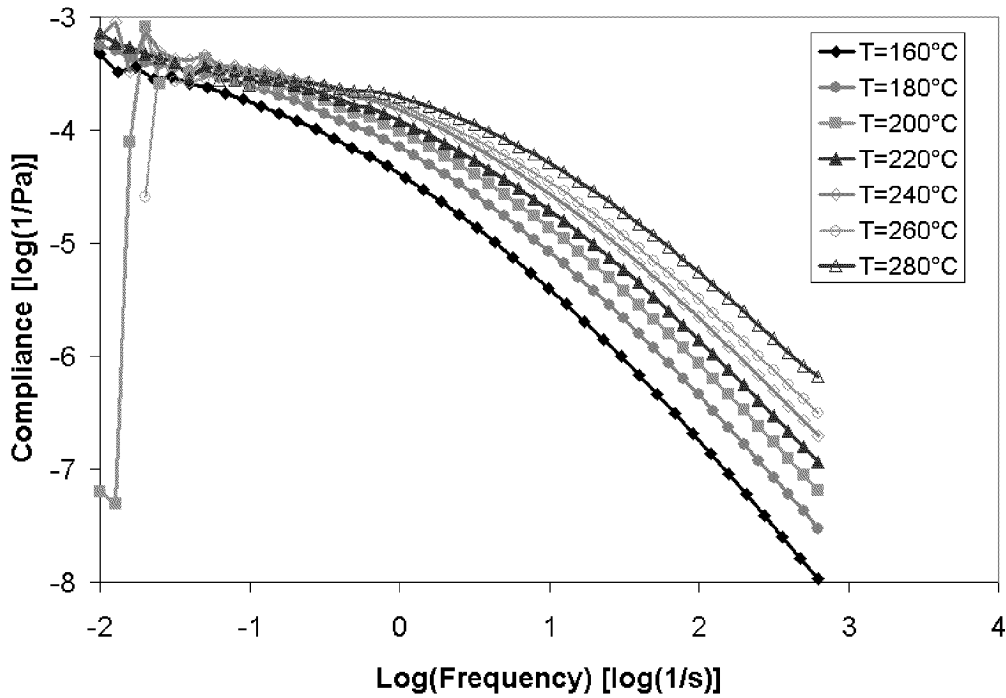


Figure B.5: Compliance versus temperature

Figure B.5 shows the measurement of the shear compliance for different temperatures. Notwithstanding the unstable measurements under the frequencies of 0.0629 s^{-1} , the figure shows that all the measurements of the shear compliance converge to the same value when the frequency converge to 0. The recoverable shear compliance is then evaluated to be:

$$J_e^0 = 10^{-3.4} \quad (\text{B7})$$

Equations B5 to B7 yield the following expression for the mechanical relaxation time:

$$t_{mech}(T) = C \exp\left(\frac{T_A}{T - T_V}\right) \quad (\text{B8})$$

where $C=8.9574 \cdot 10^{-3} \text{ s}$, $T_A=836 \text{ K}$ and $T_V=282 \text{ K}$

B.3. Determination of the molecular weight

The objective of this section is to determine the molecular weight of the polypropylene that is contained in the fiber reinforced tapes.

Since the tapes cannot be used for the molecular weight measurements, it is necessary to separate the matrix and the fibers. This is performed in three steps. First, tapes are dissolved in p-xylene at 100°C with a magnetic stirrer bar. The hot solution is filtered through a glass filter and allowed to dry in an open petri dish at ambient conditions. Last traces of solvent are removed in vacuo.

In order to observe the influence of the separation process on the measurements, the molecular weight of two additional samples is also determined. The polypropylene of both samples originates from the polypropylene granulates that are used to manufacture the tapes. The matrix of the first sample is prepared as the polypropylene coming from the tape. The resin of the second sample originates directly from the granulates.

The weight average molecular weight of the three samples is finally determined with (hot temperature) gel permeation chromatography ^[63]. Table B.1 lists the results of the measurements.

Specimen	M_w	factor $M_c=7000$	factor $M_c=7600$
granulates	240400	0.910692	0.906751
dissolved and filtered granulates	213400	0.904923	0.900713
Tapes	214600	0.905203	0.901006

Table B.1: Weight average molecular weight of the polypropylene ^[63]

The value of the factor is defined in Equation B9. It describes the influence of the molecular weight on the development of the degree of polymer chain diffusion (Equations B10). Note that Equations B1 and B2 yield to the relation given in Equation B10.

$$factor = \sqrt{1 - \sqrt{\frac{M_c}{M}}} \quad (B9)$$

$$D_{pcd} = \sqrt{1 - \sqrt{\frac{M_c}{M}}} \left(\frac{t}{t_{mech}} \right)^{1/4} \quad (\text{B10})$$

According to Table B.1, the factor is approximately constant for all samples. A magnitude of 0.9 is used in the model of the degree of polymer chain diffusion.

B.4. Numerical determination of the degree of polymer chain diffusion during the process

The determination of the degree of polymer chain diffusion during the process is performed in four steps. In order to support the explanation, a node between two layers is considered. It is supposed that the layers have been first in intimate contact at the time t_{contact} .

The first step consists to calculate the mean temperature during the current time step (t_{current}):

$$T_{\text{average}}(\text{node}, t_{\text{current}}) = \frac{T_{\text{initial}}(\text{node}, t_{\text{current}}) + T_{\text{final}}(\text{node}, t_{\text{current}})}{2} \quad (\text{B11})$$

then the corresponding reptation time is determined with Equation B2 and B8:

$$t_{\text{rep}}(\text{node}, t_{\text{current}}) = \left[1 - \sqrt{\frac{M_c}{M}} \right]^{-2} C \exp\left(\frac{T_A}{T_{\text{average}}(\text{node}, t_{\text{current}}) - T_V} \right) \quad (\text{B12})$$

where $C = 8.9574 \cdot 10^{-3}$ s, $T_A = 836$ K and $T_V = 282$ K

In order to determine the progression of the degree of polymer chain diffusion during the current time step, the time t' is calculated. It corresponds to the time that is necessary to reach the degree of polymer chain diffusion of the preceding time step ($t_{\text{current-1}}$) if the node has been heated with current temperature.

$$t'(\text{node}, t_{\text{current}}) = (D_{pcd}(\text{node}, t_{\text{current-1}}))^4 t_{\text{rep}}(\text{node}, t_{\text{current}}) \quad (\text{B13})$$

Finally, the degree of polymer chain diffusion at the end of the current time step is given by:

$$D_{pcd} = \left(\frac{t'(node, time\ step) + \Delta t}{t_{rep}(node, time\ step)} \right)^{1/4} \quad (B14)$$

The preceding operations are repeated for all nodes in intimate contact and for all time steps.

B.5. Remarks

Equations B11 to B14 can be summarized by :

$$D_{pcd}(node, t_{current}) = \left[\sum_{t_n=t_{contact}}^{t_{current}} \left(\frac{\Delta t}{t_{rep}(node, t_n)} \right) \right]^{1/4} \quad (B15)$$

or

$$D_{pcd}(node, t_{current}) = \sqrt{1 - \sqrt{\frac{M_c}{M}}} \left[\sum_{t_n=t_{contact}}^{t_{current}} \left(\frac{\Delta t}{t_{mech}(node, t_n)} \right) \right]^{1/4} \quad (B16)$$

Equations B16 enables to visualize the influence of the molecular weight on the degree of polymer chain diffusion and justify the introduction of Equation B9.

B.6. Nomenclature

β	angle
η	viscosity
σ	strength
ω	angular speed
Ω	angle
D	degree
G'	storage modulus
G''	loss modulus
J_e	shear compliance

M	molecular weight
M	torque
R	radius
t	time
T	temperature

Subscript

c	critical
mech	mechanical relaxation
pcd	polymer chain diffusion
rep	reptation
w	weight
0	zero shear rate

Reference

- [1] V. Agarwal, S.I. Güçeri, R.L. McCullough and J.M. Schultz, “Thermal Characterisation of the Laser-Assisted Consolidation Process”, *Journal of Thermoplastic Composite Materials*, 5:115-135, 1992
- [2] V. Agarwal, R.L. McCullough and J.M. Schultz, “The Thermoplastic Laser-Assisted Consolidation Process – Mechanical and Microstructure Characterization”, *Journal of Thermoplastic Composite Materials*, 9:365-380, 1996
- [3] M. Ahrens, V. Mallick and K. Parfrey, “Robotic Thermoplastic Fiber Placement Process”, *ABB Review* 2:27-34, 1998
- [4] Angst+Pfister, “Technische Informationen über ISOPLAN”, 2000
- [5] ANSYS Inc., “Theory Reference, Release 5.6”, 11th Edition, 1999
- [6] M. Avrami, “Kinetics of Phase Change, I: General Theory”, *Journal of Chemical Physics*, 7:1103-1112, 1939
- [7] M. Avrami, “Kinetics of Phase Change, II: Transformation-Time Relation for Random Distribution of Nuclei”, *Journal of Chemical Physics*, 8:212-224, 1940
- [8] M. Avrami, “Kinetics of Phase Change, III: Kinetics of Phase Change”, *Journal of Chemical Physics*, 9:177-184, 1941
- [9] L.J. Bastien and J.W. Gillespie Jr., “A Non-Isothermal Healing Model for Strength and Toughness of Fusion Bonded Joints of Amorphous Thermoplastics”, *Polymer Engineering and Science*, 31:1720-1730, 1991
- [10] B.M. Bauer, K.V. Steiner and K.U. Wolf, “Experimental Verification of Modeling and Control for the Thermoplastic Tape Placement”, *CCM* 94-24, 1994

-
- [11] E.P. Beyeler and S.I. Güçeri, "Thermal Analysis of Laser-Assisted Thermoplastic-Matrix Composite Tape Consolidation", *Journal of Heat Transfer*, 110:424-430, 1988
- [12] C.A. Butler, R.L. McCullough, R. Pitchumani and J.W. Gillespie Jr., "An Analysis of Mechanisms Governing Fusion Bonding of Thermoplastic Composites", *Journal of Thermoplastic Composite Materials*, 11:338-363, 1998
- [13] A. Cerini and M. Beretta, "Entwicklung eines Neuen Anpresssystems für den Tape-Wickelprozess", Diplomarbeit am IKB, ETHZ, 1998
- [14] M. Chao and J.W. Gillespie Jr., "The Influence of Healing and Bondline Thickness on the Mechanical Performance of Fusion-Bonded Thermoplastic Composite Joints", 39th International SAMPE Symposium and Exhibition, 39:2023-2037, 1994
- [15] J.M. Charrier, M.E. Weber and X. Wang, "Heating of Thermoplastic-Based Unidirectional Composite Prepreg Tapes", 43rd Annual Conference of the Society of the Plastic Industry, Session 7D, 1988
- [16] B.R. Cho and J.L. Kardos, "Consolidation and Self-Bonding in Poly(ether ether ketone) (PEEK)", *Journal of Applied Polymer Science*, 56:1435-1454, 1995
- [17] C.R. Choe and K.H. Lee, "Nonisothermal Crystallization Kinetics of Poly(etheretherketone) (PEEK)", *Polymer Engineering and Science*, 29:801-805, 1989
- [18] B.S. Coffenberry, D.E. Hauber and M. Cirino, "Low Cost Alternative: In-Situ Consolidated Thermoplastic Composite Structures", 38th International SAMPE Symposium and Exhibition, 38:1640-1650, 1993
- [19] P.H. Dara and A.C. Loos, "Thermoplastic Matrix Composite Processing Model", CCMS-85-10 or VPI-E-85-21, Virginia Polytechnic Institute and State University, 1985
- [20] M. Day, J.D. Cooney and D.M. Wiles, "A Kinetic Study of the Thermal Decomposition of Poly(Aryl-Ether-Ether-Ketone) (PEEK) in Nitrogen", *Polymer Engineering and Science*, 29:19-22, 1989

-
- [21] W. Dietz, "Sphärolithwachstum in Polymeren", *Colloid and Polymer Science*, 259:413-429, 1981
- [22] R.C. Don, S.T. Holmes, K.V. Steiner and J.W. Gillespie Jr., "Integrated Process Models for Control of Thermoplastic Tow Placement with On-Line Consolidation", 25th International SAMPE Technical Conference, 25:713-724, 1993
- [23] R.C. Don, R. Pitchumani and J.W. Gillespie Jr., "Simulation of the Transients in Thermoplastic Fiber Placement", 39th International SAMPE Symposium and Exhibition, 39:1521-1535, 1994
- [24] M.W. Egerton and M.B. Gruber, "Thermoplastic Filament Winding Demonstrating Economics and Properties via In-Situ Consolidation", 33rd International SAMPE Symposium, 33:35-46, 1988
- [25] M.L. Enders, "Developments in Thermoplastic Filament Winding", 22nd International SAMPE Technical Conference, 22:88-97, 1990
- [26] R. Funck, "Entwicklung Innovativer Fertigungstechniken zur Verarbeitung Kontinuierlichfaserverstärkter Thermoplaste im Wickelverfahren", *Fortschritt-Berichte VDI Reihe 2 Nr. 393*, VDI Verlag, ISBN 3-18-339302-6, 1996
- [27] P. Gallagher, "In-Situ Consolidation of Thermoplastic Thick Rings", 43rd International SAMPE Symposium and Exhibition, 43:1943-1954, 1998
- [28] M.N. Ghasemi Nejhad, R.D. Cope and S.I. Güçeri, "Thermal Analysis of In-Situ Thermoplastic-Matrix Composite Filament Winding", *Journal of Heat Transfer*, 113:304-313, 1991
- [29] M.N. Ghasemi Nejhad, J.W. Gillespie Jr. and R.D. Cope, "Prediction of Process-Induced Stresses for In-Situ Thermoplastic Filament Winding of Cylinders", 3rd Conference on Computer Aided Design in Composite Material Technology, 3:225-253, 1992
- [30] M.N. Ghasemi-Nejhad, "Issues Related to Processability during the Manufacture of Thermoplastic Composites using On-Line Consolidation Techniques", *Journal of Thermoplastic Composite Materials*, 6:130-146, 1993

-
- [31] R.W. Grenoble, B.C. Messier and J.M. Marchello, "Adhesive Bonding of Composite Ribbon During Automated Tow Placement", 29th International SAMPE Technical Conference, 29:98-107, 1997
- [32] M. Goedel, "Möglichkeiten und Grenzen des Wickelns mit Infraroterwärmung – Herstellung Endlosfaserverstärkter Wickelbauteile mit Thermoplastischer Matrix", Ph.D. thesis at RWTH Aachen, 1992
- [33] K. Ghazi Wakili and T. Frank, EMPA-Prüfbericht Nr. 414 614, 2000
- [34] S.M. Grove, "Thermal Modelling of Tape Laying with Continuous Carbon Fibre-Reinforced Thermoplastic", *Composites*, 19:367-375, 1988
- [35] I. Hagen, C. Düren, E. Lange and C. Rasche, "Einsatz Unidirektionaler Faserverstärkter Thermoplaste für die Herstellung Leichter Composite-Behälter", VDI-Berichte 1080, VDI-Verlag, 355-375, 1994
- [36] J.C. Howes and A.C. Loos, "Autohesive Strength Development in Polysulfone Resin and Graphite-Polysulfone Composites", *Journal of Thermoplastic Composite Materials*, 1:58-67, 1988
- [37] B. Hulcher, J.M. Marchello and J.A. Hinkley, "Correlation between Double Cantilever Beam and Wedge Peel Tests for Automated Tow Placement", 43rd International SAMPE Symposium and Exhibition, 43:1955-1965, 1998
- [38] J. Hümmler, S.K. Lee and K.V. Steiner, "Recent Advance in Thermoplastic Robotic Filament Winding", 36th International SAMPE Symposium and Exhibition, 36:2142-2156, 1991
- [39] F.P. Incropera and D.P. DeWitt, "Fundamentals of Heat and Mass Transfer", Fourth Edition, John Wiley and Sons, ISBN 0-471-30460-3, 1996
- [40] R.G. Irwin Jr. and S.I. Güçeri, "Parametric Study of Laser Assisted Processing of Thermoplastic Composites", *ASME-AMD Mechanics in Materials Processing and Manufacturing*, 194:319-333, 1994

-
- [41] D.L. James and W.Z. Black, "Experimental Analysis and Process Window Development for Continuous Filament Wound APC-2", ASME-HTD Thermal Processing of Materials : Thermo-Mechanics, -Controls and Composites, 289:203-212, 1994
- [42] D.L. James and W.Z. Black, "Thermal Analysis of Continuous Filament-Wound Composites", Journal of Thermoplastic Composite Materials", 9:54-75, 1996
- [43] K. Jud, H.H. Kausch and J.G. Williams, "Fracture Mechanics Studies of Crack Healing and Welding of Polymers", Journal of Materials Science, 16:204-210, 1981
- [44] J. Karger-Kocsis, "Polypropylene, Structure, Blends and Composites, Structure and Morphology", Chapman and Hall, ISBN 0-412-58430-1, 1995
- [45] D.B. Kline and R.P. Wool, "Polymer Welding Relations Investigated by a Lap Shear Joint Method", Polymer Engineering and Science, 28:52-57, 1988
- [46] H.J. Kim, S.K. Kim and W.I. Lee, "A Study on Heat Transfer during Thermoplastic Composite Tape Lay-up Process", Experimental Thermal and Fluid Science, 13:408-418, 1996
- [47] B. Lauke and K. Friederich, "Interlaminar Shear Strength Measurement of Thin Composite Rings Fabricated by Filament Winding", 5th ECCM Conference, 5:313-318, 1992
- [48] B. Lauke and K. Friederich, "Evaluation of Processing Parameters of Thermoplastic Composites Fabricated by Filament Winding", Composites Manufacturing, 4:93-101, 1993
- [49] B. Lauke, A. Schöne and K. Friederich, "High Performance Thermoplastic Composites Fabricated by Filament Winding", International Conference on Advanced Composite Materials, 883-889, 1993
- [50] B. Lauke, W. Beckert and K. Schneider, "Interlaminar Shear Strength Evaluation of Curved Composite Samples", Applied Composite Materials, 1:267-271, 1994

-
- [51] W.I. Lee and G.S. Springer, "A Model of the Manufacturing Process of Thermoplastic Matrix Composites", *Journal of Composite Materials*, 21:1017-1051, 1987
- [52] A.C. Loos and P.H. Dara, "Processing of Thermoplastic Matrix Composites", *Review of the Progress in Quantitative Non-Destructive Evaluation*, 6B:1257-1265, 1986
- [53] A.YA. Malkin, V.P. Beghishev, I.A. Keapin and S.A. Bolgov, "General Treatment of Polymer Crystallization Kinetics, Part 1 : A New Macrokinetic Equation and its Experimental Verification", *Polymer Engineering and Science*, 24:1396-1401, 1984
- [54] A.YA. Malkin, V.P. Beghishev, I.A. Keapin and Z.S. Andrianova, "General Treatment of Polymer Crystallization Kinetics, Part 2 : The Kinetics of Non-Isothermal Crystallization", *Polymer Engineering and Science*, 24:1402-1408, 1984
- [55] S.C. Mantell, Q. Wang and G.S. Springer, "Thermoplastic Tape Laying", 36th International SAMPE Symposium and Exhibition, 36:1763-1772, 1991
- [56] S.C. Mantell and G.S. Springer, "Manufacturing Process Models for Thermoplastic Composites", *Journal of Composite Materials*, 26:2349-2377, 1992
- [57] S.C. Mantell, Q. Wang and G.S. Springer, "Processing Thermoplastic Composites in a Press and by Tape Laying - Experimental Results", *Journal of Composite Materials*, 26:2378-2401, 1992
- [58] S.K. Mazumdar and S.V. Hoa, "Experimental Determination of Process Parameter for Laser Assisted Processing of PEEK/Carbon Thermoplastic Composites", 38th International SAMPE Symposium and Exhibition, 38:189-203, 1993
- [59] S.K. Mazumdar and S.V. Hoa, "Manufacturing of Non-Axisymmetric Thermoplastic Composite Parts by Tape Winding Technique", *Material and Manufacturing Processes*, 10:47-56, 1995
- [60] S.K. Mazumdar and S.V. Hoa, "Determination of Manufacturing Conditions for Hot-Gas-Aided Thermoplastic Tape Winding", *Journal of Thermoplastic Composite Materials*, 9:35-53, 1996

-
- [61] A.M. Mazzeffoli, J.M. Kenny and L. Nicolais, "Welding of PEEK/Carbon Fiber Composite Laminates", SAMPE Journal, 25:35-39, 1989
- [62] J.A. Mondo and K.A. Parfrey, "Performance of In-Situ Consolidated Thermoplastic Composite Structure", 27th International SAMPE Technical Conference, 27:361-370, 1995
- [63] P. Montag, "HT-GPC-Messungen", Auftragsnummer 589911, Polymer Standards Service, 2002
- [64] J.D. Muzzy, D.M. Abouelnasr and A.O. Kays, "Melting and Solidification of APC-2", 33rd International SAMPE Symposium and Exhibition, 33:1319-1330, 1988
- [65] J.D. Nam and J.C. Seferis, "Generalized Composite Degradation Kinetics for Polymeric Systems under Isothermal and Non-Isothermal Conditions", Journal of Polymer Science : Part B : Polymer Physics, 30:455-463, 1992
- [66] T. Ozawa, "Kinetics of Non-Isothermal Crystallization", Polymer, 12:150-158, 1971
- [67] R. Pitchumani, R.C. Don, J.W. Gillespie Jr. and S. Ranganathan, "Analysis of On-Line Consolidation during Thermoplastic Tow-Placement Process", ASME-HTD Thermal Processing of Materials : Thermo-Mechanics, -Controls and Composites, 289:223-243, 1994
- [68] R. Pitchumani, R.S. Ranganathan, R.C. Don and J.W. Gillespie, "Effects of Processing Conditions on Void Growth during Thermoplastic Fiber Placement", ASME-AMD Mechanics in Materials Processing and Manufacturing, 194:71-87, 1994
- [69] R. Pitchumani, S. Ranganathan, R.C. Don, J.W. Gillespie Jr. and M.A. Lamontia, "Analysis of Transport Phenomena Governing Interfacial Bonding and Voids Dynamics during Thermoplastic Tow Placement", Journal of Heat and Mass Transfer, 39:1883-1897, 1996
- [70] R. Pitchumani, J.W. Gillespie Jr. and M.A. Lamontia, "Design and Optimization of a Thermoplastic Tow-Placement Process with In-Situ Consolidation", Journal of Composite Materials, 31:244-275, 1997

-
- [71] J. Romagna, "Neue Strategien in der Faserwickeltechnik", Ph.D. thesis ETHZ, Nummer 12450, 1997
- [72] F. Rosselli and H. Santare, "Comparison of the Short Beam Shear (SBS) and Interlaminar Shear Device (ISD)", *Composites, Part A*, 28:587-594, 1997
- [73] F. Rosselli, H. Santare and S.I. Güçeri, "Effects of Processing on Laser Assisted Thermoplastic Tape Consolidation", *Composites, Part A*, 28:1023-1033, 1997
- [74] J.H.C. Rowan and R.N. Askander, "Filament Winding of High Performance Thermoplastic Composites", 10th International European Chapter Conference of the SAMPE, 10:11-20, 1989
- [75] H. Sarrazin and G.S. Springer, "Thermochemical and Mechanical Aspects of Composite Tape Laying", *Journal of Composite Materials*, 29:1908-1943, 1995
- [76] J.C. Seferis, C. Ahlstrom and S.H. Dillman, "Cooling Rate and Annealing as Processing Parameters for Semicrystalline Thermoplastic Based Composites", 45th SPE Annual Technical Conference and Exhibit, Plastic-Pioneering the 21st Century, ANTEC 87, 45:1467-1471, 1987
- [77] P.J. Shih and A.C. Loos, "Process Induced Thermal Stresses in Thermoplastic Filament Winding", 31st International SAMPE Technical Conference, 31:626-637, 1999
- [78] P.J. Shih and A.C. Loos, "Heat Transfer Analysis of the Thermoplastic Filament Winding Process", *Journal of Reinforced Plastics and Composites*, 18:1103-1112, 1999
- [79] P.J. Shih and A.C. Loos, "Design of Experiments Analysis of the On-Line Consolidation Process", 11th ICCM Conference, 11:92-102, 1997
- [80] F.O. Sonmez and H.T. Hahn, "Modeling of Heat Transfer and Crystallization in Thermoplastic Composite Tape Placement Process", *Journal of Thermoplastic Composite Materials*, 10:198-240, 1997

-
- [81] F.O. Sonmez and H.T. Hahn, "Analysis of the On-Line Consolidation Process in Thermoplastic Composite Tape Placement", *Journal of Thermoplastic Composite Materials*, 10:543-572, 1997
- [82] K.V. Steiner, "Einsatz einer Robotergestützten Anlage zum Bandablegen von Thermoplastischen Verbundwerkstoffen", Ph.D. thesis at the RTWH Aachen, 1995
- [83] K.V. Steiner, B.M. Bauer, R. Pitchumani and J.W. Gillespie Jr., "Experimental Verification of Modeling and Control for Thermoplastic Tow-Placement", 40th International SAMPE Symposium and Exhibition, 40:1550-1559, 1995
- [84] G.R. Strobl, "The Physics of Polymers, Concepts for Understanding their Structure and Behavior", Springer-Verlag, Second Edition, ISBN 3-540-63203-4, 1997
- [85] W.C. Sun, S.C. Mantel and K.A. Stelson, "Demonstration of Bond Quality Improvement for Closed Loop Control of Thermoplastic Tape-Laying", *Journal of Composite Materials*, 35:57-76, 2001
- [86] D. Stover, "Tape-Laying Precision Industrial Shafts", *High Performance Composites*, 29-32, 1994
- [87] M.C. Tobin, "Theory of Phase Transition Kinetics with Growth Site Impingement. I. Homogeneous Nucleation", *Journal of Polymer Science : Polymer Physics Edition*, 12:399-406, 1974
- [88] M.C. Tobin, "Theory of Phase Transition Kinetics with Growth Site Impingement. II. Heterogeneous Nucleation", *Journal of Polymer Science : Polymer Physics Edition*, 14:2253-2257, 1976
- [89] M.C. Tobin, "Theory of Phase Transition Kinetics with Growth Site Impingement. III. Mixed Heterogeneous-Homogeneous Nucleation and Nonintegral Exponents of the Time", *Journal of Polymer Science : Polymer Physics Edition*, 15:2269-2270, 1977
- [90] Y.M.P. Toso and G. Ziegmann, "Thermoplastic Filament Winding: Actual Status and Perspectives", *Filament Winding* 98, 1998

-
- [91] S. Tumkor, N. Turkmen, C. Chassapis and S. Manoochchri, "Modeling of Heat Transfer in Thermoplastic Composite Tape Lay-up Manufacturing", *International Communication in Heat and Mass Transfer*, 28:49-58, 2001
- [92] C.N. Velisaris and J.C. Seferis, "Heat Transfer Effects on the Processing-Structure Relationships of Polyetheretherketone (PEEK) Based Composites", *Polymer Engineering and Science*, 28:583-591, 1988
- [93] P. Wagner and J. Colton, "On-Line Consolidation of Thermoplastic Towpreg Composites in Filament Winding", *39th International SAMPE Symposium and Exhibition*, 39:1536-1545, 1994
- [94] *Wärme-Atlas, Sixth Edition*, VDI-Verlag, 1991
- [95] D. Wood and S.C. Mantell, "Application of Statistical Design of Experiments to Thermoplastic Tape Laying", *38th International SAMPE Symposium and Exhibition*, 38:153-162, 1993
- [96] R.P. Wool and K.M. O'Connor, "A Theory of Crack Healing in Polymers", *Journal of Applied Physics*, 52:5953-5963, 1981
- [97] R.P. Wool, "Polymer Entanglements", *Macromolecules*, 26:1564-1569, 1993
- [98] R.P. Wool, "Polymer Interfaces, Structure and Strength", Hanser/Gardner Publications, ISBN 1-56990-133-3, 1995
- [99] M.A. Yardimci, C.M. Pistor and S.I. Güçeri, "Fabrication of Non-Circular Shapes with Laser Assisted Tape Winding: Unsteady Process Analysis", *28th International SAMPE Technical Conference*, 28:1016-1026, 1996

Curriculum Vitae

Yves Marcel Pierre Toso
Citizen of Collonge-Bellerive (GE), Switzerland
Born on March 27th 1967

Experience

- 1997 - 2003 **Eidgenössische Technische Hochschule Zürich**
Ph.D. Student, “Effective Automated Tape Winding Process with On-Line Bonding under Transient Thermal Conditions”, development and validation of a simulation tool, determination of the corresponding material properties and boundary conditions
- 1996 - 1997 **Eidgenössische Technische Hochschule Zürich**
Scientific employee, development of a setup and experimental investigations of the automated tape winding process, development of a new compaction tool for this process, webmaster, coaching of mechanical engineering students
- 1994 - 1995 **Peter Siegl Ing. Büro (Weesen, Sankt-Gallen)**
Scientific employee, investigations of hypocaust heat systems
- 1994 **ABB Kraftwerke AG (Baden, Aargau)**
Practical experience, study of the heat transfer through boundary layers for gas turbine blades
- 1991 - 1992 **Département de l’enseignement public du canton de Genève**
Replacement of teachers in secondary schools in Geneva

Formation

- 1993 Diploma in mechanical engineering at the Swiss Federal Institute of Technology Lausanne (EPFL), “Energetic study of a swimming pool building (Etude énergétique d’une piscine) “
- 1987 - 1993 Study of the mechanical engineering at the EPFL
- 1987 Maturité cantonale et fédérale de type C, Collège Calvin, Geneva
- 1971 - 1987 Schools in Geneva